

CHARLES UNIVERSITY IN PRAGUE

Faculty of Science

---

Study program: Biochemistry



BSc. Samuel Pažický

Study of NKp30 oligomerization and its  
interaction with B7-H6

Studium oligomerizace proteinu NKp30  
a jeho interakce s B7-H6

Diploma thesis

Prague, 2016

Supervisor: RNDr. Ondřej Vaněk, Ph.D.

Herein I confirm that this thesis was written independently under the supervision of Dr. Ondřej Vaněk and that all referenced literature was properly cited. This work has not been submitted to receive any other or same academic title.

Prohlašuji, že jsem tuto diplomovou práci vypracoval samostatně, pod vedením školitele RNDr. Ondřeje Vaňka, Ph.D., a že jsem všechny použité prameny řádně citoval. Tato práce nebyla předložena k získání jiného nebo stejného akademického titulu.

V Praze, dne .....

Podpis

.....

## **Acknowledgement**

At first, I would like to thank my supervisor Dr. Ondřej Vaněk for his patience and valuable remarks, for steering my work in the right direction and at the same time allowing me to be an equal partner in the discussions during our laboratory meetings and talks.

Also I want to say thank you to Mgr. Jan Bláha for infinite advice on my experimental work and for sharing his valuable experience and knowledge. My thanks also go to Mgr. Barbora Kalousková who did initial experiments which preceded my work.

I would also like to acknowledge Mgr. Michal Rosůlek for measuring and evaluating mass spectrometry data, Dr. Sami Kereiche. for electron microscopy imaging, Dr. Tatsiana Charnavets for measuring and evaluating isothermal titration calorimetry measurements, Dr. Yuguang Zhao for his help with crystallization screens set-up, Dr. Karl Harlos for collection of diffraction data and Dr. Tereza Skálová for SAXS and crystallization data evaluation.

I am also really grateful for the team of the laboratory 204, members of which never failed to create a great working atmosphere.

Last but not least, I would like to mention my parents and friends whose support was irreplaceable.

*This study was supported by Czech Science Foundation (15-15181S), Charles University in Prague (GA UK No 927916) and Instruct European infrastructure project.*

## **Abstract**

NK cells are important part of immune system, recognizing and eliminating tumor cells and cells infected by viruses. For the target cell recognition, binding of ligands by activating receptors plays a crucial role. Activating receptor NKp30, protein of family of natural cytotoxicity receptors, is able to bind multiple ligands either present on tumor cell surface or being part of some viruses. B7-H6 is one of the ligands of NKp30 and its specific constitutive expression on some tumor cells and cell lines makes it an interesting biological target.

Although the NKp30/B7-H6 complex structure has been solved, structural basis of some important features of their binding is not explained yet. Soluble form of NKp30 receptor binding domain creates oligomers, presence of which is dependent on C-terminus length of its domain and its N-glycosylation; however, structural insight into formation of the oligomers and their significance is not known. Furthermore, binding affinity of NKp30 to its ligands is dependent on presence of its glycosylation and glycosylation type.

We have already found out that NKp30 oligomerization is dependent on its glycosylation. In my work, I attempted to gain detailed functional and structural information about oligomerization of NKp30 and its binding to B7-H6 by multimethodical approach including X-ray crystallography.

Answering the questions described above would not only contribute to basic research of activating receptors of NK cells but possibly may have an impact on further research of cancer diagnostics and therapy.

**KEY WORDS:** NK cell, glycosylation, oligomerization, NKp30, B7-H6

## Abstrakt

NK buňky jsou důležitou součástí imunitního systému. Jsou schopné rozeznat a zničit nádorové buňky a buňky infikované virem. Pro rozpoznání jejich cílových buněk hrají důležitou roli jejich aktivační receptory. Aktivační receptor NKp30, protein z rodiny přirozeně cytotoxických receptorů, váže několik ligandů přítomných na povrchu nádorových buněk anebo tvořících částí některých virů. B7-H6 je jedním z ligandů NKp30 a díky jeho specifické konstitutivní expresi na povrchu některých nádorů a nádorových buněk je zajímavým biologickým cílem.

Ačkoli již byla struktura komplexu NKp30/B7-H6 vyřešena, strukturní podstata některých důležitých vlastností vazby komplexu zatím nebyla vysvětlena. NKp30 tvoří oligomery, jejichž přítomnost je ovlivněna délkou C-konce NKp30 a jeho N-glykosylací, avšak strukturní podstata a ani význam těchto oligomerů nejsou známy. Navíc je vazebná afinita NKp30 k jeho ligandům ovlivněna přítomností jeho glykosylace a také jejím typem.

V naší laboratoři jsme již dříve zjistili, že oligomerizace NKp30 je závislá na jeho glykosylaci. V mé práci jsem se pokusil získat detailnější funkční a strukturní informace o oligomerizaci NKp30 a vazbě B7-H6 multimetodickým přístupem včetně rentgenové krystalografie.

Zodpovězení vznesených otázek by nejen přispělo k základnímu výzkumu aktivačních receptorů NK buněk, ale také by mohlo mít dopad na další výzkum v oblasti diagnostiky a léčby rakoviny.

**KLÍČOVÁ SLOVA:** NK buňka, glykosylace, oligomerace, NKp30, B7-H6

Acknowledgement.....	3
Abstract .....	4
Abstrakt .....	5
List of abbreviations .....	9
1. Introduction .....	11
1.1. Natural killer cells .....	11
1.1.1. Development of NK cells .....	11
1.1.2. Receptors of NK cells.....	12
1.1.3. Education of NK cells .....	16
1.1.4. Signaling in NK cells .....	17
1.1.5. Cytotoxic mechanisms of NK cells.....	17
1.1.6. Regulatory function .....	18
1.1.7. Immunological memory .....	18
1.2. NKp30.....	18
1.2.1. Structure of NKp30 .....	18
1.2.2. Genetics and isoforms .....	20
1.2.3. Ligands of NKp30 .....	21
1.2.4. Variable affinity to ligands.....	21
1.3. B7-H6 .....	23
1.3.1. Structure of B7-H6.....	23
1.3.2. B7-H6 gene .....	24
1.3.3. Expression of B7-H6.....	24
1.3.4. B7-H6 shedding .....	25
1.4. Clinical importance of NKp30 and B7-H6 .....	25
1.4.1. Potential in diagnostics .....	25
1.4.2. NKp30/B7-H6-based therapy .....	26
2. Aims of the thesis .....	29
3. Materials.....	30
3.1. Instruments and tools.....	30
3.2. Enzymes .....	31
3.3. Chemicals.....	31
3.4. Cell culture media .....	32

3.5.	Solutions .....	33
3.6.	DNA .....	34
3.7.	Cell lines and bacterial strains .....	35
4.	Methods .....	36
4.1.	Cloning and DNA manipulation .....	36
4.1.1.	Overlap extension polymerase chain reaction (OE-PCR) .....	36
4.1.2.	Agarose electrophoresis .....	37
4.1.3.	Isolation of DNA from agarose gel .....	37
4.1.4.	DNA concentration measurement .....	37
4.1.5.	Restriction cleavage.....	38
4.1.6.	Ligation .....	38
4.1.7.	Transformation .....	38
4.1.8.	Colony PCR.....	38
4.1.9.	Isolation of plasmid DNA.....	39
4.1.10.	DNA sequencing.....	39
4.1.11.	Preparation of stock amount of plasmid DNA.....	39
4.2.	Recombinant protein production .....	40
4.2.1.	HEK293 cultivation .....	40
4.2.2.	Cell density counting .....	40
4.2.3.	Transient transfection .....	40
4.3.	Protein purification.....	41
4.3.1.	Centrifugation and filtration.....	41
4.3.2.	Metal chelate affinity chromatography .....	41
4.3.3.	Protein concentrating.....	41
4.3.4.	Size exclusion chromatography .....	42
4.4.	Protein characterization .....	42
4.4.1.	Protein concentration measurement .....	42
4.4.2.	SDS-PAGE .....	42
4.4.3.	Deglycosylation.....	43
4.4.4.	Mass spectrometry .....	43
4.4.5.	Differential scanning fluorimetry .....	44
4.5.	Protein-protein interaction investigation.....	44

4.5.1.	Analytical size exclusion chromatography .....	44
4.5.2.	Sedimentation analysis.....	45
4.5.3.	Cross-linking .....	45
4.5.4.	Isothermal titration microcalorimetry .....	46
4.6.	Structural analyses.....	46
4.6.1.	LC-MS with H/D exchange .....	46
4.6.2.	Electron microscopy .....	47
4.6.3.	SAXS .....	47
4.6.4.	Protein crystallization and X-ray analysis.....	47
5.	Results .....	49
5.1.	B7-H6 production and characterization .....	49
5.1.1.	Production and purification of B7-H6_2 .....	49
5.1.2.	B7-H6_2 characterization .....	50
5.1.3.	Point mutation and cloning of mB7-H6_2.....	53
5.1.4.	Production and purification of mB7-H6_2 .....	54
5.1.5.	Characterization of mB7-H6_2 .....	55
5.1.6.	Differential scanning fluorimetry .....	56
5.1.7.	Characterization of NKp30 .....	57
5.2.	Protein interaction analysis .....	59
5.2.1.	Confirmation of protein binding.....	59
5.2.2.	Complex affinity measurement .....	63
5.3.	Study of NKp30 oligomerization .....	64
5.3.1.	Electron microscopy .....	64
5.3.2.	Small-angle X-ray scattering.....	64
5.3.3.	Mass spectrometry with H/D .....	66
5.4.	Crystallography results .....	68
6.	Discussion .....	74
7.	Conclusions.....	81
8.	Literature .....	82



## List of abbreviations

<b>B7-HX</b>	protein B7 homolog X, where X is a number
<b>BAG-6</b>	B cell lymphoma 2 associated athanogen 6
<b>BiTE</b>	bispecific T-cell engager
<b>BSA</b>	bovine serum albumin
<b>C/ml</b>	10 <sup>6</sup> cells per milliliter
<b>CD</b>	cluster of differentiation
<b>DMSO</b>	dimethyl sulfoxide
<b>DNA</b>	deoxyribonucleic acid
<b>dNTPs</b>	deoxyribonucleotide triphosphate
<b>DSG</b>	disuccinimidyl glutarate
<b>DSS</b>	disuccinimidyl suberate
<b>EDTA</b>	ethylenediaminetetraacetic acid
<b>ELISA</b>	enzyme-linked immunosorbent assay
<b>Fc</b>	constant fragment
<b>FPLC</b>	fast protein liquid chromatography
<b>HCMV</b>	human cytomegalovirus
<b>HEK</b>	human embryonic kidney cell line
<b>HER-2</b>	human epidermal growth factor receptor 2
<b>HIV</b>	human immunodeficiency virus
<b>HLA</b>	human leukocyte antigen
<b>IFN<math>\gamma</math></b>	interferon $\gamma$
<b>Ig</b>	Immunoglobulin
<b>IL</b>	Interleukin
<b>ITIM</b>	immunoreceptor tyrosine inhibition motif
<b>KIR</b>	killer immunoglobulin-like receptor
<b>LB</b>	lysogeny broth
<b>LC-MS</b>	mass spectrometry with liquid chromatography
<b>LIR</b>	leukocyte immunoglobulin-like receptors
<b>MHC-I</b>	major histocompatibility complex class I
<b>MLL5</b>	mixed-lineage leukemia protein 5
<b>MS</b>	mass spectrometry
<b>NCR</b>	natural cytotoxicity receptor
<b>NK</b>	natural killer
<b>NKp</b>	natural killer protein
<b>PAGE</b>	polyacrylamide gel electrophoresis
<b>PBS</b>	phosphate buffer saline
<b>PCNA</b>	proliferating cell nuclear antigen
<b>RNA</b>	ribonucleic acid
<b>SDS</b>	sodium dodecyl sulfate
<b>Sf9</b>	<i>Spodoptera frugiperda</i> 9 cell line
<b>SH</b>	sarcoma (Src) homolog
<b>SPR</b>	surface plasmon resonance

<b>TAE</b>	Tris-acetate-EDTA
<b>TCEP</b>	tris(2-carboxyethyl)phosphine
<b>TEMED</b>	N,N,N',N'-tetramethylethylenediamine
<b>TLR</b>	toll-like receptor
<b>Tris</b>	tris(hydroxymethyl)aminomethane

# 1. INTRODUCTION

## 1.1. Natural killer cells

Natural killer cells (NK cells) are a subset of lymphocytes discovered in 1975 as cells capable of spontaneous cytotoxic activity with no need of previous sensitization, the process termed natural cytotoxicity [1]. Therefore, they are considered to be part of innate immune system which plays an important role in early immune defense [1, 2]. In spite of that, some important features as priming, education and memory which are rather characteristic for immune cells of adaptive immunity, have been observed in NK cells recently [2, 3, 4]. As NK cells are able to recognize and kill virus infected and tumor cells, their basic and applied research provides us with important data for development of therapeutics [1, 5].

### 1.1.1. Development of NK cells

As for all immune cells, development of NK cells occurs in bone marrow in multiple stages [1, 2]. First, hematopoietic stem cell may develop into myeloid or lymphoid progenitor cell [2]. From lymphoid progenitor cell, T and B lymphocytes' progenitor may be developed on one hand and precursor NK cell on the other hand. Subsequently, based on cytokine regulation, precursor NK cell develops into immature NK cell which afterwards matures into mature NK cell. Each step of development occurs in bone marrow with an exception of maturation which in restricted form can also occur in spleen, lymph nodes and peripheral blood. Alternatively, early stage thymocytes (precursor cells of T lymphocytes) can differentiate into NK cells [2].

Expression level of surface proteins is specific for each developmental step [2]. Early developmental stages can be distinguished by expression of CD133, CD34, CD33, CD117 and CD244 receptors. Expression of CD56 receptor and subsequently CD94/NKG2A heterodimeric receptor is characteristic for prematuration stage. Mature NK cells are characterized by lowered CD94/NKG2A expression. For proper development, presence of specific interleukins, cytokines and contact with stromal cells is crucial [2].

Eventually, two major subsets of NK cells can be distinguished: NK CD56<sup>low</sup> subset (around 90%) with decreased CD56 but increased CD16 and Ig-like receptors expression level is more

abundant in peripheral blood whereas NK CD56<sup>high</sup> subset (around 10%) is predominant in secondary lymphoid tissues, expresses high levels of CD56 but little or no CD16 and produces pro-inflammatory cytokine interferon gamma (IFN $\gamma$ ) and tumor necrosis factor alpha (TNF $\alpha$ ) after stimulation by macrophages [2].

### **1.1.2. Receptors of NK cells**

Mature NK cells possess the ability to recognize tumor cells and cells infected by some viruses [1, 2, 6]. For their recognition they use palette of inhibitory and activating receptors. Inhibitory receptors bind to human leukocyte antigen (HLA) molecules and this binding triggers inhibition of NK cells activation. Activating receptors bind to specific molecules expressed on target cells and this binding induces activation of NK cells. Whether the NK cell is or is not activated is decided by outcome of a slight balance of inhibitory and activating signals [1, 2, 7]. Both inhibitory and activating receptors are classified in two structural groups: C-type lectin-like receptors and immunoglobulin-like receptors [1, 6].

#### **1.1.2.1. C-type lectin-like receptors**

Ly49 is family of C-type lectin-like receptors which are mainly inhibitory [1, 6]. These receptors are expressed in mice but not in primates and humans. Ly49 receptors bind major histocompatibility complex class I (MHC-I) proteins with bound peptide and their affinity is variable. MHC-I are proteins which present peptides from proteins present within cells and their downregulation is often linked to virus infection or malign transformation [6]. Interestingly, these receptors bind their ligands not only in *trans* (receptor and ligand are not on the same cell) but also in *cis* (receptor and ligand are on the same cell), which subsequently leads to different outcomes [8]. It has been suggested that *cis* binding is significant for regulation of education of NK cells [8].

CD94-NKG2A/C/E are heterodimeric C-type lectin-like receptors which bind non-classical MHC-I [6]. In humans and primates, this is HLA-E molecule which itself binds peptides derived from classical MHC-I. For NK cells, this is an indirect way to monitor level of MHC-I expression level on target cell surface. However, among these receptors both inhibitory and activating are abundant. Importance of this phenomenon is not explained yet [6].

NKG2D, another C-type lectin-like activating receptor, forms homodimer and binds several MHC class I chain-related (MIC) molecules and UL16-binding proteins (ULBP) [6]. Expression of these ligands is induced as a response to DNA damage and cellular stress in malignant cells and presence of virus in a cell can lead to posttranscriptional upregulation of ligand expression. Importance of NKG2D for NK cell activation is illustrated by several ways of immune evasion strategies concerning this receptor. One of them is production of soluble ligands of NKG2D by target cells which serve as decoy ligands for NK cells. Additionally, transforming growth factor- $\beta$ 1 produced by tumor cells causes downregulation of NKG2D expression on NK cells [6].

Killer cell lectin-like receptor G1 (KLRG1) inhibits NK cell function after binding of classical cadherins (important cell-adhesion molecules) which are expressed on healthy cells [6]. In agreement, decrease of E-cadherin expression found in malignant epithelial tumors helps tumors to metastasize, but also makes tumor cells more vulnerable to NK cell killing [6].

#### **1.1.2.2. Immunoglobulin-like receptors**

Absence of Ly49 family of receptors in primates and humans is compensated by presence of killer immunoglobulin-like receptors (KIR) [1, 6]. KIRs are composed of two or three immunoglobulin-like (Ig-like) domains, single transmembrane domain and long or short cytoplasmic domain. There are inhibitory and activating KIRs which vary in signaling routes they use. Similarly to Ly49, KIRs bind HLA-A, -B and -C proteins with bound peptide [6].

Another group of inhibitory receptors called leukocyte immunoglobulin-like receptors (LIRs) is thought to be less dominant compared to other receptors as they bind MHC-I molecules with lower affinity [1, 6]. After ligand binding they inhibit NK cells activation. On the other hand, one of LIRs has been shown to bind cytomegalovirus protein UL18 with much greater affinity, leading to increase of NK cell activity [6].

2B4, also an Ig-like receptor, binds CD48, a molecule expressed on surface of all hematopoietic cells [6]. Different outcome after 2B4 binding has been observed. As activation or inhibition signals are mediated by recruited adaptor proteins, it has been proposed that triggering outcome might be dependent on developmental stage of NK cells.

Moreover, this outcome has been shown to be influenced by specific isoforms of 2B4 receptor [6].

Another group of Ig-like receptors are natural cytotoxicity receptors [1, 6, 7]. Since receptor NKp30, the main subject of this thesis, belongs to this group, a separate chapter is devoted for this receptor family.

### 1.1.2.3. Natural cytotoxicity receptors

Family of activating Ig-like receptors called natural cytotoxicity receptors (NCRs) consists of natural killer proteins NKp30, NKp44, NKp46 [6, 7]. These receptors were grouped together for their ability to activate NK cells and kill the tumor cells *in vitro*. Besides that, they do not share any similarity in the amino acid sequence or in the structure. All of them are type I transmembrane proteins comprised of one or two immunoglobulin extracellular domain, a transmembrane  $\alpha$ -helix with positively-charged amino acid enabling an interaction with signaling adaptor protein and short C-terminal domain (Fig. 1) [7].

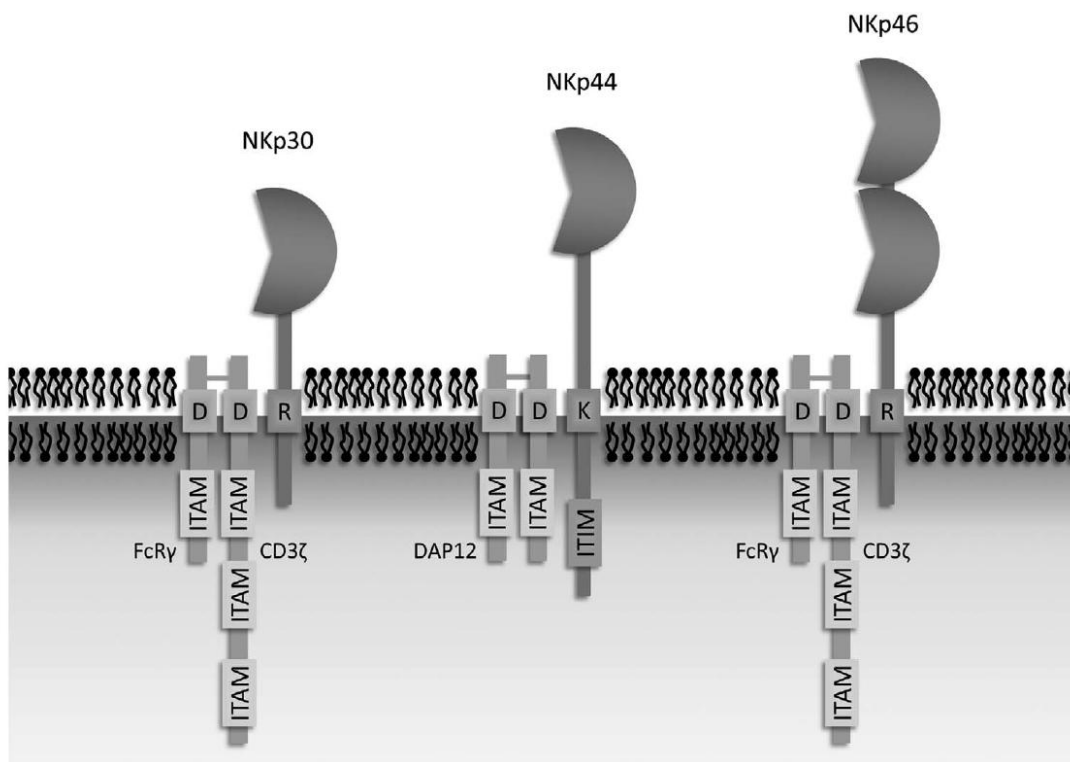


**Figure 1: Scheme of NCRs domain arrangement and associated signaling molecules.** Letters K, R, D are amino acids responsible for protein-protein contact, ITAM - immunoreceptor tyrosine-based activating motif, ITIM - immunoreceptor tyrosine inhibition motif.

NCRs can bind a diverse group of ligands [7]. Several proteins of viral envelopes such as influenza hemagglutinins, hemagglutinin neuraminidase of Sendai virus and Newcastle disease virus, hemagglutinin of vaccinia virus and ectromelia virus, envelope glycoproteins of the dengue and West Nile virus and protein pp65 of human cytomegalovirus were found to be ligands of NCRs. Interestingly, presence of sialic acid on N- and also O-glycosylation patterns of NCRs is generally important for binding of viral ligands [7].

NKp44 is also able to bind cell wall molecules of several bacterial strains, nevertheless these interactions do not activate NK cells and their relevance has been proposed to be in prolongation of time the NK cells stay activated [7]. NKp46 binds vimentin, intracellular protein of *Mycobacterium tuberculosis*, which is secreted by macrophages and vascular endothelial cells and subsequently activates NK cells cytotoxicity. Importance of NCRs (particularly NKp30 and NKp46) was also recorded for *Plasmodium falciparum* protein binding, however these data remain an issue [7].

All NCRs also have the ability to bind heparan sulfates [7, 9]. For this binding, NCRs have to be glycosylated. Generally, they recognize structures containing two to three sulfate groups per disaccharide unit; however their affinity differs with heparan sulfate length and sulfate group positions. Heparan sulfates are not able to activate NK cells and therefore are considered to act as co-ligands [7, 9].

Two cellular protein ligands of NKp44 were found, both active in cell nucleus under normal conditions [7]. Proliferating cell nuclear antigen (PCNA), which is normally involved in DNA replication, was demonstrated to have inhibitory effect on NK cells mediated by immunoreceptor tyrosine inhibition motif (ITIM) of NKp44 intracellular domain, which was previously considered to be non-functional. PCNA is overexpressed on decidual trophoblasts during first trimester of gestation; therefore PCNA is thought to contribute to immune system tolerance in uterus. Presumably, tumor cells abuse this mechanism to escape the cytotoxicity mediated by NK cells [7].

Another cellular ligand of NKp44 is termed NKp44L, which is an isoform of mixed-lineage leukemia protein 5 (MLL5) [7]. Normally, MLL5 plays its role in cell cycle regulation, however, its isoform NKp44L was found to be expressed in some tumor cell lines and CD4<sup>+</sup> T lymphocytes infected by human immunodeficiency virus (HIV) [7].

Similarly to NKp44, three cellular ligands of NKp30 were also investigated: B cell lymphoma 2 associated antigen 6 (BAG-6), a multifunctional protein present in cell nucleus and cytoplasm; protein B7 homolog 6 (B7-H6), specifically expressed on some tumor cell lines and galectin-3, surface protein of some tumors [7, 10]. NKp30 and its ligands are described in a separate chapter (1.2).

#### **1.1.2.4. Other receptors of NK cells**

Several receptors of NK cells (both Ig-like and C-type lectin-like) are considered to be co-stimulatory, as they are not able to activate NK cells sufficiently to trigger NK cell activation [6]. Natural killer receptor protein 1 (NKR-P1) family consists of both activating and inhibitory receptors. DNAX accessory molecule 1 (DNAM-1) receptor binds several molecules which are sign of cellular stress on the target cell. Paired Ig-like type 2 receptors (PILs) recognize ligands with O-glycosylation, thereby widening the target cell range. Additionally, NK cells also express toll-like receptors (TLR), which bind molecules specific for pathogenic organisms. TLRs enhance cytotoxicity and induce IFN $\gamma$  production [6].

NK cells also recognize opsonized cells through binding of fragment constant (Fc) domain of IgG antibody with their Fc receptor CD16. This also leads to their activation in the process called antibody dependent cellular cytotoxicity (ADCC) [1, 6].

#### **1.1.3. Education of NK cells**

Certain clones of NK cells do not express all receptors on their surface and their combination varies among the clones [2, 4, 11]. Therefore, NK cells must possess a mechanism by which they set an activation threshold specific for given combination of receptors. Major mechanism of setting this threshold is considered to be education [4, 11]. In this process, inhibitory receptors of NK cells (Ly49 in mice and KIRs in humans) bind MHC-I molecules. In the arming model, NK cells are hypo-responsive by default and are educated by interaction with MHC-I. In the disarming model, NK cells are responsive by default and can be disarmed if they lack receptors for MHC-I, resulting in NK cell anergy [11]. Cis-interaction model proposes that *cis* interaction between inhibitory receptor and MHC-I on NK cell sequesters inhibitory receptors which make NK cells more responsive to activating signals [8, 11].



Rheostat model proposes that education of NK cells is rather quantitative and depends on quantity of received inhibitory signal [11].

#### **1.1.4. Signaling in NK cells**

After ligand binding by NK cell receptors, signal pathways based mainly on phosphorylation are initialized [2, 6]. Activating receptors transmit signal through associated proteins (such as DAP12) containing immunoreceptor tyrosine-based activating motifs (ITAMs) [6]. Tyrosine residue is phosphorylated followed by sarcoma (Src) homology 2 (SH2) domain-containing kinase recruitment leading to triggering of a signal cascade which results in cytotoxic effects of NK cells. Most of the inhibitory receptors contain immunoreceptor tyrosine inhibition motifs (ITIMs) in their C-terminal cytoplasmic chain. Phosphorylation of ITIMs leads to recruitment of Src homology 2 domain-containing phosphatases (SHPs). Further pathways imply phosphorylation and dephosphorylation events which lead to inhibition of activation pathways. Alternative activation of NK cells involves adaptor protein DAP10 which signals via phosphatidylinositol-3 kinase and further signaling pathways. In comparison, DAP10 signaling results in cytotoxicity whereas DAP12 signaling additionally contributes to cytokine secretion [6].

#### **1.1.5. Cytotoxic mechanisms of NK cells**

After activation, NK cells utilize several cytotoxic mechanisms to kill target cell [1, 2]. These mechanisms are similar to those used by cytotoxic T lymphocytes [1]. Granules of NK cells migrate to cytoplasmic membrane on cell-cell contact site, where they fuse with membrane and their content is diffused in between the two cells [1, 2]. This process is called degranulation. Granules contain protein perforin, which creates small pores on target cell. These pores can cause cell death by osmotic lysis, but rather they make cell cytoplasm accessible for granzymes, proteases from granules. Granzymes cleave precursors of caspases, which cause cell apoptosis. The other cytotoxic mechanism is mediated by Fas-ligand (FasL), receptor on surface of NK cells which binds Fas receptor on target cell and triggers its apoptosis [1, 2].

### **1.1.6. Regulatory function**

In addition to direct immunological impact on elimination of target cells, NK cells also play an important role in regulation of other immune cells [2]. They are able to kill immature dendritic cells and thus influence their homeostasis [2]. Furthermore, killing of target cells by NK cells can lead to cross-presentation of apoptotic peptides by dendritic cells which afterwards can activate T lymphocytes. NK cells can also influence adaptive immunity. By IFN $\gamma$  secretion NK cells promote priming of T lymphocytes in inflamed lymph nodes. T lymphocytes can be also killed by NK cells in case they do not possess enough of MHC-I on their surface [2].

### **1.1.7. Immunological memory**

Until recently, immunological memory was considered to be signature of a daptive immunity [2, 3]. However, there is evidence that innate immune cells including NK cells are also capable to "remember" after exposure to some stimuli [3]. NK memory cells response is quantitatively and qualitatively increased in case of repeated stimulation. For example, after stimulation with human cytomegalovirus (HCMV), higher amount of NK cell subset with CD94-NKG2C receptor is abundant in peripheral blood. After reexposure to HCMV, NKG2C-positive NK cells demonstrate enhanced function. Similarly, NK memory cells can originate after stimulation by hapten, other viruses and also cytokines. In some cases, tissue-specific homing has been detected and furthermore, epigenetic changes in NK memory cells were recorded [3].

## **1.2. NKp30**

Natural killer protein 30 (NKp30; also Natural cytotoxicity receptor 3, NCR3; also CD337) is an immunoglobulin-like activating receptor of NK cells discovered in 1999 [7, 12]. Together with NKp44 and NKp46, NKp30 is a member of family of natural cytotoxicity receptors [7, 12].

### **1.2.1. Structure of NKp30**

NKp30 is type I transmembrane protein, consisting of N-terminal immunoglobulin domain, short 15-amino-acid-long domain termed stalk domain, a transmembrane  $\alpha$ -helix and

C-terminal cytoplasmic domain [12, 13]. Structurally, NKp30 is part of CD28 family of proteins [12, 13]. All CD28 family proteins have an N-terminal signal sequence which is cleaved during protein trafficking, one V-shaped immunoglobulin domain (IgV domain), one transmembrane domain and one or two intracellular domains [13]. Intron-exon arrangement is similar, too (Fig. 2). From CD28 family, closest homolog of NKp30 is inducible T-cell costimulator (ICOS) with 25% sequence similarity. Interestingly, most of the CD28 family members bind to proteins of B7 family, which is also true for NKp30 [13].

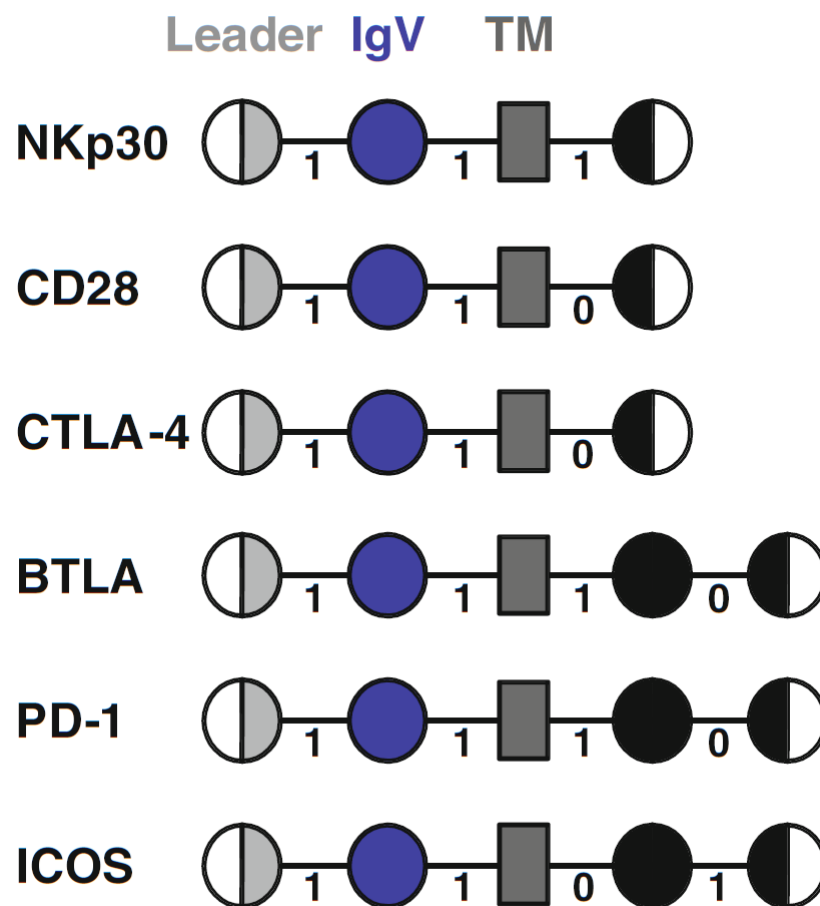


**Figure 2: Gene structure of NKp30 compared to other CD28 family members.** "Leader" - signal sequence, "IgV" - V-type immunoglobulin domain, "TM" - transmembrane domain, white - untranslated regions, "0"/"1" – zero/one intron, respectively.

Structure of NKp30 was solved by X-ray crystallography for NKp30 in an unbound state [14] and in bound state with B7-H6 [15].

### 1.2.2. Genetics and isoforms

In human, NKp30 is encoded by gene located in the class III region of the major histocompatibility complex on chromosome 6 [12]. In this region, many immunologically important molecules as cytokines, complement molecules and heat shock proteins, are encoded. Interestingly, ligand of NKp30, BAG-6, is also encoded within this region [12].

By alternative splicing, various isoforms of NKp30 can be produced, distinguished in shape of immunoglobulin domain (V-shaped, IgV; C-shaped, IgC) and C-terminus length (three variants) [16]. Combination of these can result in six possible isoforms termed as NKp30x, where x is a letter indicating particular isoform. NKp30a-c possess IgV domain and NKp30d-f possess IgC domain (Fig. 3). Functional difference among IgV isoforms was investigated. NKp30a and NKp30b both enhanced IFN $\gamma$  and interleukin 2 (IL-2) production after NK cells stimulation *ex vivo*, however, NKp30c did not. Similarly, upon incubation with tumor cells expressing B7-H6, NKp30c-transfected NK cells did not show any sign of activation compared to other NK cells. On the other hand, NKp30c-transfected cells produced inhibitory interleukin IL-10 upon stimulation. These function outcome differences are thought to be caused by weak association of NKp30c with its adaptor signaling molecule CD3 $\zeta$ . Additionally, individuals with gastrointestinal sarcoma have worse therapeutic prognosis when NKp30c expression level is relatively higher [16].

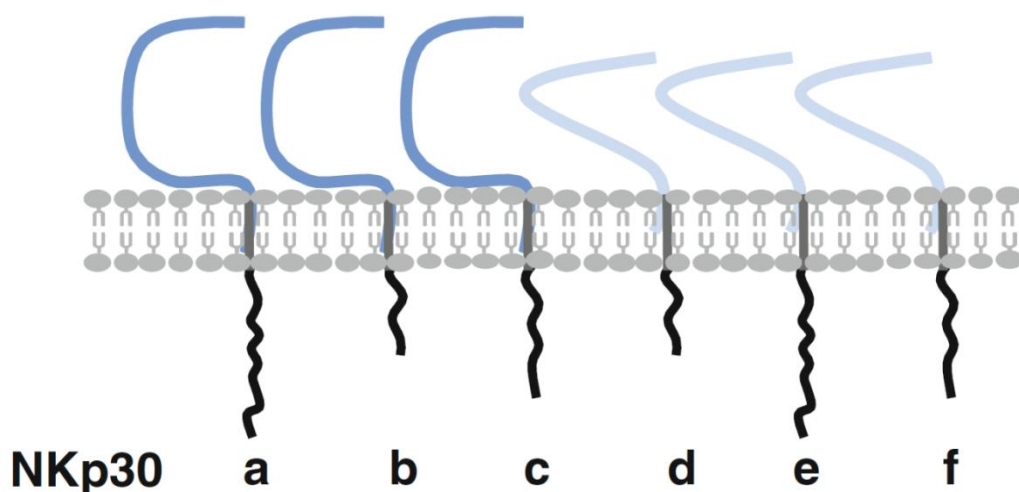


**Figure 3: Schematic comparison of length and extracellular domain shape of NKp30 isoforms.** Isoforms structurally differ in their extracellular domain shape (IgC for NKp30a-c and IgV for NKp30d-f) and intracellular domain length. Functionally, isoforms differ in their ability to activate NK cell after ligand binding.

### **1.2.3. Ligands of NKp30**

Few non-cellular ligands of NKp30 were identified at first [7]. Heparin and heparan sulfate act as co-ligands, binding only to glycosylated NKp30 [9]. Binding of *Plasmodium falciparum* erythrocyte membrane protein-1 (fcEMP1) is yet to be confirmed or disproved [7, 17]. Although both of these ligands trigger activation of NK cells, other non-cellular ligands have inhibitory effect [7]. These are viral ligands: hemagglutinin of the ectromelia and vaccinia virus and protein pp65 released from human cytomegalovirus [7, 18]. In case of pp65, its binding to NKp30 does not prevent binding of its other ligands [18] since pp65 uses another binding site and causes dissociation of NKp30-CD3 $\zeta$  complex resulting in disrupted activating signaling pathway [7, 18].

Later, three specific cellular ligands of NKp30 were identified [7]. B cell lymphoma 2 associated antigen 6 (BAG-6) is large protein involved in many intracellular processes as response to DNA damage, gene regulation, protein targeting, protein quality control, defective protein degradation and also immunoregulation [19]. Under stress conditions and in some tumor cells, BAG-6 is recruited onto the cell membrane in an unknown manner and there interacts with NKp30 [19]. B7-H6 is a membrane protein constitutively expressed on some tumor cell lines and tumor cells [20]. Both of these proteins may also appear on the surface of exosomes [19]. Additionally, both of them were also found in soluble forms which are derived from their membrane forms by proteolytic cleavage termed shedding. These soluble forms inhibit activation of NK cells [19, 21]. The most recently discovered ligand of NKp30 is galectin-3, which almost completely blocks NK cell cytotoxicity. Galectin-3 is expressed on the surface of some tumors [10].

### **1.2.4. Variable affinity to ligands**

Although the structure of NKp30 bound to B7-H6 is known (Fig. 4, p. 22), proteins in this structure were produced in bacteria and insect cell line, respectively [14, 15]. Moreover, NKp30 in this structure lacks short stalk domain [14, 15]. However, both glycosylation and stalk domain presence were shown to impact the binding affinity of NKp30 [22]. Stalk domain influences the oligomerization state of NKp30: NKp30 with no stalk domain creates only monomer and dimer whereas NKp30 with stalk domain forms oligomers in addition [23]. Interestingly, the dimer of NKp30 can be seen in its structure (construct without stalk

domain produced in *E. coli* [14] but not in the bound state [15]. Nevertheless, the presence of oligomers positively correlates with NKp30 affinity to its ligands, although its differences are not in orders of magnitude [23]. Affinity differences in order of magnitude are caused by N-glycosylation [22]. Using point mutation analysis, glycosylation at asparagine 42 was shown to be essential for binding of ligands and glycosylation at asparagines 68 and 121 also plays a significant role [22].

Furthermore, various affinities were measured for NKp30 binding, depending on the protein production system used (Tab. 1) [14, 15, 22, 23]. Whilst the affinity measured for both NKp30 and B7-H6 isolated from *E. coli* was 2.5 - 3.5  $\mu$ M [14] and in case of B7-H6 isolated from Sf9 insect cell line 1  $\mu$ M [15], the affinity of the same protein pair produced in human embryonic kidney cell line HEK293T (providing human complex N-glycosylation pattern [24]) was approx. 100 nM (depending on stalk domain length) [22]. Even higher affinity was recorded for NKp30 produced in Sf9 insect cell line and B7-H6 produced in HEK293T cells: dependent on oligomeric state of NKp30, affinity was between 1 nM and 2 nM (Tab. 1) [23]. Interestingly, affinity of NKp30 produced in HEK293T cells and BAG-6 isolated from insect cell line was 64 nM, but for BAG-6 isolated from *E. coli* twice as strong [25].

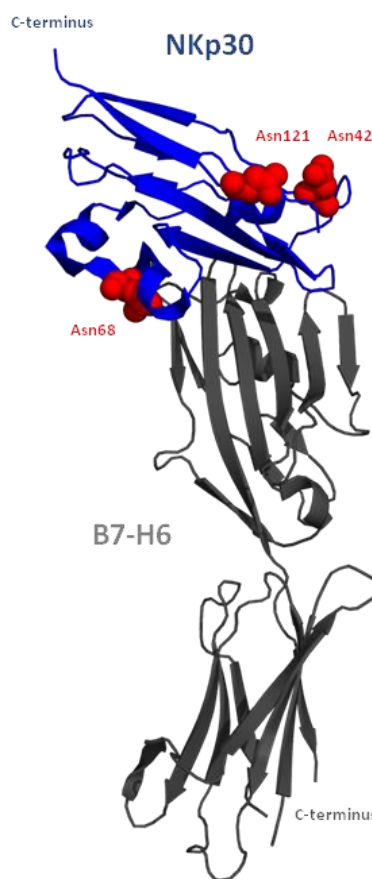


**Figure 4: Structure of NKp30/B7-H6 complex (PID 3PV6).** Glycosylation sites of NKp30 are highlighted.

**Table 1:** Comparison of measured affinities of NKp30/B7-H6 interaction found in the literature.

Production system		Affinity measurement	
NKp30	B7-H6	Result	Method
<i>E. coli</i>	<i>E. coli</i>	2.5 – 3.5 $\mu$ M	SPR
<i>E. coli</i>	Sf9 insect cell line	1 $\mu$ M	SPR
HEK293T human cell line	HEK293T human cell line	75 - 150 nM	SPR
Sf9 insect cell line	HEK293T	1 – 2 nM	ELISA

In our laboratory, we found out that the formation of NKp30 oligomers depends on its N-glycosylation [26]. NKp30 produced in HEK293S cell line with knocked-out N-acetylglucosaminyltransferase I formed oligomers but appeared only as monomer after enzymatic deglycosylation [26]. However, the structural basis of NKp30 oligomerization and basic questions of how stalk domain and glycosylation impact NKp30 affinity as well as physiological importance of these effects on NK cells remain to be elucidated.

### **1.3. B7-H6**

Protein B7 homolog 6 (B7-H6) was discovered as a binding partner of NKp30 in 2009 [20]. Since then, a lot of research has been provided to define its expression specificity on various tumor cell lines and its clinical potential.

#### **1.3.1. Structure of B7-H6**

B7-H6, similarly to NKp30, is a type I transmembrane protein [20]. It comprises of two extracellular immunoglobulin domain (IgC and IgV),  $\alpha$ -helical transmembrane domain and short C-terminal sequence homologous to GAG protein (Fig. 5, p. 24). C-terminal sequence contains various signaling motifs such as ITIM, SH-2 and SH-3-binding motifs [13, 20]. These motifs initialize signal transduction after NKp30 binding, though the signal outcome is not known [13]. The closest structural homologs of B7-H6 are B7-H1 and B7-H3 and therefore B7-H6 is part of B7 family of proteins [13, 20]. Members of B7 family are mostly co-stimulatory or co-inhibitory ligands of various immune cells and bind members of CD28 protein family. However, B7-H6 is an exception to that [13].

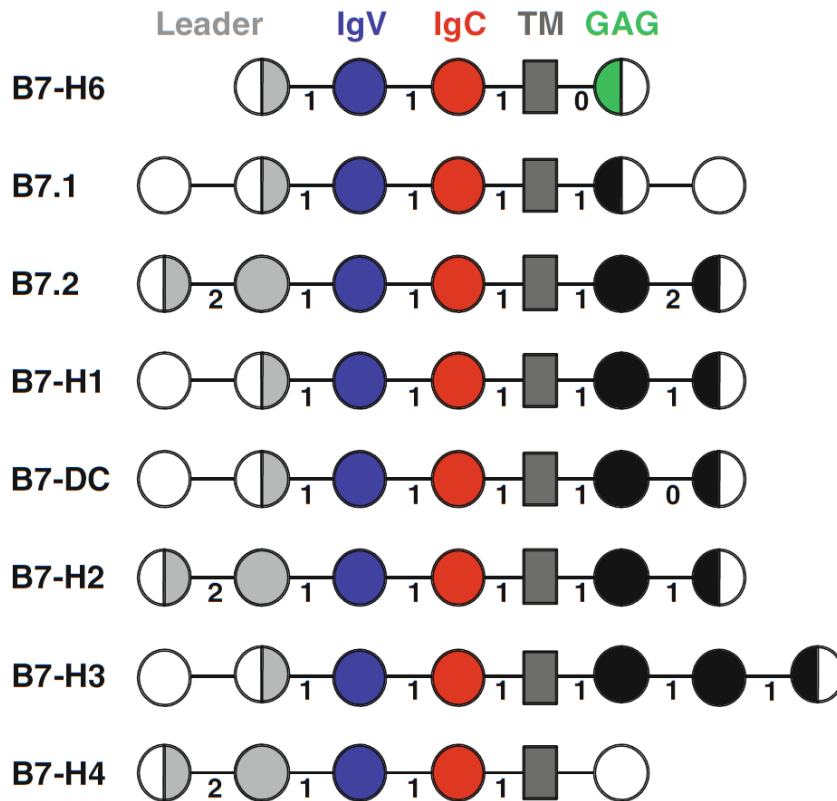


**Figure 5: Comparison of gene arrangement of various B7 family members.** "Leader" - signal sequence, "IgV" - V-shaped immunoglobulin domain, "IgC" - C-shaped immunoglobulin domain, "TM" - transmembrane domain, "GAG" - GAG domain, white - untranslated regions, "0"/"1"/"2" – zero/one/two introns, respectively.

### 1.3.2. B7-H6 gene

B7-H6 is encoded on chromosome 11 [20]. It is well conserved among the primates, but not among the other mammals [13, 20]. In *Mus musculus*, where the GAG domain is missing, only sequence homology with first exon was found and there is no B7-H6 expressed in this specie. This suggests co-evolution of B7-H6 with NKp30, which is also not expressed in *Mus musculus* [13].

### 1.3.3. Expression of B7-H6

Strikingly, constitutive expression of B7-H6 was not recorded on any healthy cells; however it has been detected on several tumor cell lines both *ex vivo* and *in vivo*, making B7-H6 an exemplary adept marker for tumor recognition [13, 20]. Subsequently, induced expression of B7-H6 in monocytes and neutrophils was observed, too [27]. Expression of B7-H6 in these cells was induced by agonists of toll-like receptors TLR2, TLR4, TLR5 and TLR8, interleukin



IL-1 $\beta$  and tumor necrosis factor alpha (TNF $\alpha$ ). In all cases, the kinetics of B7-H6 mRNA and protein expression was similar. B7-H6 mRNA appeared early, peaking between 3 to 12 hours after induction and returning to normal state within 24 hours. Surface expression of B7-H6 was stable up to 48 hours after induction. Similarly, presence of soluble or exosomal form of B7-H6 was also induced by the same factors. Supporting *in vitro* studies, soluble and membrane form of B7-H6 were found in blood of patients with systemic inflammatory response syndrome. Cell-surface expression was restricted to patients presenting sepsis and was selective for CD14<sup>+</sup> CD161<sup>+</sup> pro-inflammatory-type monocytes. Soluble or exosomal form of B7-H6 was present only in blood of patients presenting sepsis caused by Gram-negative bacteria [27].

#### **1.3.4. B7-H6 shedding**

Generally, shedding is a proteolytic event used by tumor cells to escape immune system by cleaving extracellular parts of membrane ligands of receptors of immune cells [1]. Using combination of various metalloprotease inhibitors and RNA silencing method, proteases responsible for B7-H6 shedding were identified as disintegrin and metalloproteinase domain-containing proteins (ADAMs) ADAM-10 and ADAM-17 [21]. Inhibition of these proteases leads to enhanced cytotoxicity of NK cells.

In agreement, increased levels of soluble B7-H6 form were also found in blood of patients with late stages of melanoma, which proposes clinical significance of B7-H6 [21]. Similarly, soluble B7-H6 form was found in blood of patient with ovarian carcinoma, which leads to decreased NKp30 production on surface of NK cells and increased reactivity threshold of NK cells [28].

### **1.4. Clinical importance of NKp30 and B7-H6**

As constitutive expression of B7-H6 is restricted to certain tumor cells, major investigation has been focused on potential utilization of NKp30/B7-H6 pair in clinical praxis.

#### **1.4.1. Potential in diagnostics**

Expression of B7-H6 was found in astrocytoma [29], non-small cell lung cancers [30] and human gastric carcinoma [31]. In all cases, expression level was not connected to tumor size

or pathological state of patient, but positively correlated with differentiation state of tumor cells. Information about tumor differentiation can help making choice of therapy approach [29, 30, 31]. Furthermore, expression of B7-H6 was found to correlate with cancer progression and survival of patients in human ovarian cancer [32]. B7-H6 was also found to be expressed on salivary epithelial cells of patients with Sjögren's syndrome, an autoimmune disorder effecting minor salivary glands [33]. Indeed, NK cells are accumulated there and probably cause inflammation in NKp30/B7-H6 binding-dependent manner [33].

Expression of NKp30 on NK cells negatively correlates with occurrence of acquired immunodeficiency syndrome (AIDS) in patients infected by HIV [34]. On the other hand, NKp30 expression is upregulated in hepatitis B virus (HBV) patients and patients with acute-non-chronic liver failure [35]. In contrast, NKp30 expression level of hepatitis C virus 2 (HCV-2) patients was decreased [36]. Proportion of expression levels of various NKp30 isoforms was also shown to be important in some pathological states. High-risk neuroblastoma patients had decreased activating isoforms NKp30a and NKp30b, but not inhibitory NKp30c [37]. In agreement, sporadic and recurrent pregnancy loss correlates with NKp30a and NKp30b upregulation in the placental tissue [38].

#### **1.4.2. NKp30/B7-H6-based therapy**

B7-H6 has already been utilized therapeutically, though it was not known previously: several standard tumor therapeutics and therapeutic methods were shown to enhance B7-H6 expression on tumor cells, making them an easier target for NK cells. Among studied therapeutics, this is caused by cisplatin, 5-fluorouracil, radiation therapy and cytokine therapy [39].

Several bipolar protein therapeutics, utilizing NKp30/B7-H6 binding to enhance tumor elimination by NK or other cells, were developed [40, 41, 42, 43].

B7-H6:7D8 consists of extracellular domain of B7-H6 and single chain fragment variable of anti-CD20 antibody 7D8 [40]. CD20 is mainly expressed on B cells; therefore this bipolar molecule mediates contact of B and NK cells and triggers NK cell activation. This therapeutic protein is aimed to treat lymphoma and leukemia. Moreover, B7-H6:7D8 also acts

synergistically with rituximab, a monoclonal antibody against CD20, and with daratumumab, monoclonal antibody against CD38 [40].

Another investigated bipolar protein consists of B7-H6 extracellular domain and single chain fragment variable of anti-HER2 (human epidermal growth factor receptor 2) antibody (Fig. 6) [41]. As HER2 is protein specifically expressed on breast cancer cells, this potential therapeutics enhances cytotoxicity of NK cells against these target cells [41].

Converse approach is utilized in case of so-called BiTE (bispecific T-cell engager) molecules, where single chain fragment variable of antibodies against B7-H6 of tumor cells and against CD3 of T lymphocytes are produced as one protein [42]. This BiTE is able to activate cytotoxic T lymphocytes which show therapeutic efficiency against ovarian cancer, lymphoma, melanoma and ovarian cancer on mouse models [42].

Fused extracellular domain of NKp30 and constant region of IgG1 was able to induce macrophages-mediated antibody-dependent cellular cytotoxicity against prostate tumor cell lines. This therapeutic protein was also able to slow down tumor progression rapidly and to distinguish between benign and malign cell lines [43].

Moreover, T lymphocytes were modified by insertion of chimeric antigen receptors (CARs) [44] consisting of single chain fragment variable of anti-B7-H6 antibody fused to various transmembrane domains (CD28, CD8, CD3 $\zeta$ ) and various signaling domains (CD28, CD3 $\zeta$  or both). Such modified T lymphocytes were able to bind B7-H6 as well as initialize IFN $\gamma$  secretion, which subsequently stimulated other immune cells [44].

Minimalistic approach was chosen by one research group which investigated the ability of B7-H6-derived peptides to initiate immune response [45]. These peptides were shown to

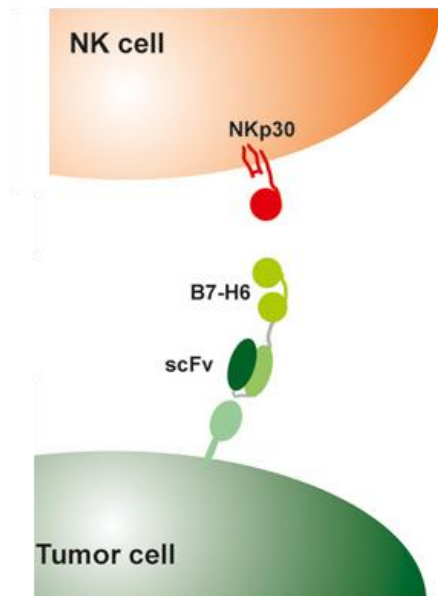


**Figure 6: Example of a bipolar therapeutic protein.** The protein binds to NKp30 on one side by B7-H6 extracellular domain and to HER-2 by single-chain fragment-variable part of antibody on the other side.

bind NKp30 on surface of NK cells and partially activate NK cells. Moreover, these peptides did not show any signs of cell toxicity towards healthy cells [45].

An interesting approach of utilizing dendritic cells derived exosomes (called Dex) is already in phase II clinical trial phase [46]. Membrane-bound BAG-6, ligand of NKp30, is present on these exosomes. Results show that patients with non-small cell lung cancer tolerate the treatment and Dex increases NKp30-dependent cytotoxicity of NK cells [46].

## **2. AIMS OF THE THESIS**

The aim of this thesis was to prepare soluble extracellular domain of protein B7-H6 and characterize the protein. Furthermore, formation of NKp30 oligomers by multimethodical approach was to be investigated. The next goal was to explain how and why glycosylation, oligomerization and C-terminal chain length influence its affinity to B7-H6 ligand. Finally, crystallization and X-ray structure solution of the glycosylated NKp30/B7-H6 complex was to be attempted.

### 3. MATERIALS

#### 3.1. Instruments and tools

Analytical ultracentrifuge Proteomelab XL-I	Beckman Coulter, USA
Automatic pipettes	Discovery HTL, Poland
Automatic pipettes	Pipetman Gilson, USA
Burner	Závod Votice, Czech republic
Burner Fuego SCS	VERKON, Czech Republic
Camera Cyber-shot DSC W570	SONY, Japonsko
Centrifuge Allegra X-22R	Beckman Coulter, USA
Centrifuge EBA 12R	Hettich, Germany
Centrifuge tubes Oak Ridge	Sigma, USA
Centrifuge Universal 320 R	Hettich, Germany
Column Acclaim C185 PepMap	Thermo Scientific, USA
Column HiTrap Talon Crude 5 ml	GE Healthcare, USA
Column Superdex 200 10/300 GL	GE Healthcare, USA
Column Superdex 200 Increase 10/300 GL	GE Healthcare, USA
Concentrators Amicon Ultra (MWCO 10,000)	Millipore, USA
Cooker	ETA, Czech Republic
Deionized water source Milli Q	Millipore, USA
Electron microscope Tecnai G2 Sphera	FEI, USA
Flow box BIO 126	LABOX, Czech Republic
Flow box Clean Air	PMV, Netherland
Formulatrix storage and imaging system	Formulatrix, USA
Freezer box Ultra-low UDF-U53V (-80 °C)	Sanyo, Japan
Gel/PCR DNA Fragments Extraction kit	Geneaid, USA
Glutathione Sepharose 4B	GE Healthcare
Hemocytometer	Sigma-Aldrich, USA
High-Speed Plasmid Mini Kit	Geneaid, USA
HPLC system ÄKTA basic	GE Healthcare, USA
Hydra pipetting robot	Art Robbins Instruments, USA
Incubator IR 1500	LABsystem Praha, Czech Republic
Incubator, CO <sub>2</sub> MCO-18 AIC	Sanyo, Japan
Magnetic stirrer MM2A	Laboratorní přístroje Praha, Czech republic
Microcalorimeter MicroCal iTC <sub>200</sub>	Malvern Instruments, UK
Microcentrifuge MiniStar silverlin	VWR, USA
Microscope (inverse) AE31	Motic, Germany
Microwave oven KOR 6L05	Daewoo Electronics, UK
Mr. Frosty freezing container	Nalgene, USA
Nucleobond Xtra Maxi	Macherey-Nagel, Germany
pH meter Φ 200	Beckman Coulter, USA
Pipetter Pipetus	Hirschmann, Germany

Plastics for cell cultures	Sigma, USA
Power supply for electrophoresis EC 250-90EC	Apparatus Corporation, UK
Precision balance KB1200-2	Kern, Germany
Rotary evaporator CentriVap DNA	Labconco, USA
Set for agarose electrophoresis	Biokeystone, USA
Set for SDS-PAGE	Bio-Rad, Germany
Shaker Celltron	Infors HT, Switzerland
Shaker Multitron Cell	Infors HT, Switzerland
Spectrometer Bruker solarix XE 12 T	Bruker, USA
Spectrophotometer DeNovix DS-11+	DeNovix, USA
Spectrophotometer UV/VIS UV4-500	UNICAM, UK
Square glass bottles with membrane screw caps	P-Lab, Czech republic
Sterile filters (0,22 µm)	TPP, Switzerland
Termocycler Rotor-Gene 2000	Corbett Life Science, USA
Termocycler Progene	Techne, UK
Termocycler Techgene	Techne, UK
Ultracentrifuge ProteomLab XL-I	Beckman Coulter, USA
Ultrasonic water bath	P-Lab, Czech Republic
Ultrasound homogenizer Sonoplus	Bandelin, Germany
UV lamp (300 nm)	Ultra-Lum, USA
UV lamp (312 nm)	UVItec, UK
Vortex shaker	VELP Scientifica, Italy
Water bath	Memmert, Germany
Water bath TW2	Julabo, Germany

### 3.2. Enzymes

Combi PPP Mastermix	New England Biolabs, USA
Endoglycosidase F1	Prepared in house
RNAsa A	Lach-Ner, Czech republic
Q5 DNA polymerase	New England Biolabs, USA
T4 DNA ligase	New England Biolabs, USA
Trypsin	Sigma, USA
Restriction endonuclease Agel	New England Biolabs, USA
Restriction endonuclease KpnI	New England Biolabs, USA

### 3.3. Chemicals

1 kb DNA standard	New England Biolabs, USA
100 bp DNA standard	New England Biolabs, USA
2-mercaptoethanol	Sigma, USA

Acrylamide	Sigma, USA
Agar	Oxoid, UK
Agarose	Sigma, USA
Ampicillin	Biotika, Slovakia
Ammonium persulfate (APS)	Serva, USA
Buffer NEB1	New England Biolabs, USA
Buffer Q5	New England Biolabs, USA
Buffer for T4 DNA ligase	New England Biolabs, USA
Bromphenol blue	Lachema, Czech republic
Coomassie Brilliant Blue R-250	Fluka Chemika, Switzerland
Deuterium oxide	Armar AG, Switzerland
DMSO	Finnzymes, Finland
dNTPs	Top-Bio, Czech republic
DSG	Thermo Scientific, USA
DSS	Thermo Scientific, USA
EDTA	Jersey Lab Supply, USA
Ethylmorpholine	Thermo Scientific, USA
GoodView II DNA stain	Ecoli, Slovakia
Iodoacetamide	Thermo Scientific, USA
L-arginine.HCl	Sigma, USA
L-glutamine	Sigma, USA
IPEI 25 kDa	Polysciences, USA
N,N'-Methylenbisacrylamide	Serva, USA
PCR H <sub>2</sub> O	Top-Bio, Czech republic
Pluronic F-68	Sigma, USA
Q5 enhancer	New England Biolabs, USA
SDS	Jersey Lab Supply, USA
Sodium azide	Serva, USA
Sypro Orange	Thermo Scientific, USA
TCEP	Thermo Scientific, USA
TEMED	Serva, USA
Trypan blue	Sigma, USA
Trypton	Oxoid, UK
Valproic acid	Sigma, USA
Yeast extract	Imuna Pharm, Slovakia
Other common chemicals	Lach-Ner, Czech republic

### 3.4. Cell culture media

#### ExCell 293 (Sigma, USA)

- commercial medium supplied in powder form, dissolved as stated in instruction [47] and filtered. L-glutamine to 4mM final concentration was added prior to use.



### **Freestyle F17 (Gibco Invitrogen, USA)**

- commercial medium supplied in liquid sterile form. Prior to use, L-glutamine and Pluronic F-68 were added to final concentration of 4 mmol/l and 0.1%, respectively.

### **Ex/F17**

- mixture of ExCell 293 and Freestyle F17 in 1:1 ratio.

### **Lysogeny broth (LB) medium**

- 1% trypton, 0.5% yeast extract, 1% NaCl, pH 7.4

## **3.5. Solutions**

- **Solutions for electrophoreses and deglycosylation**

AA solution for SDS-PAGE	29% acrylamide, 1% N,N'-methylen-bis-acrylamide
Destaining buffer for SDS-PAGE	35% ethanol, 10% acetic acid
Electrode solution for SDS-PAGE (10x)	0.25M Tris, 1.9M glycine, 1% (w/v) SDS, pH 8.3
Elution buffer for Glutathione Sepharose 4B	20mM Tris, 150mM NaCl, 10mM NaN <sub>3</sub> , 10 mM glutathione, pH 8.0
Sample buffer for agarose electrophoresis (10x)	30% glycerol, bromphenol blue in TAE
Sample buffer for SDS-PAGE (5x, non-reducing)	31,5mM Tris, 10% (v/v) glycerol, 0,005% (w/v) bromphenol blue, 1% (w/v) SDS, 10mM NaN <sub>3</sub> , pH 6.8
Sample buffer for SDS-PAGE (5x, reducing)	100 µl of mercaptoethanol in 5x non-reducing sample buffer for SDS-PAGE
Staining solution for SDS-PAGE	45% methanol, 10% acetic acid, 0.25% Comassie Brilliant Blue R250
TAE buffer	40mM Tris, 20mM CH <sub>3</sub> COOH, 1mM EDTA

- **Solutions for chromatography**

Elution buffer for metal-chelate chromatography	50mM Na <sub>2</sub> HPO <sub>4</sub> , 300mM NaCl, 10mM NaN <sub>3</sub> , 250mM imidazole, pH 7.0
---	--

MES buffer	20mM MES, 100mM NaCl, 10mM NaN <sub>3</sub> , pH 5.0
Mobile phase for size exclusion chromatography	10mM HEPES, 150mM NaCl, 10mM NaN <sub>3</sub> , pH 7.5
PBS buffer	50mM Na <sub>2</sub> HPO <sub>4</sub> , 300mM NaCl, 10mM NaN <sub>3</sub> , pH 7.0

- **Solutions for cell cultures**

PBS buffer for cell cultures	10mM Na <sub>2</sub> HPO <sub>4</sub> , 150 mM NaCl, 2mM KCl, 2mM KH <sub>2</sub> PO <sub>4</sub> , pH 7.0
Linear polyethylenimine solution	10 mg/ml linear polyethylenimine in PBS for cell cultures
Trypan blue solution	0.4% trypan blue in PBS for cell cultures

- **Solutions for working with DNA**

TES buffer	10mM Tris, 2mM EDTA, 150mM NaCl, 1mM NaN <sub>3</sub> , pH 8.0
RES	50mM Tris-HCl, 100 µg/ml RNAsa A, pH 8.0
LYS	0.2M NaOH, 1% SDS
NEU	3.1M CH <sub>3</sub> COOK, pH 5.5
EQU	0.1M CH <sub>3</sub> COONa, 0.6M NaCl, 0.15% Triton X-100, pH 5.0
WASH	0.1M CH <sub>3</sub> COONa, 825mM NaCl, pH 5.0
ELU	100mM Tris-HCl, 1.25M NaCl, pH 8.5

For every solution, deionized water was used as a solvent unless stated otherwise.

### 3.6. DNA

- **Vectors**

pTW5sec\_B7-H6\_2  
pTW5sec\_LBD  
pTW5sec\_NKp30\_del

The preparation of the vectors is described elsewhere [48].

- **Primers**

B7-H6_C212S_FW	5'-TTTAATGTCAGTACTAGCAGCTTGAAGCTGAACT-3'
B7-H6_C212S_REV	5'-AGTTCAGCTTCAAGCTGCTAGTGACATTTAAA-3'
B7-H6_FW	5'-AAAAACCGGTGATCTGAAAGTAGAGATGATGGCAGG-3'
B7-H6_2_REV	5'-TTTTGGTACCCAGGGTAAAGTTGCTCCTCAAGGG-3'

The primers were purchased from Sigma (USA).

### **3.7. Cell lines and bacterial strains**

<i>E. coli</i> DH5 $\alpha$	Thermo Scientific, USA
HEK 293S GnTI <sup>-</sup>	ATCC, USA

## 4. METHODS

### 4.1. Cloning and DNA manipulation

#### 4.1.1. Overlap extension polymerase chain reaction (OE-PCR)

To perform a point mutation, three PCR reactions were set up. For the reaction, a template, two primers, deoxyribonucleotides (dNTPs), Q5 buffer, Q5 enhancer and Q5 High Fidelity DNA polymerase were mixed and water was added to 50  $\mu$ l.

Initial step of OE-PCR was provided by two separate PCR reactions (PCR-A and PCR-B). For both, pTW5sec\_B7H6\_2 plasmid was used as a template. By these reactions, overlapping DNA sequences with point mutations were created. Reaction details are given in Table 2.

PCR-A and PCR-B reactions were set up as follows. First the reaction mix was heated up to 95 °C for 5 min. The second step cycled 30 times: 95 °C for 30 sec, then annealing at 56 °C for 30 sec and polymerization at 72 °C for 1 min. After 30 cycles, samples were tempered at 72 °C for 8 min and finally cooled to 4 °C.

**Table 2:** Composition of PCR-A and PCR-B reactions.

PCR-A	Amount	PCR-B	Amount
B7-H6_1_FW	5 $\mu$ l	B7-H6_C212S_FW	5 $\mu$ l
B7-H6_C212S_REV	5 $\mu$ l	B7-H6_2_REV	5 $\mu$ l
Q5 buffer	10 $\mu$ l	Q5 buffer	10 $\mu$ l
Q5 enhancer	10 $\mu$ l	Q5 enhancer	10 $\mu$ l
pTW5sec_B7-H6_2	20 - 50 ng	pTW5sec_B7-H6_2	20 - 50 ng
dNTPs	1.5 $\mu$ l	dNTPs	1.5 $\mu$ l
Q5 HF polymerase	0.5 $\mu$ l	Q5 HF polymerase	0.5 $\mu$ l
PCR H <sub>2</sub> O	to 50 $\mu$ l	PCR H <sub>2</sub> O	to 50 $\mu$ l

For OE-PCR, products of the previous PCRs A and B were used as template. These overlapping products anneal together and whole DNA sequence is amplified subsequently. Reaction details are given in Table 3 (p. 36); the same reaction sequence as above was used.

**Table 3:** Composition of OE-PCR reaction.

<b>OE-PCR</b>	<b>Amount</b>
B7-H6_1_FW	5 $\mu$ l
B7-H6_2_REV	5 $\mu$ l
PCR A product	10 - 30 ng
CD product	10 - 30 ng
Q5 buffer	10 $\mu$ l
Q5 enhancer	10 $\mu$ l
dNTP's	1.5 $\mu$ l
Q5 pol	0.5 $\mu$ l
PCR H2O	to 50 $\mu$ l

#### **4.1.2. Agarose electrophoresis**

Agarose electrophoresis was used for isolation and evaluation of PCR products. 1.25% agarose gel was prepared by dissolving 0.80 g of agarose in 65 ml of TAE buffer in microwave oven for approx. 2 min. After the solution was cooled to approx. 50 °C, 4  $\mu$ l of GoodView DNA stain were added, the solution was mixed and poured into the electrophoresis chamber.

To 50  $\mu$ l of sample, 5  $\mu$ l of 10x concentrated DNA loading buffer was added. Sample was divided into two wells. Next to the samples, DNA marker was added into a well. Electrophoresis ran 20 minutes at 180 V and DNA was visualized under UV lamp with wavelength of 312 nm.

#### **4.1.3. Isolation of DNA from agarose gel**

Gel containing the DNA of expected size was cut out and transferred to a 1.5 ml tube. Extraction was provided with Gel/PCR DNA Fragments Extraction Kit according to manual [49]. DNA was eluted by sterile water heated to 65 °C.

#### **4.1.4. DNA concentration measurement**

Concentration of DNA was measured by UV light absorption using DeNovix Ds-11+ spectrophotometer. 1  $\mu$ l of sample was used for the measurement of absorbance at 260 nm and sample purity was evaluated according to ratio of absorbances at 260 and 280 nm. DNA was concentrated by evaporation using SpeedVac DNA 110 rotary evaporator.

#### **4.1.5. Restriction cleavage**

Both plasmid and PCR product restriction cleavage were performed as follows. 20 µl of the restriction reaction was prepared by adding 1.5 µl of AgeI and 1.5 µl of KpnI restriction endonucleases, 2 µl of NEB1 buffer, 2 µl of 10x concentrated BSA, 300 ng of pTW5sec\_B7-H6\_2 plasmid and sterile water to the final volume. Restriction reaction was carried out at 37 °C for one hour and the samples were subsequently heated to 65 °C for 20 min to deactivate the restriction endonucleases. Restricted plasmid (termed pTW5sec\*) was purified by agarose electrophoresis and gel extraction.

#### **4.1.6. Ligation**

Approximately 100 ng of purified pTW5sec\* and 100 ng of PCR product were mixed with 2 µl of T4 DNA ligase buffer, 1 µl of T4 DNA ligase and water in 10 µl reaction volume. Reaction was carried out for 1 hour at laboratory temperature.

#### **4.1.7. Transformation**

Competent *Escherichia coli* DH5α bacteria were stored at -80 °C. Prior to transformation, they were thawed on ice and 20 µl of ligation reaction was added to 50 µl of bacteria suspension. Mixture was incubated on ice for 30 min and subsequently spread on an agar plate (1.5 % agar and 100 µg/ml ampicillin in LB medium) tempered to 37 °C. Bacteria were grown overnight at 37 °C.

#### **4.1.8. Colony PCR**

From agar plates, 4 colonies were randomly chosen and resuspended in 6 µl of sterile water in 0.2 ml PCR tubes; 2 µl of forward primer pTT5\_FW and 2 µl of reverse primer pTW5sec\_B7-H6\_2\_REV and finally 10 µl of 2x concentrated Combi PPP Mastermix (containing Taq polymerase, dNTPs and stabilizing agents) were added. Thermal profile of the reaction was the same as in chapter 4.1.1. Finally, 10 µl of reaction products were loaded on agarose gel and the correct size of products was verified by agarose electrophoresis.

#### **4.1.9. Isolation of plasmid DNA**

For isolation of plasmid DNA, bacterial colonies were picked up from agar plate and resuspended in 5 ml of LB medium with ampicillin (100 µg/ml) in 50 ml Falcon tubes. In Falcon tubes, bacteria were grown overnight on shaker at 37 °C and rotational speed 220 revolutions per minute (RPM). Afterwards, the bacteria were centrifuged and the plasmid DNA isolated using High-Speed Plasmid Mini Kit according to manual [50]. The DNA was eluted by 50 µl sterile water.

#### **4.1.10. DNA sequencing**

DNA sequence inserted into the plasmid was verified by sequencing. In 0.2 ml tubes, two reactions were mixed, one with addition of pTT5\_FW primer and one with addition of pTT5\_rev primer. Approx. 300 ng of plasmid in 7 µl and 1 µl of primer were mixed.

Afterwards, 6 µl of sequencing reaction mix was added into tubes in DNA sequencing laboratory of Faculty of Science of Charles University by RNDr. Štěpánka Hrdá. Analysis was performed by Genetic Analyzer 3130 (Applied Biosystems) with 16 capillaries.

#### **4.1.11. Preparation of stock amount of plasmid DNA**

For preparation of stock amount of plasmid DNA, bacteria were grown in larger volume. Colonies grown on agar plate were resuspended and transferred to 0.5 l of LB medium (ampicillin 100 µg/ml) in 2 l Erlenmeyer flask. The bacteria were grown overnight on shaker at 37 °C and rotational speed 220 RPM. Afterwards, the bacteria were centrifuged at 4500 x g for 1 hour, resuspended in 30 ml of TES buffer and centrifuged at 4500 x g for 15 minutes. Next isolation steps were done as stated in manual of PureLink™ HiPure Plasmid DNA kit (Macherey-Nagel, Germany). Bacterial pellet was resuspended in 18 ml of RES buffer. 18 ml of LYS buffer was added subsequently and the tube was inverted five times to gently mix its content. After 5 minutes, 18 ml of NEU buffer was added and tube was inverted five times again. Afterwards, the tube was centrifuged at 20,000 x g for 20 minutes and the supernatant was loaded on equilibrated NucleoBond® Xtra Midi Column through filtration paper. On the column the DNA was subsequently washed by 25 ml of WASH buffer and eluted by 15 ml of ELU buffer. Eluate was mixed with 10.5 ml of isopropanol and the mixture was centrifuged at 16,000 x g, 4 °C. After 30 minutes, the supernatant was

decanted, the pellet was washed by 70% ethanol and the DNA was centrifuged at 16,000 x g, 4 °C for 10 minutes. The supernatant was decanted again and the DNA pellet was dried in rotary evaporator and dissolved in 1 ml deionized water.

## **4.2. Recombinant protein production**

For the protein production, human cell line HEK293S GnTI<sup>-</sup> (further mentioned as HEK293) was used. All manipulation with HEK293 cells was done in sterile flow hood in the room for GMO manipulation of II risk category. Production of LBD and NKp30 has already been described [26].

### **4.2.1. HEK293 cultivation**

HEK293 cells were cultivated in square shaped glass bottles with gas permeable lids in Multitron Cell shaker at 37 °C, 180 RPM and 5% CO<sub>2</sub>. The bottles were filled from 30% up to 40% of their nominal volume and ExCELL293 and Freestyle F17 media in 1:1 ratio were used as growth medium. Twice per week, cell density and presence of contaminants were controlled by light microscopy. When the cell density exceeded 4 million cells per milliliter of culture (C/ml), the suspension was subcultivated with fresh growth medium to 0.2 C/ml cell density.

### **4.2.2. Cell density counting**

To estimate the cell density, 20 µl of cell suspension was mixed with 160 µl of 0.4% trypan blue solution to distinguish between live and dead cells: dead cells are stained blue. The sample was transferred onto hemocytometer and counted. The number of cells on hemocytometer multiplied by factor 10<sup>4</sup> results in the cell density in C/ml unit.

### **4.2.3. Transient transfection**

Prior to transfection, HEK293 cells were grown in larger volume (200 or 400 ml) of growth media to reach sufficient amount of cells. The volume of growth medium containing 800 million HEK293 cells was transferred into 50ml Falcon tubes and centrifuged for 5 minutes at 90 x g. Cells were resuspended in 34 ml of ExCELL293 medium and transferred into a clean glass square bottle. 800 µg of DNA (1 µg per 1 million cells) was diluted in 6 ml of PBS. DNA consisted of three plasmids: 88% of DNA was expression plasmid



pTW5sec\_mB7-H6\_2 and the rest were plasmids expressing cell cycle regulatory proteins, pTW5sec\_p27 (10%) and pTW5sec\_aFGF (2%). DNA in PBS solution was filtered through 0.22 µm filter into the flask with cells. Subsequently, linear 25 kDa polyethyleneimine (IPEI) was added to reach the DNA:IPEI w/w ratio 1:3. Cells were incubated on shaker for 4 hours at 37 °C and afterwards, 1.6 ml of 0.5 M valproic acid and ExCELL293 medium up to 400 ml were added. Cells were harvested after seven days of production.

### **4.3. Protein purification**

#### **4.3.1. Centrifugation and filtration**

As recombinant proteins were produced with signal sequence causing them to be secreted from the cells, after production firstly the conditioned cultivation medium was separated from the cells. HEK293 cultures were centrifuged 1 hour at 3900 x g and 20 °C. Supernatant was filtered through 0.22 µm filter and diluted with PBS buffer by a factor of two.

#### **4.3.2. Metal chelate affinity chromatography**

Recombinant proteins were produced with a histidine tag, therefore enabling the proteins to be purified by metal chelate affinity chromatography. For purification, two 5 ml HiTrap TALON columns connected to FPLC system were used. These columns were stored in 20% ethanol and equilibrated by PBS prior to protein purification. After washing, diluted medium was loaded onto the column and the column was washed by PBS afterwards. For elution, PBS with 250mM imidazole was used and eluted protein was pooled.

#### **4.3.3. Protein concentrating**

For protein concentrating, Amicon Ultra (MWCO 10,000) concentrators were used. Concentrators were filled by protein solution and centrifuged at 3900 x g at 20 °C until the volume decreased to 0.5 ml. This step was repeated until the whole protein solution was concentrated in the concentrator. Finally, protein solution was concentrated to 200 - 250 µl. The solution was transferred into a microtube which was centrifuged for 5 minutes at 30000 x g and 20 °C.

#### 4.3.4. Size exclusion chromatography

Superdex 200 Increase or Superdex 200 column connected to HPLC system were stored in 20% ethanol. Prior to purification, the column was equilibrated by mobile phase. Additionally, 1 ml sample injection loop was washed by mobile phase and the centrifuged sample was injected on the column. The sample was separated on the column and the fractions were collected automatically.

### 4.4. Protein characterization

#### 4.4.1. Protein concentration measurement

Concentration of proteins was measured by UV light absorption using DeNovix Ds-11+ spectrophotometer. Protein molar extinction coefficient and molecular weight were calculated from amino-acid sequence using ProtParam tool on ExPASy server [51]. Using these values protein concentration was calculated from the absorbance measured at 280 nm.

#### 4.4.2. SDS-PAGE

For the purity and homogeneity validation of the sample, twice 5  $\mu$ l of each fraction was used for sodium dodecyl sulfate polyacrylamide gel electrophoresis (SDS-PAGE). Both running and stacking gel were prepared by mixing water, 30% AA, 1.5 M Tris buffer (pH 8.8 and 6.8, respectively), 10% SDS, TEMED and 10% APS (Tab. 4). First, the running gel was mixed and after polymerization, the stacking gel was added on top of it. Into the stacking gel, the sample comb was inserted to create the wells. Polymerized gels were placed in the electrophoresis chamber.

**Table 4: Volumes of components of one 15% PAGE.** APS was added as last to prevent precocious polymerization. Tris buffer pH was 8.8 for running gel and 6.8 for stacking gel.

Gel component	Running gel	Stacking gel
H <sub>2</sub> O	0.92 ml	0.7 ml
30% AA	2.0 ml	0.25 ml
1.5M Tris buffer	1.0 ml	0.12 ml
10% SDS	40 $\mu$ l	10 $\mu$ l
TEMED	40 $\mu$ l	10 $\mu$ l
APS	1.75 $\mu$ l	1.5 $\mu$ l

The samples were prepared in duplicate - with non-reducing and with reducing sample buffer. 5  $\mu$ l of the sample was mixed with 2  $\mu$ l of 5x sample buffer and 3  $\mu$ l of water. The

samples were boiled for 5 minutes in water bath, centrifuged and loaded into the wells of polyacrylamide gel. Eventually, a protein standard was loaded into one well.

Electrophoresis ran for 70 minutes at 220 V. At the end, the gels were stained by staining solution (at least 20 min) and unstained by destaining solution (60 min twice). Gels were digitalized by scanning.

#### **4.4.3. Deglycosylation**

Deglycosylation was used to prepare deglycosylated proteins for further measurements and for their characterization in combination with SDS-PAGE. For deglycosylation of native NKp30 construct protein, the protein HEPES solution at 1 mg/ml was mixed with 10x G5 reaction buffer (1:10) and endoglycosidase F1 (EndoF1) was added. The mass ratio of protein to EndoF1 was 1:200. In case of mB7-H6\_2 construct, no reaction buffer was added and instead glycerol was added to 20%.

For deglycosylation of denatured protein, small amount of protein (20 µg) was mixed with 10x GP reaction buffer and boiled for 10 minutes in water bath. Subsequently, deglycosylation was provided as stated above. Deglycosylation conditions were 2 hours and 37 °C for NKp30\_del and B7-H6\_2 and overnight at laboratory temperature for mB7-H6\_2.

For deglycosylation analysis, 5 µl of the sample was loaded onto SDS-PAGE. For purification of deglycosylated protein, 100 µl of Glutathione Sepharose 4B was added into the reaction tube and incubated on a shaker for 1 hour. Afterwards, the tubes were centrifuged (5 min, 200 x g, 20 °C) and the supernatant was transferred into clean tubes. This step was repeated. Finally, the tubes were centrifuged at 20000 x g (5 min, 20 °C) and the supernatant was transferred into a clean tube.

Glutathione Sepharose resin was regenerated by adding 1 ml of elution buffer for Glutathione Sepharose 4B, incubating for 5 min, 20 °C and centrifuging the resin (5 min, 200 x g, 20 °C). Regenerated resin was stored in 20% ethanol and 4 °C.

#### **4.4.4. Mass spectrometry**

Protein characterization by mass spectrometry was done by Mgr. Michal Rosůlek, Institute of Microbiology of Academy of Sciences of the Czech Republic.

5  $\mu\text{g}$  of protein sample was diluted 2x by 50mM ethylmorpholine buffer with 10% acetonitrile and 0.25  $\mu\text{g}$  of trypsin (pH 8.5). The protein was cleaved by trypsin overnight at 37 °C. Afterwards, the solvent was evaporated in rotary evaporator and peptides were dissolved in 0.5% formic acid with 2.5% acetonitrile. Final concentration of peptides was 0.05  $\mu\text{g}/\mu\text{l}$ .

1  $\mu\text{l}$  of peptide solution was injected on Acclaim C18 PepMap 100 column (0.1 $\times$ 20 mm, average particle size 5  $\mu\text{M}$ , size of pores 100 Å) connected to HPLC system. Desalting was done in three minutes with flow rate 10 ml/min. After three minutes, gradient of mobile phases was applied on the column (phase A: 0.1% formic acid with 2% acetonitrile; phase B: 0.1% formic acid with 98% acetonitrile) with flow rate 0.5  $\mu\text{l}/\text{min}$ . Eluted peptides were separated on reverse phase analytical column (Acclaim C18 PepMap 100; 0.1 $\times$ 150 mm, average particle size 3  $\mu\text{m}$ , pore size 100 Å) at 60 °C.

The measurement was performed on FT-ICR mass spectrometer Bruker solariX XR 12T in positive mode. For data evaluation, DataAnalysis 4.2 and MSLinks softwares were used.

#### **4.4.5. Differential scanning fluorimetry**

Differential scanning fluorimetry was performed using Sypro Orange stain. Its 5000x stock solution was diluted to 50x concentrated solution. The samples were prepared by mixing 4  $\mu\text{l}$  of the protein with 10  $\mu\text{l}$  of 2x screen buffer and 1  $\mu\text{l}$  of 50x concentrated Sypro Orange stain. Samples were filled by HEPES up to 20  $\mu\text{l}$ . As a blank, sample with no protein was used and for comparison, glycosylated and deglycosylated samples with no screen buffers were also used. The data were collected on Rotor-Gene 2000 Real-Time Cycler with excitation wavelength of 300 nm. Fluorescence was measured at 570 nm. The temperature increased stepwise, 0.5 °C each 30 seconds from 25 °C to 95 °C. Measured data were evaluated using OriginPro 8.

### **4.5. Protein-protein interaction investigation**

#### **4.5.1. Analytical size exclusion chromatography**

First, each protein was injected and separated on Superdex 200 Increase column separately. Protein concentration was 20  $\mu\text{M}$  and injection volume 100  $\mu\text{l}$ . Afterwards, equimolarly

mixed proteins were incubated for 2 hours at room temperature (100  $\mu$ l, each 20  $\mu$ M) and separated on the column. Peak shift was observed and analyzed by OriginPro 8.

#### **4.5.2. Sedimentation analysis**

Sedimentation analysis was provided by Dr. Ondřej Vaněk using analytical ultracentrifuge ProteomeLab XL-I using sedimentation velocity experiment. 20  $\mu$ M protein solutions were used for the measurement. Analysis was performed at 48000 RPM and 20 °C using An50-Ti rotor. 200 absorbance scans were taken in 4 min interval at 280 nm wavelength. As a reference, HEPES buffer was used. Buffer density and viscosity and partial specific volume of analyzed proteins were predicted by SENDTERP [52] software and data were analyzed by software SEDFIT [53].

#### **4.5.3. Cross-linking**

The cross-linking reaction set-up and subsequent MS measurements were done by Mgr. Michal Rosůlek.

For cross-linking reaction, 10  $\mu$ g of deglycosylated mB7-H6\_2 at 20 $\mu$ M concentration was mixed with 20 $\mu$ M glycosylated NKp30 at 1:2 molar ratio. 10x and 20x higher amount of mixture of deuterated and non-deuterated DSG and DSS was added (DSS and DSG were both dissolved in DMSO at 2  $\mu$ g/ $\mu$ l). After one hour, the samples were boiled in sample buffer and loaded on SDS-PAGE. Bands from SDS-PAGE were cut out and unstained in ultrasound water bath in 1:1 mixture of 50mM ethylmorpholine buffer and acetonitrile. The solution was being changed for a new one until the gels were unstained. Finally the gels were dehydrated by 100% acetonitrile, the solution was taken away and gels were dried in rotary evaporator.

Subsequently the samples were reduced by 20mM tris(2-carboxyethyl)phosphine (TCEP) in 100mM ethylmorpholine buffer at 70 °C for 3 minutes. TCEP was washed out from the gel by 50mM ethylmorpholine buffer which was overlaid by 50mM iodacetamide in 100mM ethylmorpholine buffer for alkylation. The samples were incubated in darkness for 30 minutes. Cleavage of the proteins was done by trypsin at 37 °C overnight: the gels were overlaid by trypsin dissolved in 50mM ethylmorpholine buffer in 10% acetonitrile in water at 5 ng/ $\mu$ l concentration. The peptides were alternately washed from gel by 50  $\mu$ l of 80% acetonitrile with 0.5% formic acid and 50  $\mu$ l of 0.5% formic acid (3x). The peptide

solution was always transformed into a new tube. Finally, the peptide solutions were dried and the peptides were resuspended by 0.5% formic acid to concentration 0.05 mg/ml.

The measurements and data evaluation were done as described in chapter 4.4.4.

#### **4.5.4. Isothermal titration microcalorimetry**

MicroCal iTC<sub>200</sub> (Malvern) was used for measuring of thermodynamic parameters of NKp30/B7-H6 binding. The measurements were done in cooperation with Dr. Tatsiana Charnavets. First, control heat was determined by 10 injections of 4 µl of buffer (HEPES) from syringe into the same buffer in the cell. For protein binding measurement, 200 µl of 10µM B7-H6 was used in the cell and 0.5 mM NKp30 (as LBD expression construct) in the syringe. Initial injection of 0.4 µl of NKp30 was followed by 19 injections of 2 µl of NKp30. Injection duration was 4 s and injection spacing was 150 s. The measurement was done at 25 °C and the cell solution was stirred at 1000 RPM. The data were evaluated using Origin software.

### **4.6. Structural analyses**

#### **4.6.1. LC-MS with H/D exchange**

H/D exchange and successive mass spectrometry were performed in cooperation with Mgr. Michal Rosůlek. 10 µl of 100 µM protein samples were diluted in 190 µl of heavy water. After several time delays, 20 µl of diluted samples were mixed with 40 µl of quenching buffer and incubated for 3 minutes on ice. Finally, these samples were frozen in liquid nitrogen. The time delays between sample dilution in heavy water and sample quenching were 20 s, 2 min, 10 min, 30 min, 1 hour and 4 hours.

Prior to MS measurement, samples were thawed on ice and injected on pepsin and nepenthesin protease columns connected in series. Then the peptides were separated by reverse phase column. MS spectrum measurement of eluted peptides was performed on FT-ICR mass spectrometer Bruker solarix XR 12T in positive mode and DeutEx software was used for data evaluation.

#### **4.6.2. Electron microscopy**

Electron microscopy (EM) was performed in cooperation with Sami Kereiche, Institute of Cellular Biology and Pathology of First Faculty of Medicine of Charles University. Oligomeric fractions of NKp30 were mixed and their concentration was adjusted to 1 mg/ml. 5  $\mu$ l of sample were applied to glow-discharged carbon-coated copper grids containing continuous carbon support film. After 1 min, excess solution was removed with filter paper and 5  $\mu$ l of 2% uranyl acetate was loaded on the grid. After additional 1 min, excess uranyl acetate was removed by filter paper.

The images were recorded at a final magnification of 500,000 x in Tecnai G2 Sphera 20 microscope (FEI, Hillsboro, OR, USA) equipped with a LaB6 cathode and a 2048 $\times$ 2048 Gatan Ultrascan 1000 CCD camera (Gatan, Inc, Pleasanton, USA) of a pixel size 14  $\mu$ m. The microscope was operated at the accelerating voltage of 120 kV.

#### **4.6.3. SAXS**

Synchrotron SAXS data were collected on the European Molecular Biology Laboratory at beamline P12 at PETRA III storage ring at the Deutsches Elektronen-Synchrotron DESY (Hamburg, Germany). Protein samples were prepared in various concentrations (0.6 - 10 mg/ml) in HEPES buffer. The data were normalized to the intensity of transmitted beam and the scattering of the buffer was subtracted by PRIMUS software [54]. The collected data were evaluated by Dr. Tereza Skálová, Biotechnology Institute, AS CR.

#### **4.6.4. Protein crystallization and X-ray analysis**

Protein crystallization was performed at the Division of Structural Biology of the Nuffield Department of Clinical Medicine at the University of Oxford. Crystallization was done by sitting drop method in 400 nl volume (200 nl of protein solution and 200 nl of crystallization reagents) using Hydra instrument. First, the robot transferred reagents into the reservoir well. Subsequently, reagents from each reservoir were transferred onto every corresponding crystallization position. Then, 200 nl of protein solution was added into reservoir drop. Finally, the plates were sealed by a transparent foil to prevent evaporation of drops.

For initial screening, four commercially available screens (Index, Proplex, PACTpremier, Block; prepared in house) were tested for mB7-H6 in complex with two constructs of NKp30 (eight screens together). Proteins were concentrated up to 10 mg/ml prior to drop set-up. For optimization, protein concentration of 6.6 mg/ml was used and protein to crystallization reagent was 1:2 (100 nl + 200 nl). The choice of optimization screens was based on initial results. All crystallization plates were stored in Formulatrix Storage and Imaging System at 21 °C. Diffraction data collection was kindly performed by Dr. Karl Harlos at Diamond Light Source synchrotron. Preliminary data analysis was performed by Dr. Tereza Skálová.



## 5. RESULTS

### 5.1. B7-H6 production and characterization

For protein production, constructs cloned in pTW5sec plasmid were used. Preparation of these plasmids is described elsewhere [48]. Similarly, production and purification of constructs of protein NKp30, termed LBD (Leu19 – Arg130) and NKp30\_del (Leu19 – Arg143), are described elsewhere [26]. NKp30\_del construct consists of three amino acids which are not cleaved from secretion signal (ITG) at N-terminus, whole NKp30 extracellular domain, two additional amino acids (GT), His-tag consisting of 8 histidines and glycine at C-terminus. LBD, in comparison to NKp30\_del, does not contain short stalk domain which is C-terminal part of extracellular domain of NKp30 (Fig. 7).

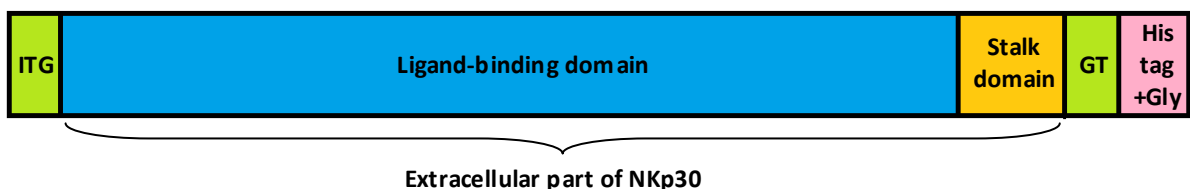


**Figure 7: NKp30 constructs.** N-terminal ITG sequence is followed by ligand-binding domain and short 13-amino-acid-long stalk domain (which is not contained in LBD construct), GT sequence, histidine tag (8 histidines) and C-terminal glycine.

#### 5.1.1. Production and purification of B7-H6\_2

For protein B7-H6, pTW5sec plasmids for two constructs, termed B7-H6\_1 (distal Ig domain; Asp25 - Val140) and B7-H6\_2 (whole extracellular domain; Asp25 - Leu245) were cloned previously (Fig. 8, p. 50) [48]. In both cases, extracellular part of B7-H6 is expressed with additional amino acids at N-terminus and C-terminus as described for NKp30 constructs. B7-H6\_1 contains N-terminal immunoglobulin domain of B7-H6 and B7-H6\_2 contains both extracellular immunoglobulin domains.

ITGDLKVEEMAGGTQITPLNDNVTIFCNIFYSQPLNITSMGITWFWKSLTFDKEV  
 KVFEFFGDHQEAFRPGAIIVSPWRLKSGDASLRLPGIQLEEAGEYRCEVVVTPLKA  
 QGTVQLEVVASPASRLLLDQVGMKENEDKYMCESSGFYPEAINITWEKQTQKFPH  
 PIEISEDVITGPTIKNMDGTFNVTSLKLNSSQEDPGTVYQCVVRHASLHTPLRS  
 NFTLGTHHHHHHHG

**Figure 8: Sequence of B7-H6 constructs.** ITG - terminal amino acid residues from signal sequence, N - asparagines with predicted N-glycosylation, C - cysteines forming disulfide bridges, C - odd cysteine, H - histidine tag. **BLUE amino acids** are not part of B7-H6\_1 construct.

Each domain contains one disulfide bridge (C48 - C122 and C163 - C228). Moreover, the C-terminal domain contains one odd cysteine.

Production of both proteins in HEK293 cell line was tested, however, only B7-H6\_2 could be produced and purified (Fig. 9). Protein yield after purification was 5 mg from 1 l cell culture.

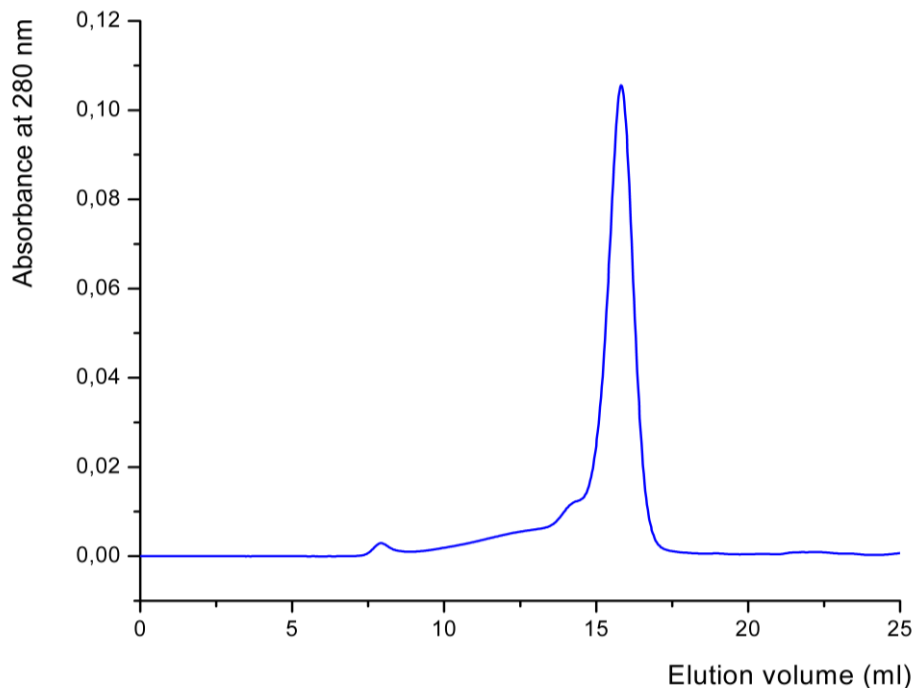


**Figure 9: Size exclusion chromatography of B7-H6\_2.** Protein isolated from 400 ml of cell culture media using metal chelate chromatography was further purified by SEC on Superdex 200 column with yield of 5 mg per liter of media. Small peak (at around 14.5 ml, absorbance under 0.02) indicates possible dimerization of the protein.

### 5.1.2. B7-H6\_2 characterization

On the chromatogram from size exclusion chromatography (SEC) (Fig. 9), small peak at lower elution volume and high peak at higher elution volume were observed. To evaluate protein

purity and homogeneity, SDS-PAGE analysis was performed. In reducing buffer, protein appeared as monomer (33 kDa; Fig. 10, right), however, in non-reducing buffer, protein of size of a dimer (58 - 72 kDa) of B7-H6\_2 in the first two SEC fractions was detected (Fig. 10, left). B7-H6 forms two disulfide bridges and has one additional cysteine residue which suggests that the protein formed covalent dimer via its odd cysteine residue.

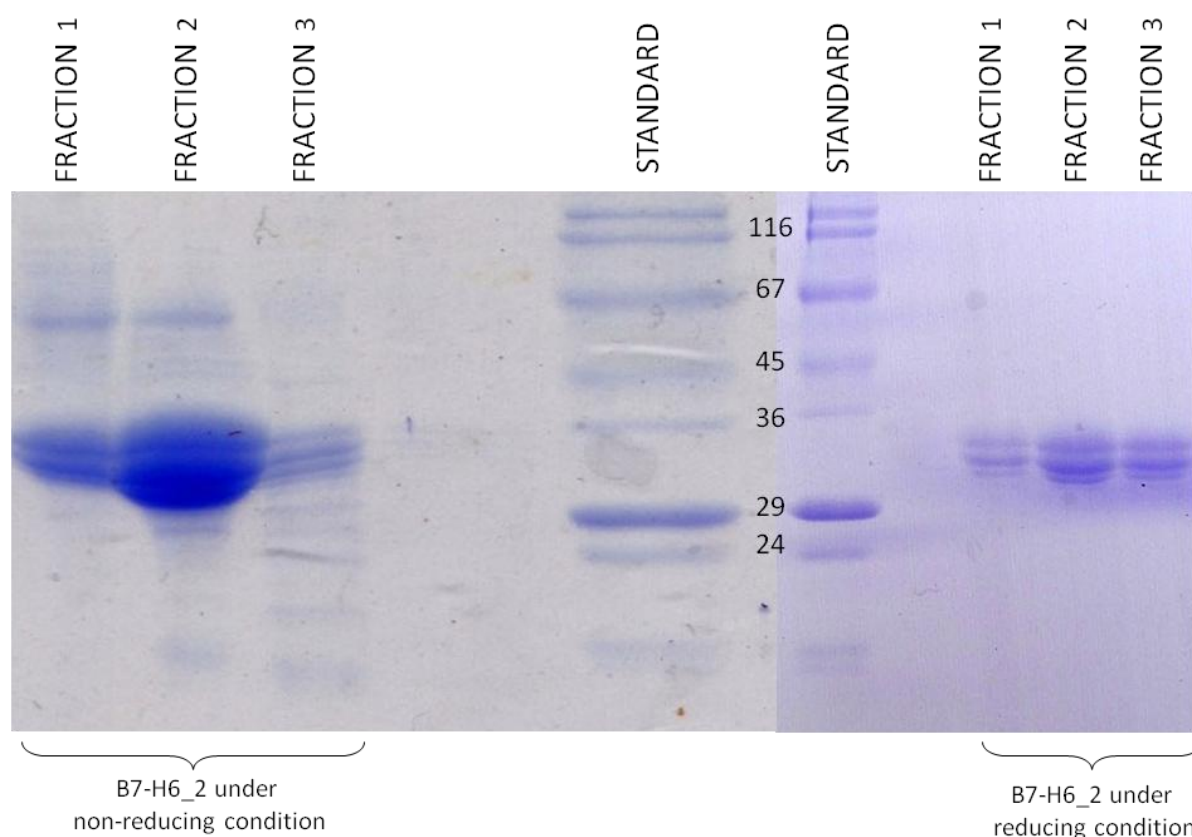


**Figure 10: SDS-PAGE analysis of B7-H6\_2.** First three fractions of B7-H6\_2 peak from SEC were taken and loaded on 15% SDS-PAGE under non-reducing (left) and reducing (right) condition. Dimers (approx. 66 kDa) are visible in first two fractions of B7-H6\_2 in non-reducing sample buffer, but not in reducing sample buffer, where only monomer (approx. 33 kDa) occurs.

Deglycosylation was performed with and without denaturing buffer and samples were loaded on SDS-PAGE, too (Fig. 11, p. 52). Glycosylated sample consists of two major forms which suggests that some protein N-glycosylation sites are not always occupied (composition of N-linked oligosaccharide moieties is homogeneous due to the cell line used for protein expression [24], but glycosylation is not always present at all sites). Deglycosylation of native protein led to drop of the protein mass to 26 kDa, as expected for deglycosylated B7-H6\_2. As mass of one oligosaccharide from HEK293S GnTI<sup>-</sup> cell line is

1217 Da (5x mannose and 2x N-acetylglucosamine), this suggests as much as six glycosylation sites at extracellular domain of B7-H6. Six N-glycosylation sites are predicted for B7-H6 extracellular domain according to amino-acid sequence [55] and until now, four have been confirmed [55]. Deglycosylation in denaturing buffer was not complete, presumably because of partial inactivation of EndoF1 under these conditions; therefore multiple bands can be seen on the polyacrylamide gel corresponding to individual partially deglycosylated protein forms.

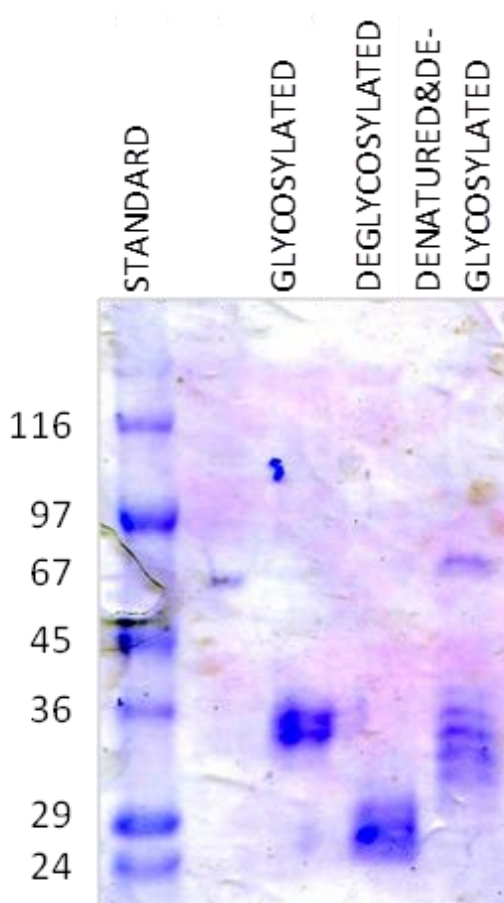


**Figure 11: Deglycosylation analysis of B7-H6\_2.** Samples of glycosylated, deglycosylated and protein deglycosylated in denaturing environment were resolved on reducing 15% SDS-PAGE gel. After deglycosylation the protein mass shifted to expected value of 26 kDa. Deglycosylation in denaturing buffer revealed that multiple glycosylation sites of B7-H6 are occupied.

In agreement, mass spectrometry confirmed that cysteine bridges of B7-H6\_2 were not linked correctly (according to published structure [15]; not shown).

Sedimentation analysis was also performed for B7-H6\_2 (Fig. 12, p. 53). SEC fraction with the highest protein concentration was used and adjusted to 0.5 mg/ml. Majority of the protein

behaved as monomer (sedimentation at 2.5 S), but small amount of putative dimer (4 S) and tetramer (6.1 S) species were observed, too (Fig. 12). Moreover,  $f/f_0$  frictional ratio equaled 1.5 which, in agreement with published structure, indicates prolonged shape of the molecule.

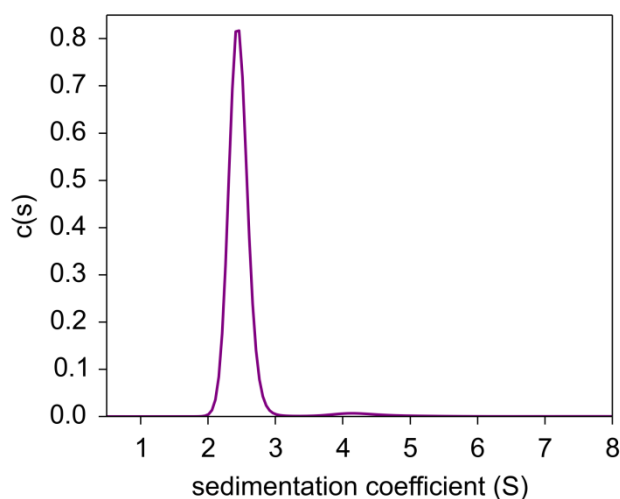


**Figure 12: Sedimentation analysis of B7-H6\_2.** Protein at 0.5 mg/ml concentration was analyzed by sedimentation velocity experiment at 48,000 RPM and 20°C, resultant data were analyzed in Sedfit software and are shown as fitted continuous size distribution  $c(s)$  of sedimenting species with respect to their sedimentation coefficient given in Svedberg units (S).

### 5.1.3. Point mutation and cloning of mB7-H6\_2

As B7-H6\_2 formed covalent dimers, point mutation of odd cysteine by OE-PCR was performed. The odd cysteine was identified as C212 according to published structure (PID 3PV6; Fig. 13).

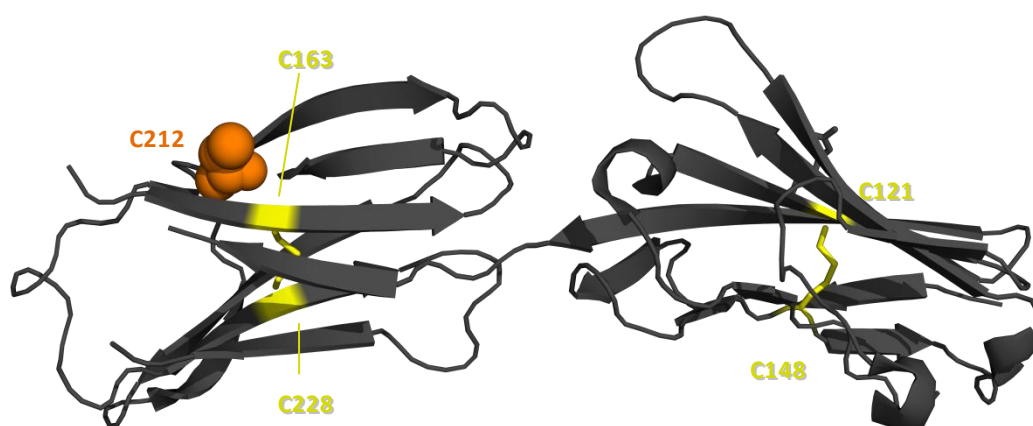


**Figure 13: Cysteines in B7-H6.** Structure of B7-H6 extracellular domain (PID 3PV6) with highlighted disulfide bonds (yellow) and odd cysteine 212 (orange). B7-H6\_2 formed covalent dimer, therefore point mutation C212S was performed.

Cysteine 212 was exchanged for serine (mutation C212S; Fig. 14) and product of OE-PCR was cloned into pTW5sec vector, resulting in pTW5sec\_mB7-H6\_2 which encoded protein construct termed mB7-H6\_2.

G	T	C	A	C	T	A	G	C	T	G	C	T	T	G	A	A	G
V	T	S	C	L	K												
G	T	C	A	C	T	A	G	C	A	G	C	T	T	G	A	A	G
V	T	S	S	L	K												
209																	214

**Figure 14: Point mutation C212S.** Mutation was verified by DNA sequencing.

#### 5.1.4. Production and purification of mB7-H6\_2

mB7H6\_2 was produced in HEK293 cell line and purified as stated in chapter 4.3. Surprisingly, introduced point mutation rapidly increased protein yield up to 47 mg per 1 l of cell culture medium (Fig. 15).

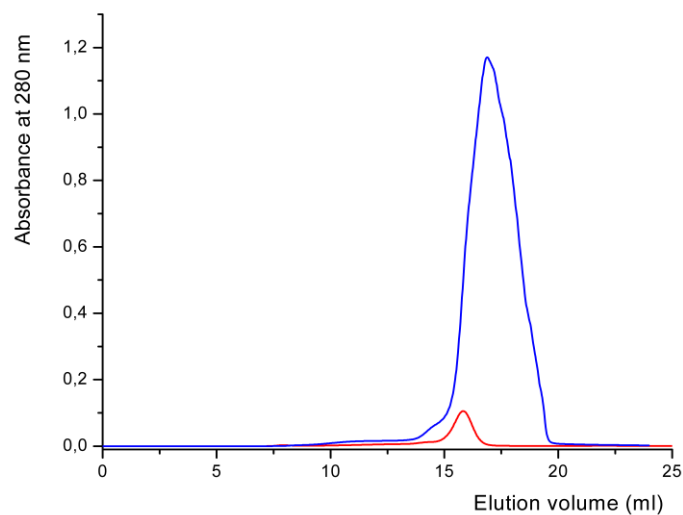


**Figure 15: Size exclusion chromatography of mB7-H6\_2.** Comparison of SEC chromatograms of wild-type B7-H6\_2 (red) and mB7-H6\_2 (blue). Proteins isolated from 400 ml of cell culture media using metal chelate chromatography were further purified by SEC on Superdex 200 column. Point mutation C212S led to almost ten-fold increase in yield, up to 47 mg per 1 l of cell culture medium

### 5.1.5. Characterization of mB7-H6\_2

Purity and homogeneity of mB7-H6\_2 fractions from SEC were investigated by SDS-PAGE. Compared to B7-H6\_2, mB7-H6\_2 is more homogenous and does not form covalent dimers. Deglycosylation of mB7-H6\_2 leads preferentially to complete deglycosylation of the protein with only minor presence of partially glycosylated proteins (Fig. 16).

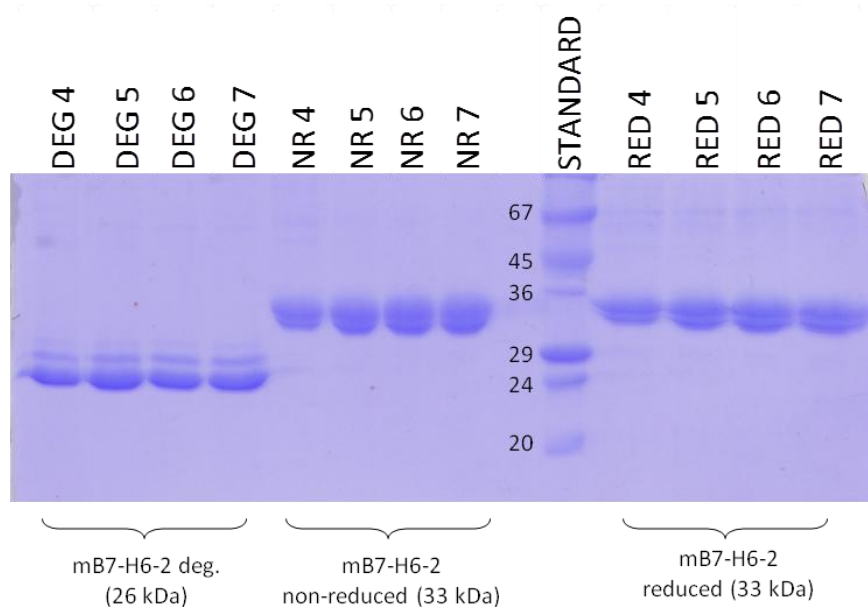


**Figure 16: Deglycosylation of mB7-H6\_2.** 15% SDS-PAGE of deglycosylated (left) and glycosylated non-reduced (middle) and glycosylated reduced mB7-H6\_2, fractions 4 - 7 from SEC. Mass of the protein after deglycosylation shifted to expected value of 26 kDa. Protein dimers are not observed in non-reduced state. Standard – molecular weight standards in kDa.

For mass spectrometry analysis of disulfide bonds and occupancy of predicted glycosylation sites, deglycosylated mB7-H6 was used. Deglycosylation by endoglycosidase F1 leaves one reminiscent N-acetylglucosamine on the glycosylation site, therefore the deglycosylated protein can be used for such analysis. The sequence coverage was 79%. The correct conformation of disulfide bonds was confirmed and five occupied glycosylation sites were detected. The sixth glycosylation site at Asn242 could not be observed because the last 15 amino acids were not covered by any detected peptide.

### 5.1.6. Differential scanning fluorimetry

Deglycosylation of mB7-H6\_2 in standard buffer condition led to its precipitation. Therefore, better buffer conditions for deglycosylation and storage of protein were sought by differential scanning fluorimetry. 25 various conditions were screened (Fig. 17) and protein melting points were analyzed.

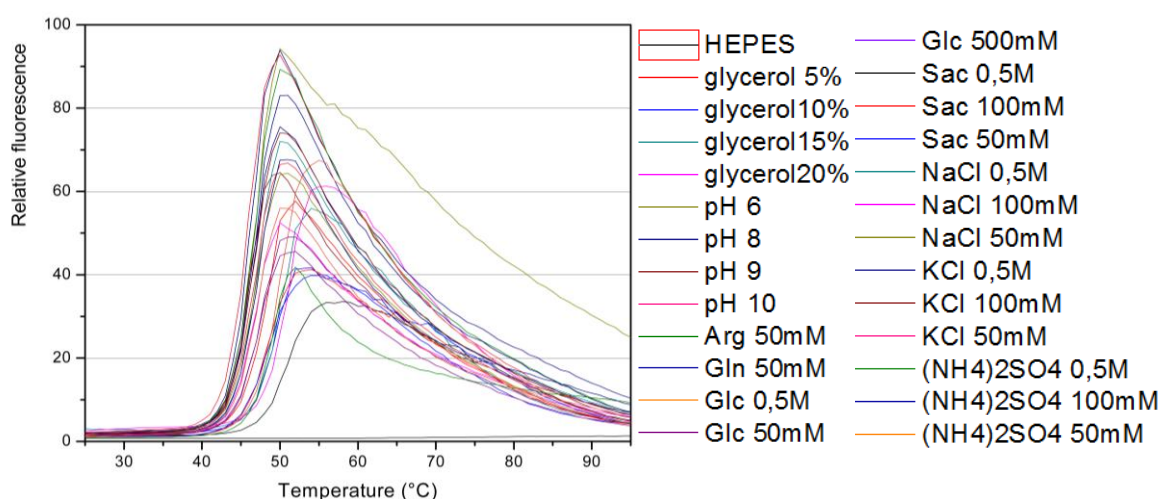


**Figure 17: Melting curves of mB7-H6\_2 with different reagents.** Specific reagents are stated in legend; Arg – L-arginine, Gln – L-glutamine, Glc – glucose, Sac – saccharose. HEPES buffer was used as a control (its signal is not rising with increasing temperature).

Melting points can be extrapolated by finding inflection point of sigmoid melting curves in the previous graph (Fig. 17). By depicting the data as negative derivative of relative fluorescence ( $-d(RF)/T$ ) the melting points correspond to minima of melting curves (Fig. 18).

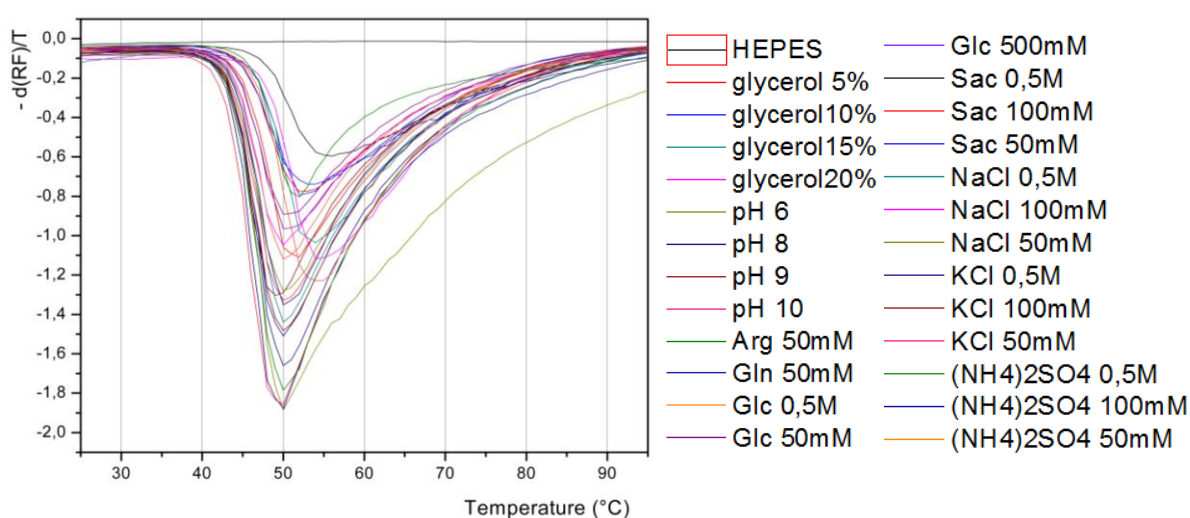


**Figure 18: Negative derivation of relative fluorescence ( $-d(RF)/T$ ) dependence on temperature.** Minima correspond to the melting points. Highest melting point was detected for 0.5M saccharose (56 °C). Specific reagents are stated in legend; Arg – L-arginine, Gln – L-glutamine, Glc – glucose, Sac – saccharose.



The highest melting point was recorded for 0.5M saccharose (56 °C; Fig. 19), however 20% glycerol (melting point 54 °C) was chosen for deglycosylation and storage at low temperatures (-20 °C). Furthermore, no buffer for deglycosylation (pH 5.5) was added into reaction as pH other than neutral destabilizes the protein.

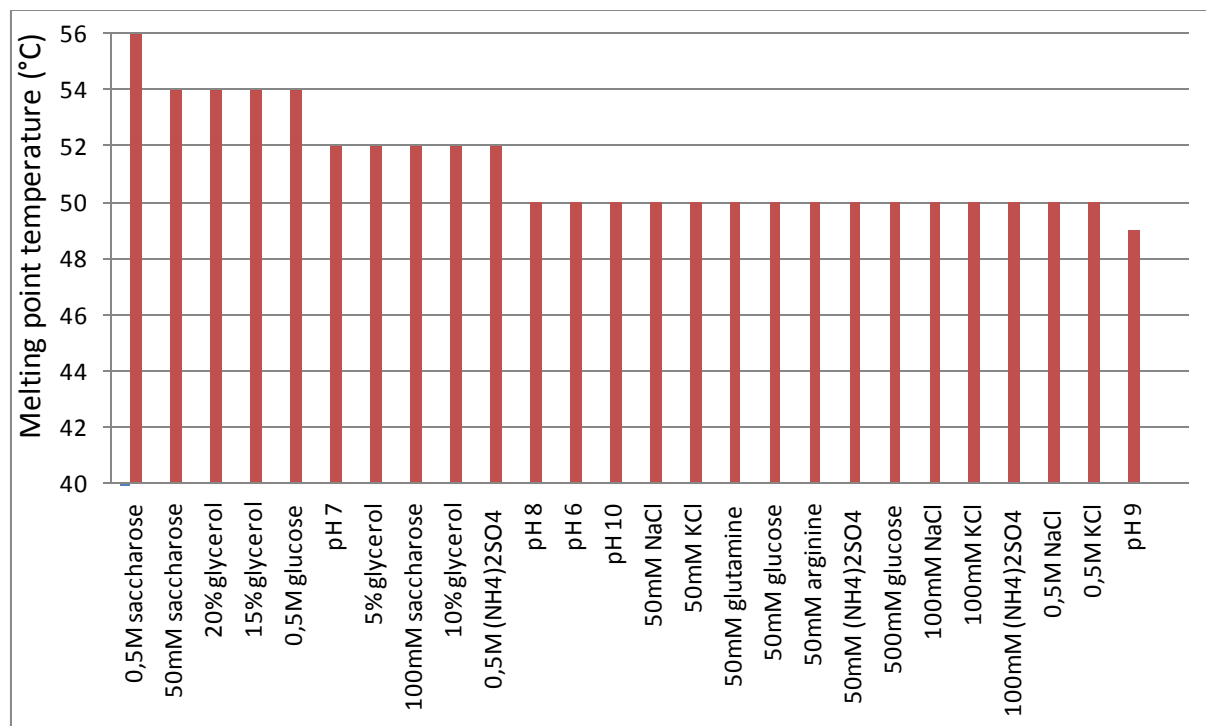


**Figure 19: Summary of B7-H6 melting points under various conditions.** 25 conditions were examined. 0.5M saccharose was found to be the most stabilizing agent. pH values other than 7 had destabilizing effects.

### 5.1.7. Characterization of NKp30

Multiple glycoforms of NKp30 can be seen on SDS-PAGE [26], therefore its glycosylation pattern was analyzed by mass spectrometry. NKp30<sub>del</sub> construct was used for the analysis. According to the sequence, three N-glycosylation sites are predicted for NKp30. By direct protein mass spectrometry, measured mass of the intact protein was majorly 17671.87 Da which suggested the protein has two occupied N-glycosylation sites (Fig. 20, p. 58). Minor form with higher mass (three occupied N-glycosylation sites) was also detected, albeit at much lower intensities in mass spectrum and it should be at least 10x less abundant in the sample. By LC-MS analysis of peptide fragments Asn42 and Asn121 were detected as 100% occupied; Asn68 was just partially glycosylated. Glycosylation of Asn42 is mainly important for further studies as it has been shown to be crucial for increased NKp30 binding affinity [9].

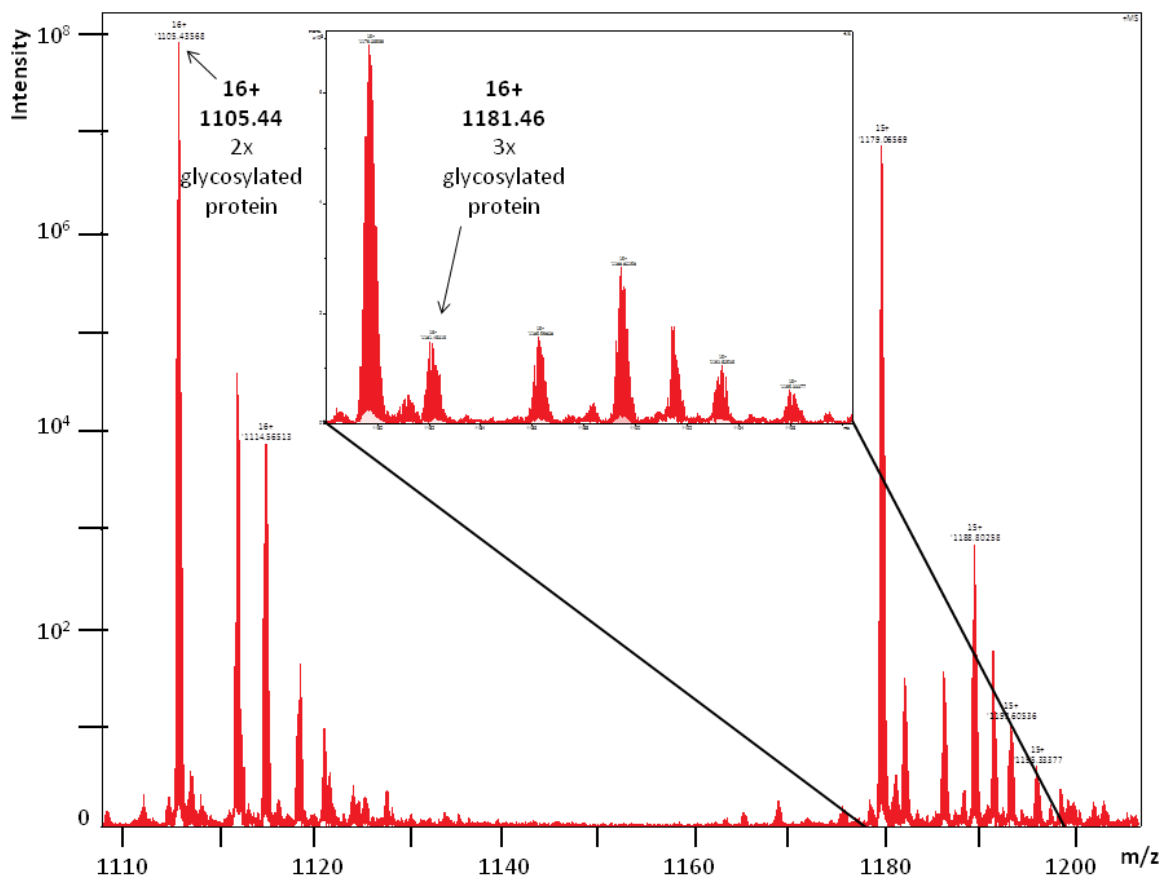


**Figure 20: Signals from direct protein mass spectrometry.** Peak with observed 1105.44 m/z value corresponds to 16x charged protein with two occupied N-glycosylation sites. Intensity of the peak is at  $10^8$  order of magnitude. Peak with observed 1181.46 m/z value and intensity at  $10^2$  corresponds to 16x charged protein with three occupied N-glycosylation sites which is less than 10x abundant.

In MS spectrum, expected glycosylation motif for protein produced in HEK293S GnTI<sup>-</sup> cells [24] was confirmed (Fig. 21, p. 59). The highest signal in the spectrum corresponds to peptide with N-linked oligosaccharide composed of 7 monosaccharide units, followed by lower fragmentation signals showing gradual loss of masses corresponding to hexose (relative molecular mass 162) and N-acetylhexosamine (relative molecular mass 203).

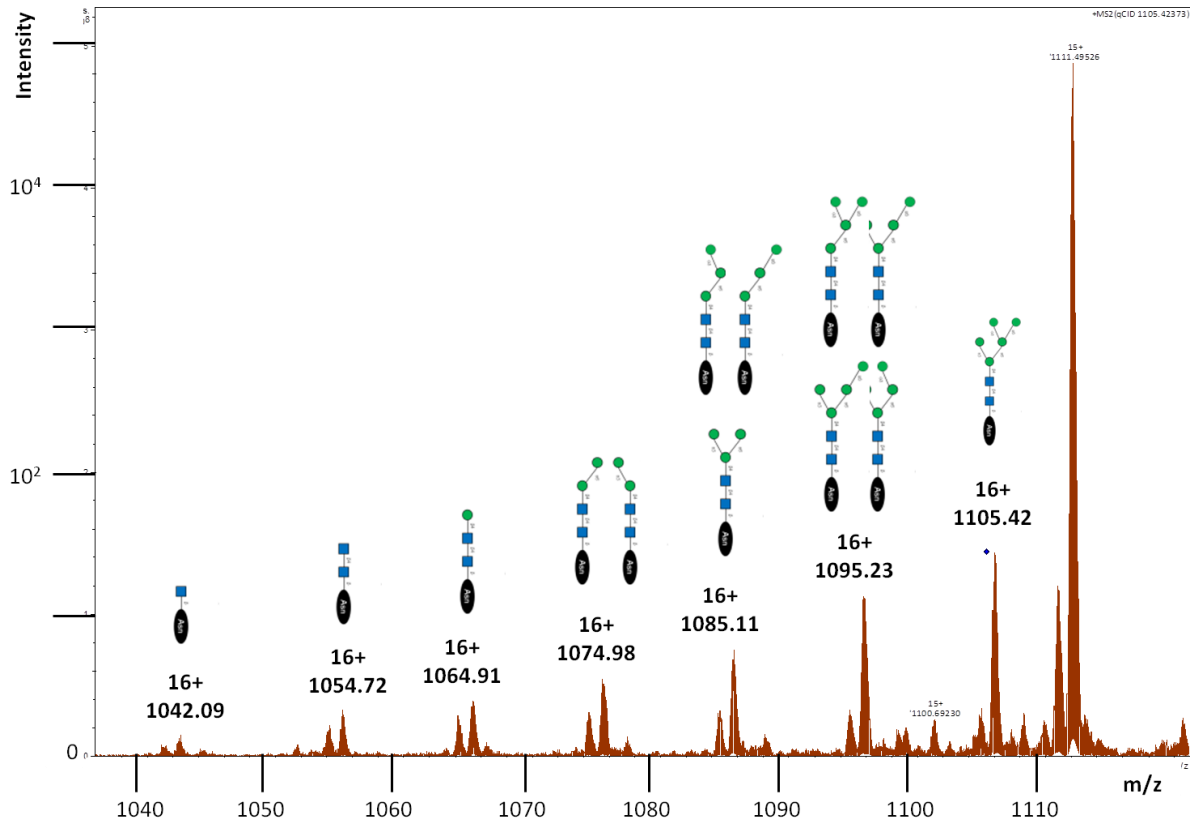


**Figure 21: Example of MS spectrum of peptide with N-glycosylation.** The highest peak with charge 16+ corresponds to NKp30 peptide with full glycosylation (2x N-acetylglucosamine and 5x mannose). Loss of mass in other peptides due to fragmentation corresponds to loss of one mannose (relative molecular mass 162, which is 10.2 on m/z x-axis with charge z=16). Loss of mass of the first peptide (on the left in spectrum) corresponds to loss of one N-acetylglucosamine (relative molecular mass 203, which is 12.7 on m/z x-axis with charge z=16). Possible oligosaccharide structures of distinct peptides are depicted by symbolic nomenclature of monosaccharide representation (green round - mannose, blue square - N-acetylglucosamine).

## 5.2. Protein interaction analysis

### 5.2.1. Confirmation of protein binding

First, both NKp30\_del and mB7-H6\_2 (further B7-H6 only) proteins were mixed (both in 20 $\mu$ M concentration and 100  $\mu$ l volume) and loaded on SEC column. By comparison of elution volume of the expected protein complex and elution volumes of both individual proteins, complex formation was confirmed (Fig. 22, p. 60).

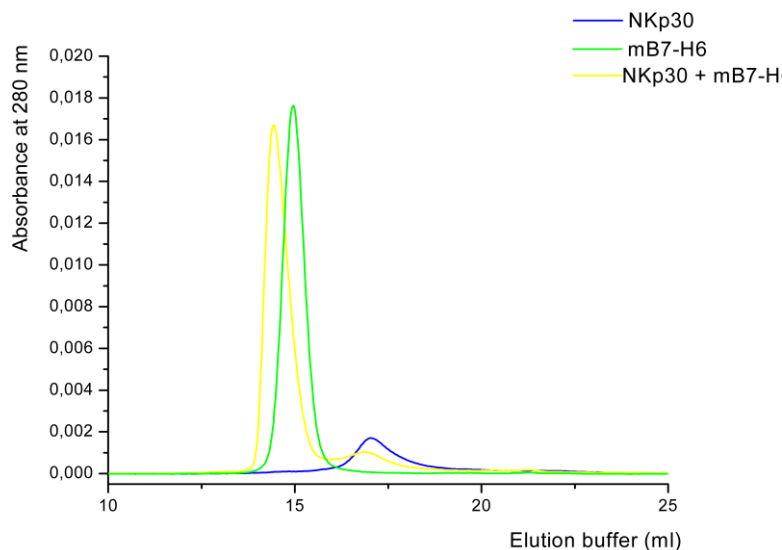


**Figure 22: NKp30/B7-H6 complex formation analysis.** Size exclusion chromatography of NKp30\_del (blue), mB7-H6\_2 (green) and their equimolar mixture (yellow) was performed on Superdex 200 Increase column. Peak shift was detected for the mixture of proteins indicating their binding. Excess NKp30 in the chromatogram of protein complex can be explained by inaccurate protein concentration measurement. The difference in peak height between NKp30 and B7-H6 is caused by their very distinct absorption coefficients.

By analytical ultracentrifugation, the binding of NKp30 and B7-H6 proteins in 1:1 molar ratio was definitely confirmed (Fig. 23, p. 61). Glycosylated NKp30 sedimented predominantly at 1.7 S (monomer) and marginally at 3.5 S (dimer or trimer species). B7-H6 sedimented predominantly at 2.4 S (monomer) and marginally at 4.4 S (dimer). Mixture of the proteins sedimented as a complex at 3.1 S and relatively small peak of sedimentation at 1.7 (monomer of NKp30) was detected. Signal of NKp30 monomer was presumably caused by excess of free NKp30 in the mixture due to incorrect protein concentration measurement.

Finally, the complex binding was detected on SDS-PAGE after cross-linking reaction with DSG (disuccinimidyl glutarate) and DSS (disuccinimidyl suberate) (Fig. 24, p. 61).

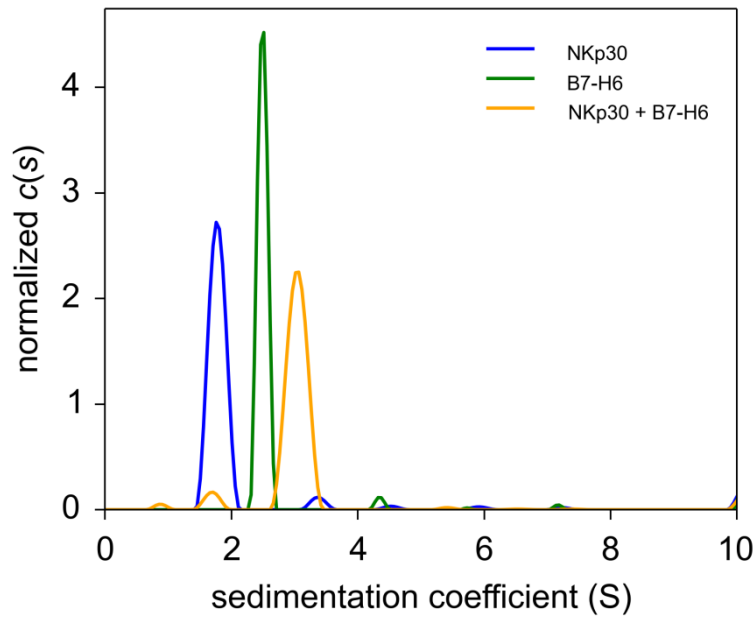


**Figure 23: Sedimentation analysis of NKp30/B7-H6 complex formation.** Proteins at 20 $\mu$ M concentration were analyzed by sedimentation velocity experiment at 48000 RPM and 20°C, resultant data were analyzed in Sedfit software and are shown as fitted continuous size distribution  $c(s)$  of sedimenting species with respect to their sedimentation coefficients given in Svedberg units (S); distributions are normalized by area under the curve. Sedimentation coefficient differences between individual NKp30 and B7-H6 proteins and their mixture prove complex formation. Excess NKp30 was detected in the complex sample, similarly to analytical SEC, indicating inaccurate NKp30 concentration measurement.

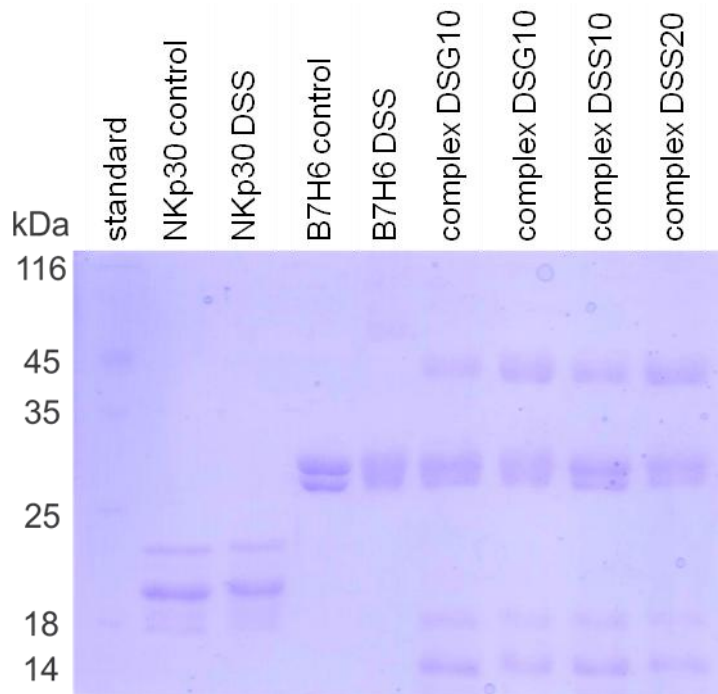


**Figure 24: Cross-linking of NKp30/B7-H6 complex.** 15% SDS-PAGE of non-cross-linked proteins (controls) and NKp30, B7-H6 and their complex cross-linked using DSS and DSG reagents (for details see chapter 4.5.3). NKp30 is present in multiple glycosylation forms at 16 – 19 kDa. B7-H6 was deglycosylated and two remaining glycosylation forms at 29 kDa can be seen. For cross-linked complex, additional band at 45 kDa appears.

For cross-linking reaction, glycosylated NKp30 and mB7-H6\_2 (which was deglycosylated to avoid covering of putative amino acid residues which could react with cross-linking reagents) were used. On SDS-PAGE bands around 45 kDa for cross-linked protein complex can be seen. Analysis of the MS data from cross-linked proteins resulted in only one identified intermolecular cross-link by DSG between N-terminus of NKp30 and lysine 74 of B7-H6 (Fig. 25).

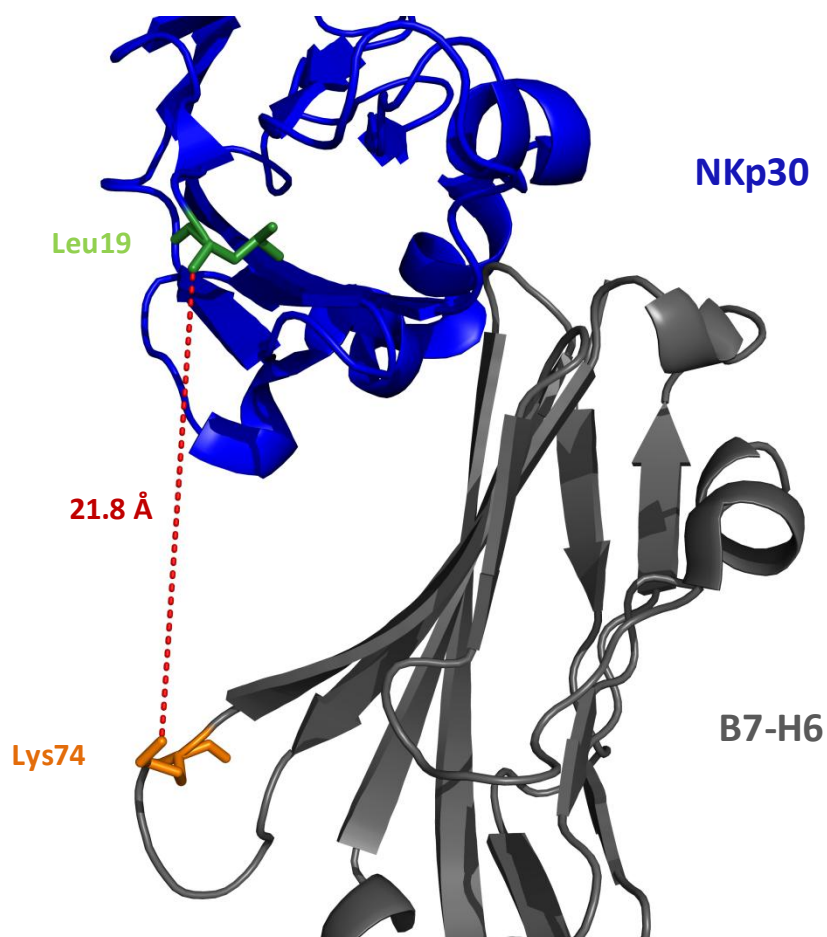


**Figure 25: Visualization of cross-link identified in NKp30/B7-H6 complex.** Crystal structure of NKp30/B7-H6 complex (PID 3PV6) with highlighted distance among Lys74 of B7-H6 and Leu19 of NKp30. Three additional amino acids are missing at NKp30 N-terminus in this structure as compared to our NKp30 expression construct.

Length of DSG molecule is 7.7 Å and the distance between N-terminal Leu19 of NKp30 and Lys74 of B7-H6 is 21.8 Å, according to published structure (PID 3PV6). However, N-terminus of our NKp30 expression construct has three more amino acids (ITG) and the complex itself may be flexible enough to overcome the distance observable in the crystal structure and be able to react with DSG at both sites.

## 5.2.2. Complex affinity measurement

Isothermal titration calorimetry was used to measure affinity of LBD/B7-H6 binding (for simplicity, LBD construct of NKp30 that does not form oligomers, was used). Here, only preliminary results are presented (Fig. 26).

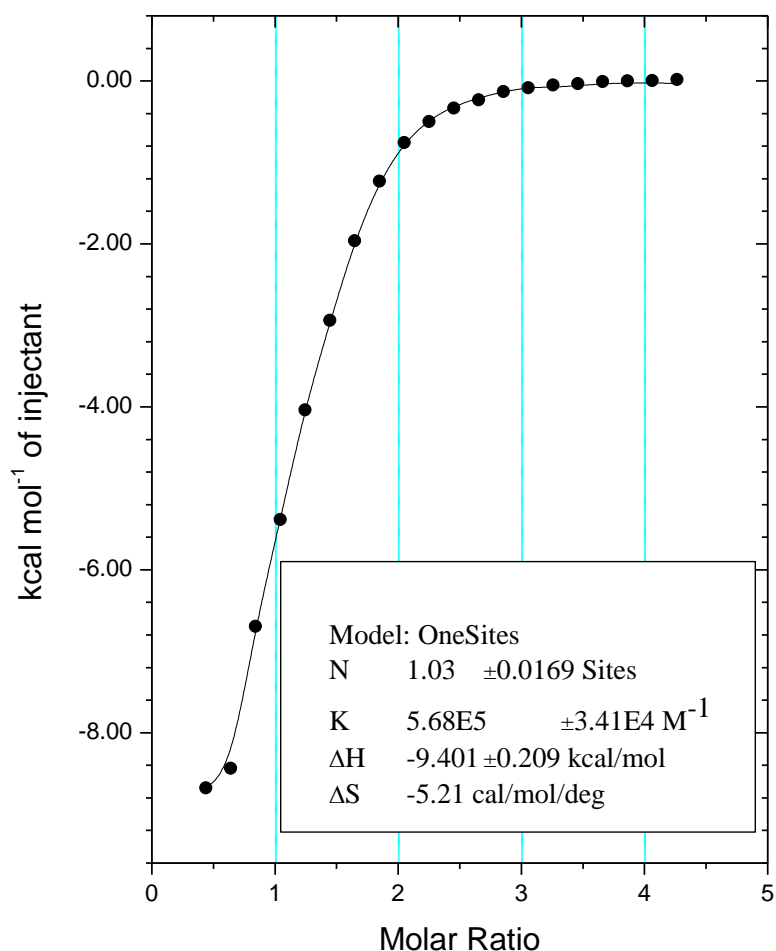


**Figure 26: An example of titration curve from ITC measurement.** 10 $\mu$ M B7-H6 solution in the cell was titrated by 0.5mM solution of LBD (for details, see chapter 4.5.4). Measured affinity ( $K_D$ ) in this case is 1.8 $\mu$ M

From the titration curves, affinity of the proteins was calculated as 5.8  $\mu$ M in average. In comparison with other affinity measurements of this complex available from literature, this result is comparable with lowest affinities measured for both constructs produced in *E. coli* (2.5 - 3.5  $\mu$ M) [14] or NKp30 construct produced in *E. coli* and B7-H6 construct produced in Sf9 insect cell line (1.0  $\mu$ M) [15]. The affinity is one order of magnitude weaker than reported in case of proteins produced in HEK293T cell line [22].

## 5.3. Study of NKp30 oligomerization

### 5.3.1. Electron microscopy

NKp30 oligomers were imaged by negative stain electron microscopy with glow discharge (Fig. 27). As representative sample of oligomers, various oligomeric fractions from size exclusion chromatography of NKp30\_del construct were joined into one sample and concentration of the sample was adjusted to 1 mg/ml.

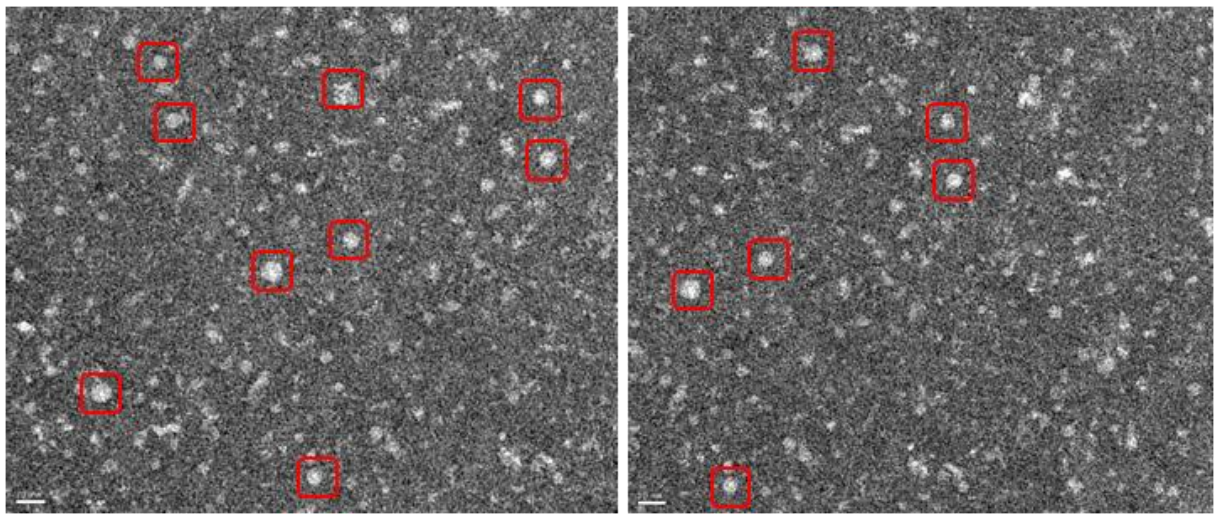


**Figure 27: Electron microscopy images of NKp30 oligomers.** Particles of various sizes can be seen on the images, with the largest form having diameter about 15 nm (some of them highlighted by red squares). Pooled oligomeric fractions from SEC of NKp30\_del construct were used.

On the EM images, particles of various sizes can be seen which can be caused by dynamic equilibrium of several oligomer types of NKp30\_del construct. Predominant particles have diameter about 15 nm which is in agreement with published data [23]. In comparison, average diameter of NKp30 extracellular domain is approx. 4.2 nm, according to the published structure (PID 3PV6).

### 5.3.2. Small-angle X-ray scattering

Small-angle X-ray scattering (SAXS) was measured for both NKp30 constructs: dimeric fraction of LBD (Fig. 28 and 29, p. 65) and oligomeric fraction of NKp30\_del (Fig. 30, p. 66) at various protein concentrations. In both cases, envelope shape has been shown to be dependent on the protein concentration which is in agreement with our previous studies [26].



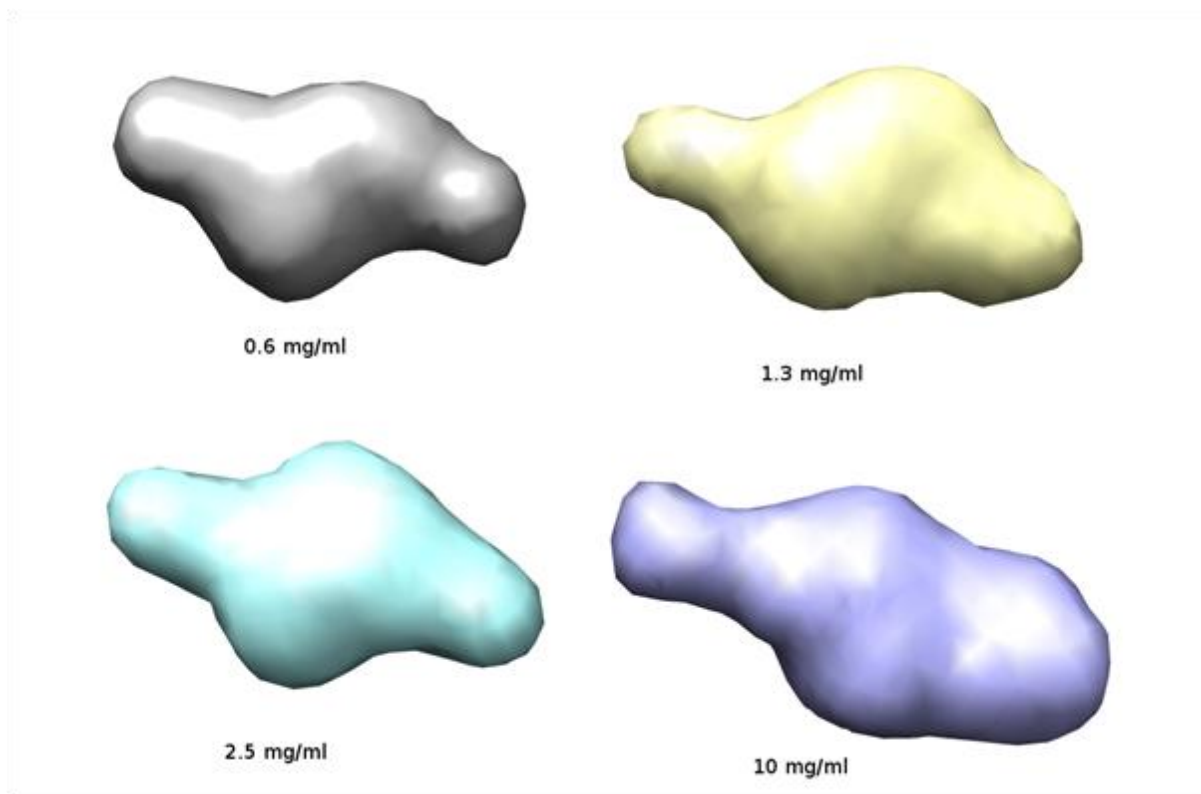


**Figure 28: SAXS envelopes for LBD at various concentrations.** The size of the LBD envelope rises with increasing concentration of the protein. Size of lower concentration envelopes agrees with size of two LBD molecules.

Asymmetric unit of published LBD structure (PID 3NOI) and our structure of LBD dimer (see next chapter), which is similar to published LBD dimer (PID 3NOI), were fitted into the SAXS envelope from LBD sample at concentration 0.6 mg/ml in Chimera software (Fig. 29).

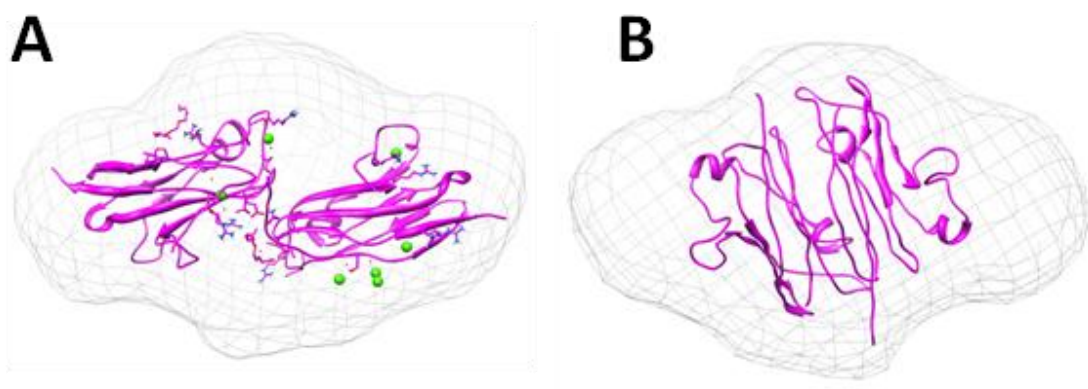


**Figure 29: SAXS envelope for LBD with two fitted LBD molecules.** Size of the LBD envelope correlates with size of two LBD molecules. **(A)** Fit of asymmetric unit of published structure of dimeric NKp30 (PID 3NOI) into the envelope of LBD at concentration 0.6 mg/ml. **(B)** Fit of dimer from our structure (which is similar to published structure, see chapter 5.4) into the envelope of LBD concentration 0.6 mg/ml.

The models were fitted using Chimera software with assumption of two-fold rotation symmetry of the dimer. The fit was evaluated by Crysol software [56]. Surprisingly, asymmetric unit of LBD from PID 3NOI structure fits into the SAXS envelope better (chi-square value 1.24) than LBD dimer observed within our crystal structure (chi-square value 1.40; see chapter 5.4).

For NKp30\_del construct, data collected at low protein concentration (0.4 and 1.0 mg/ml) had non-linear Guinier plot and thus low quality. The model was generated for the samples at 2.4, 5.0 and 9.7 mg/ml. For 9.7 mg/ml sample, average of 20 models with random input parameters resulted in small ball-shaped envelope which suggest that these data are not reproducible. For the samples with other concentration, the model resulted in paraglide-shaped envelope (Fig. 30). The model at 2.4 mg/ml is more credible as the whole protein mass calculation resulted in almost same molecular mass of approx. 90 kDa. Clearly, the longer NKp30 construct tends to form much larger oligomeric species than shorter LBD.

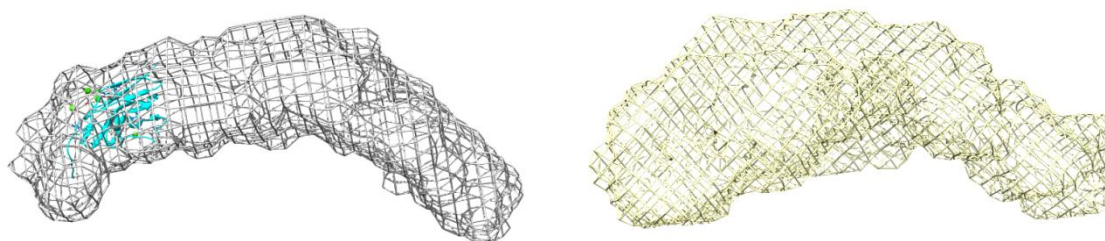


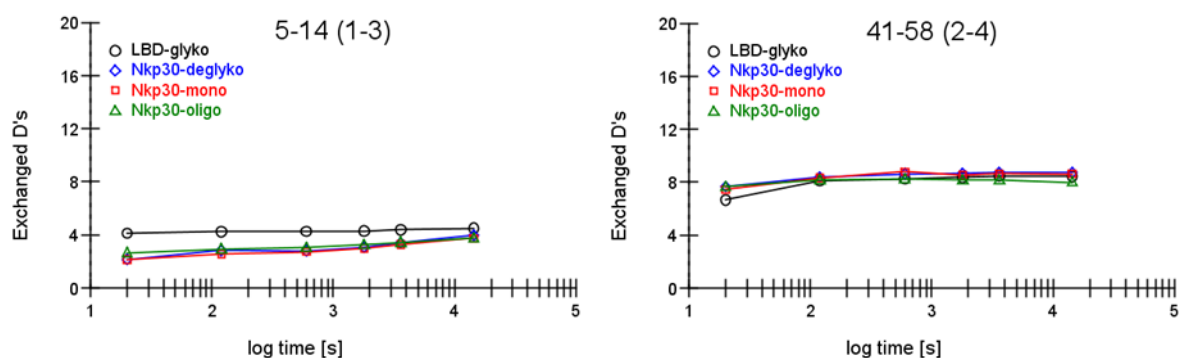
**Figure 30:** SAXS envelopes of NKp30\_del at 2.4 mg/ml (left) and 5 mg/ml (right). For size comparison, one NKp30\_del molecule is visualized inside the left envelope.

### 5.3.3. Mass spectrometry with H/D

Interaction surface of NKp30 oligomers and possible additional interaction surface of NKp30/B7-H6 was investigated using mass spectrometry with H/D exchange. After peptide cleavage optimization the sequence coverage reached for LBD and NKp30 was 72% and 75%, respectively. Coverage of B7-H6 sequence was 78%.

To investigate NKp30 oligomers, various forms of the protein were used (Fig. 31, p. 67). Glycosylated monomeric fraction of LBD collected from SEC was compared to deglycosylated

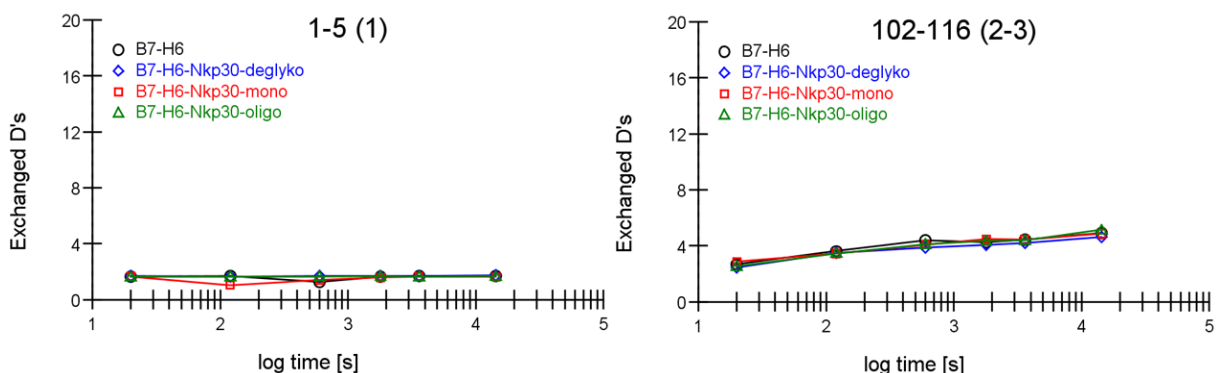
NKp30 monomer, glycosylated NKp30 monomer and joined fractions of glycosylated NKp30 oligomers.



**Figure 31: Typical results of H/D exchange of two LBD and NKp30 peptides.** Number of exchanged deuteriums (Y-axis) in distinct times (X-axis) is compared among glycosylated monomer of LBD (LBD-glyko), deglycosylated NKp30 (NKp30-deglyko), glycosylated monomer of NKp30 (NKp30-mono) and glycosylated oligomers of NKp30 (NKp30-oligo). No significant changes in deuteration between the samples were detected in most of the peptides. Peptide numbering is correlated to construct sequence. Numbers assign the peptide segment and numbers in brackets assign its charge state.

The recorded differences of deuteration of distinct forms of NKp30 were small or none.

To investigate NKp30/B7-H6 complex interface and influence of different NKp30 forms on it, several samples were compared: B7-H6 protein alone, B7-H6 mixed with deglycosylated NKp30, glycosylated monomeric fraction of NKp30 and oligomeric fraction of NKp30 (Fig. 32).

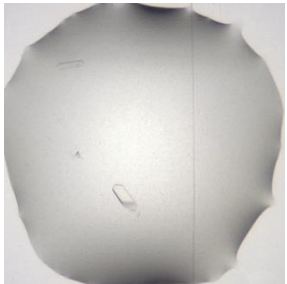
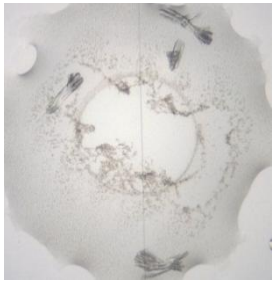
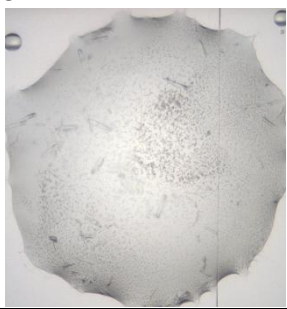
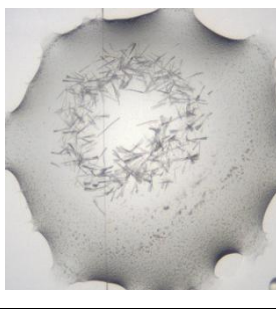


**Figure 32: Typical results of H/D exchange of two B7-H6 peptides.** Number of exchanged deuteriums (Y-axis) in distinct times (X-axis) of single B7-H6 molecule is compared to equimolar mixture of B7-H6 with deglycosylated NKp30 (B7-H6-NKp30-deglyko), with glycosylated monomer of NKp30 (B7-H6-NKp30-mono) and with glycosylated oligomers of NKp30 (B7-H6-NKp30-oligo). Again, no significant changes in deuteration between the samples were detected in most of the peptides. Peptide numbering is correlated to construct sequence. Numbers assign the peptide segment and numbers in brackets assign its charge state.

Again, no significant differences in numbers of H/D exchanges were recorded. Overall, not only differences in deuteration of different samples but also deuteration itself was very small, therefore no conclusion can be made based on these results.

## 5.4. Crystallography results

Four random optimization screens with LBD/B7-H6 and NKp30\_del/B7-H6 mixtures were set up to further investigate the structural basis of glycosylation and oligomerization role in the protein complex. Few crystals from LBD/B7-H6 mixture grew after 3 - 4 weeks (Fig. 33).

<p><b>1</b></p> 	<p>0,1M magnesium chloride 0,1M MES pH 6</p>	<p><b>2</b></p> 	<p>20% (w/v) PEG 4000 0,1M sodium citrate pH 4.5</p>
<p><b>3</b></p> 	<p>0,1M sodium citrate pH 5.5</p>	<p><b>4</b></p> 	<p>0,1M sodium citrate 20% (w/v) PEG 8000 pH 5</p>

**Figure 33: Pictures of four drops from initial screening with grown crystals.** All crystals grew from protein mixture of LBD and B7-H6. Diffraction of the crystal from drop in panel 1 was tested; however, the resolution was too low. Size measure is not provided by the imaging system; the total drop volume was 400 nl.

In most of the drops of NKp30\_del/B7-H6 only precipitation occurred and no crystal was observed. Diffraction data were measured for one of the crystals (Fig. 33, No. 1), however, their resolution was too low. Based on the information from initial screening, six optimization screens were designed with helpful advises by Dr. Yuguang Zhao. Concentration of the protein was decreased to 6.6 mg/ml and the protein to crystallization reagents ratio was changed to 1:2.

The first optimization screen was gradient screen, screening for pH (4.5 - 7) and PEG 6000 concentration (5% - 10%). The same gradient was used for the second optimization screen

but random additives were added. The third optimization plate was set up with the same gradient screen again but the drops were seeded by crystals from initial screen (Fig. 33, p. 68, No. 4). For the fourth screen, Proplex matrix was used (as in the initial screen), but the drops were seeded by the same crystals again. For last two optimization screens, 1:1 protein:reagents ratio was used with protein concentration 10 mg/ml. The fifth optimization screen was gradient screen with 0.1M sodium citrate, screening for PEG 6000 concentration (5 - 15%) and pH (4.5 - 7). The same gradient was screened in the sixth optimization screen with additional seeding.

Increased number of crystals grew in the drops of optimizations screens and for few of them diffraction data were collected again. The best diffraction data were collected from crystal grown in the condition of the sixth optimization screen (Fig. 34). The condition was 0.1M sodium citrate, 11.7% PEG 6000, pH 6.7 and the drop was seeded by previously gained protein crystal needles. Diffraction resolution was 3.4 Å.

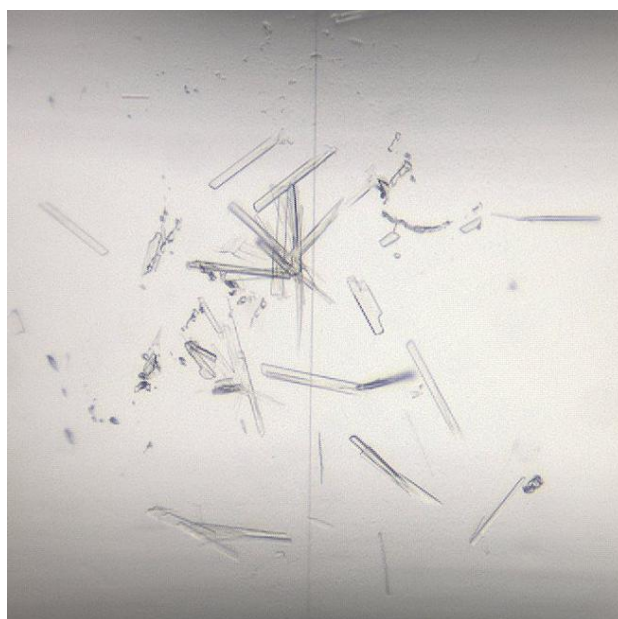


**Figure 34: Crystals of LBD/B7-H6 complex.** Protein solution (10 mg/ml) was mixed with precipitant (0.1M sodium citrate, 11.7% PEG 6000, pH 6.7) in 1:1 ratio (200 nl + 200 nl) and the drops were seeded by previously grown protein crystal needles. Diffraction data were collected to 3.4 Å resolution.

Structure of the complex was solved by molecular replacement using previously solved NKp30/B7-H6 structure (PID 3PV6) and preliminary structural model was built. An asymmetric unit of the crystal contains two molecules of LBD and three molecules of B7-H6 (Fig. 35, p. 70). The arrangement of molecules in the crystal is different compared to the

arrangement of molecules in the published structure of the complex (PID 3PV6). For further description purpose, molecules in asymmetric unit are termed B7-H6\_A, B7-H6\_B, B7-H6\_C, LBD\_A and LBD\_B, as shown in figure 35 below.

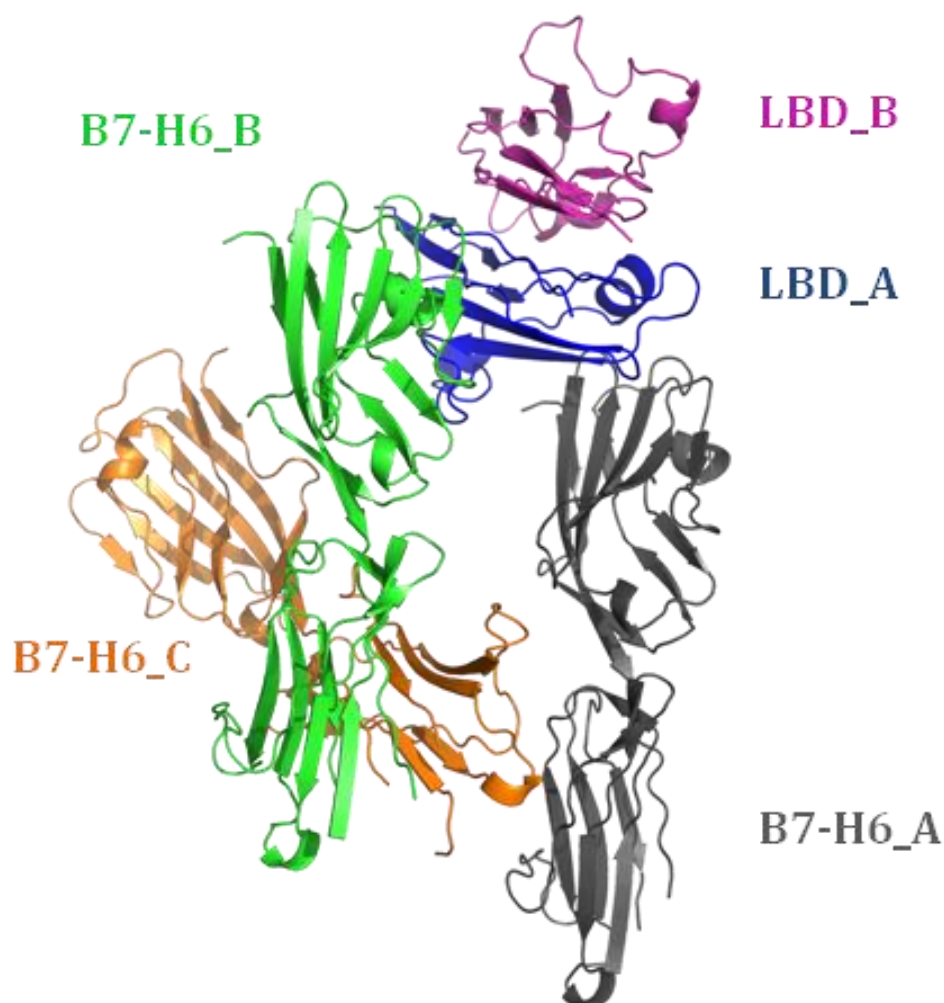


**Figure 35: Asymmetric unit of crystal structure of LBD/B7-H6 complex.** In asymmetric unit, three molecules of B7-H6 (termed B7-H6\_A, B7-H6\_B and B7-H6\_C) and two molecules of LBD (termed LBD\_A and LBD\_B) are visible. The arrangement of molecules in the crystal is different than the arrangement in the published structure of the complex (PID 3PV6).

When other asymmetric units are viewed in the crystal, the dimer of two complexes of LBD/B7-H6 (LBD\_A/B7-H6\_A and LBD\_B/B7-H6\_B) is revealed (Fig. 36, p. 71). Similar dimer was already observed in the crystal structure of NKp30 (PID 3NOI) but not in the crystal structure of NKp30/B7-H6 dimer.



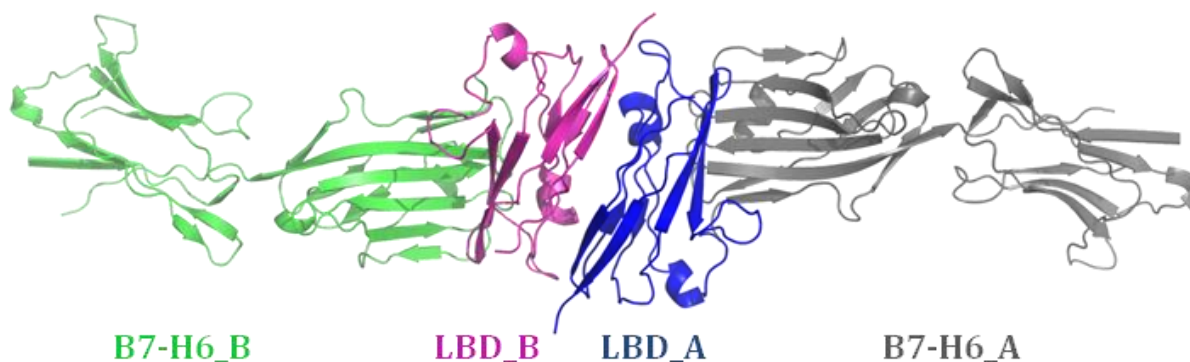


**Figure 36: Dimer of NKp30/B7-H6 complex.** A dimer of two LBD/B7-H6 complexes is observable in the structure. Dimer of LBD is similar to published structure (PID 3NOI). Both pairs of molecules bind to each other almost identically and when compared to published structure of the complex (PID 3PV6), the binding mode of the proteins is also very similar.

The dimer of LBD has 2-fold rotation symmetry about an axis perpendicular to the plane of incidence (rotation by an angle of  $180^\circ$ , as visualized in Fig. 37). Noticeably, a glycosylation site at Asn42 of one LBD molecule (LBD\_A) is located closely to the C-terminal stalk domain of the second LBD molecule (LBD\_B). Glycosylation of this site has been shown to be crucial for NKp30/B7-H6 complex binding previously [22]. Interestingly, only one of the LBD molecules (LBD-A) has electron density which indicates presence of glycosylation.

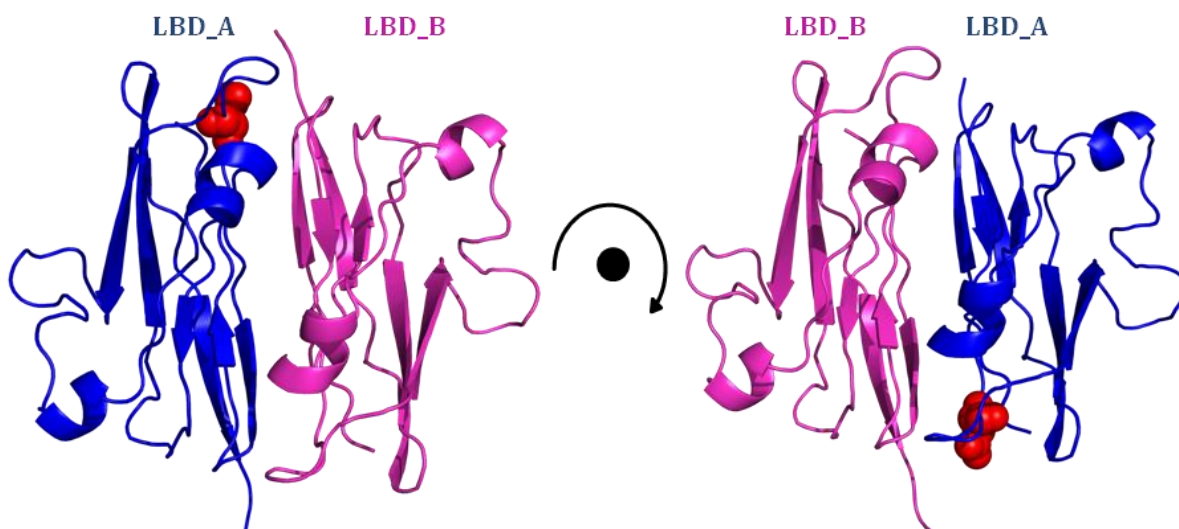


**Figure 37: Putative non-covalent dimer of LBD.** The dimer has two-fold rotation symmetry. Glycosylation site at Asn42 of LBD\_A is close to C-terminal stalk domain of LBD\_B. Electron densities at two glycosylation sites (Asn42 and Asn121) are observable for LBD\_A but not for LBD\_B.

In the electron density map of LBD\_A, two electron densities corresponding to one monosaccharide unit are visible at glycosylation sites Asn42 and Asn121 (Fig. 38). Occupancy of these glycosylation sites is in agreement with mass spectrometry data (chapter 5.1.7). The rest of the oligosaccharides is not visible due to their flexibility or structure low resolution.

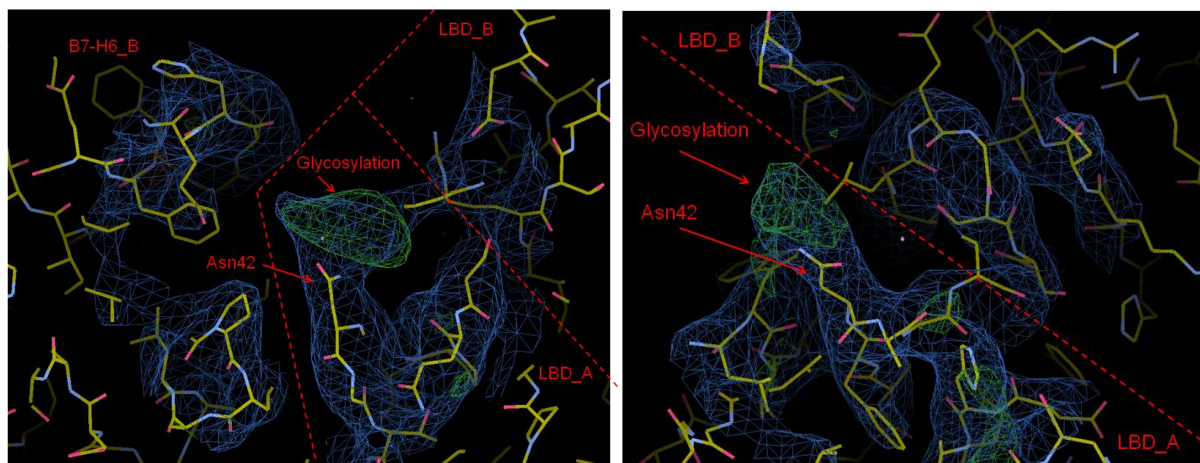


**Figure 38: Glycosylation in electron density of LBD\_A.** Green color indicates presence of so far unmodeled electron density, in this case corresponding to one monosaccharide unit visible at glycosylation site Asn42 (left) and Asn121 (right). Glycosylation at Asn42 is in proximity of LBD\_A dimeric partner LBD\_B and glycosylation at Asn121 is in proximity of B7-H6\_B.

For comparison, the putative non-covalent dimer of LBD from present crystal structure was aligned to the structure of published LBD dimer (PID 3NOI; Fig. 39).

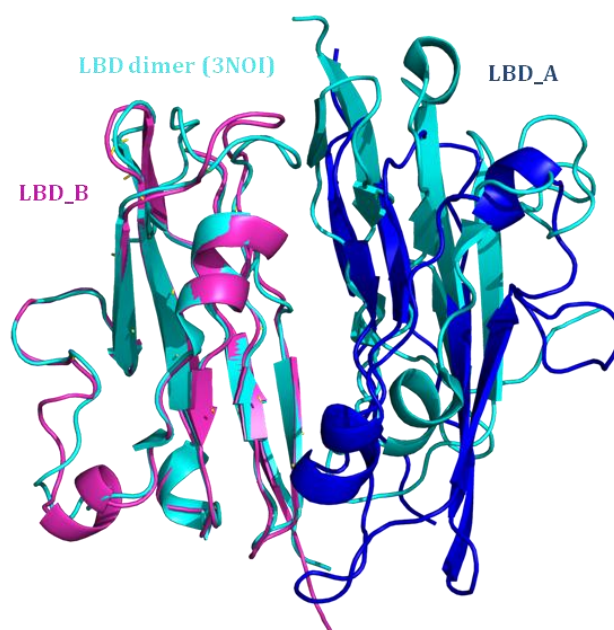


**Figure 39: Alignment of LBD dimers.** The dimer has two-fold rotation symmetry. Glycosylation site at Asn42 of LBD\_A is close to C-terminal stalk domain of LBD\_B.



In the published structure of NKp30 dimer (PID 3NOI), only one additional amino acid (Gln130) is visible compared to our structure. The dimers are visibly similar with the same two-fold rotation symmetry, however, the molecules of dimer in the published structure are more distant and the dimer is present in a more open form, while in the LBD dimer of LBD/B7-H6 complex the two LBD molecules are in comparably closer formation.

In the present crystal structure, one LBD molecule makes contact with two B7-H6 molecules. One of the B7-H6 molecules binds LBD with similar spatial arrangement as in already published complex structure (PID 3PV6; i. e. LBD\_A/B7-H6\_A in Fig. 40A), however, the other B7-H6 molecule makes contact with the same LBD molecule (e. g. LBD\_A/B7-H6\_B) near Asn121 of LBD, which has been shown to be crucial for the binding (Fig. 40B) [22].

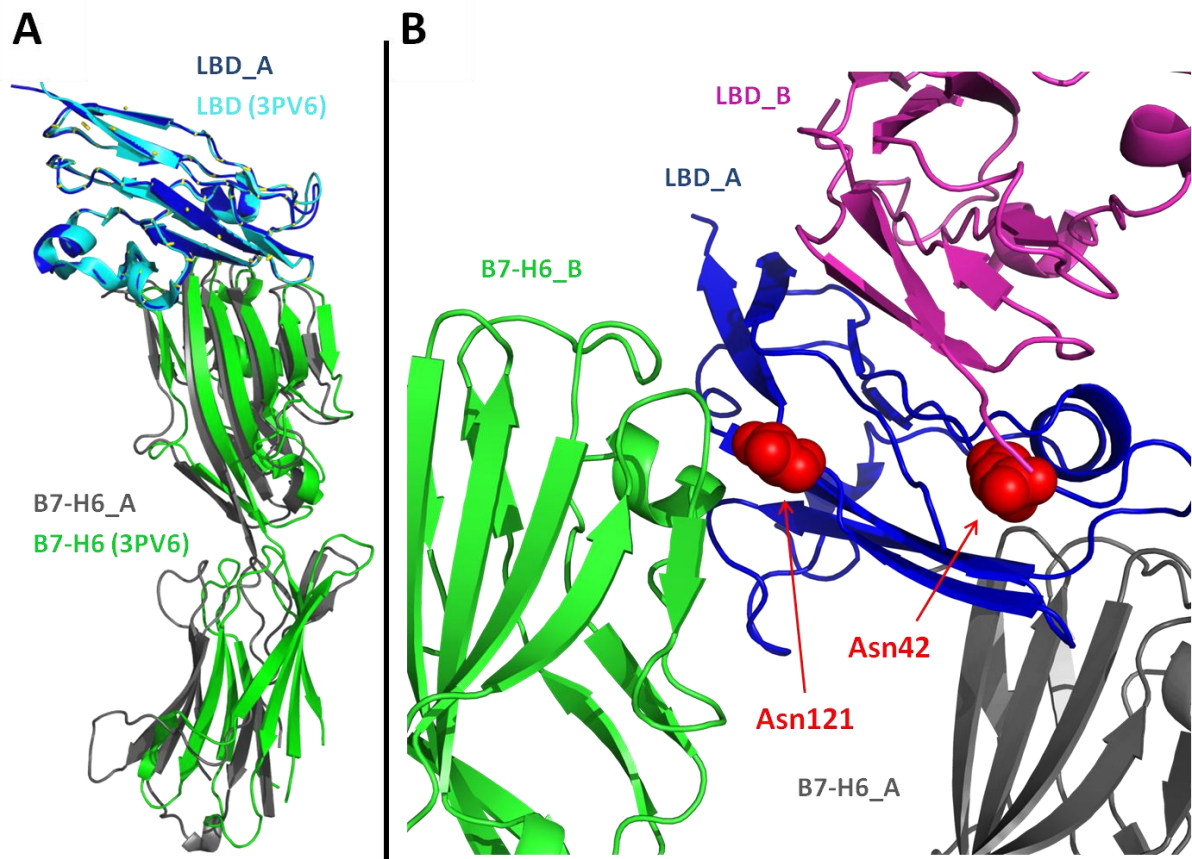


**Figure 40: (A) Alignment of NKp30/B7-H6 complexes.** LBD molecule was aligned to NKp30 of published structure (PID 3PV6). Small differences in B7-H6 orientation, mainly of C-terminal Ig domain, are visible. **(B) Glycosylation sites of LBD.** LBD\_A is glycosylated at Asn42 and Asn121 which are close to LBD\_A and B7-H6\_B, respectively.

## 6. DISCUSSION

The essential part of this work was the preparation of stable and soluble extracellular part of B7-H6 protein. This was first achieved by transient transfection of HEK293 cells using expression construct with wild-type B7-H6 sequence. However, further analysis showed that the protein was inhomogeneous and created covalent dimer due to its odd cysteine C212. In agreement, this cysteine is located on the molecule's surface and is therefore able to react and create additional disulfide bonds with other cysteine residues. Such heterogeneity would presumably prevent protein crystallization which requires very homogeneous samples, therefore a point mutation C212S was introduced. Serine was chosen because of its side chain similarity to cysteine. The production of the mutated form of B7-H6 led to tenfold increase of its production. The explanation of this phenomenon can lie in lowered energy consumption of HEK cells, which would otherwise spend the energy for eliminating of improperly folded protein and production of chaperons and other protein production stabilizing agents. Further analysis of mutated B7-H6 by mass spectrometry showed expected configuration of disulfide bridges.

Moreover, at least five out of six glycosylation sites were found to be occupied. Presence of different glycoforms can prevent crystal growth or cause low quality of diffraction data due to flexibility of oligosaccharide chains. Therefore, deglycosylated B7-H6 was used for crystallization of the complex. Unluckily, deglycosylation under standard condition led to protein precipitation, therefore differential scanning fluorimetry was performed and stabilizing conditions for deglycosylation reaction and protein storage were found.

Basic protein characterization was also performed for NKp30. Correct connection of a disulfide bridge was confirmed and occupancy of glycosylation sites was investigated. Two glycosylation sites were occupied in majority of the protein sample. These sites were Asn42 and Asn121. This information was important for further studies of NKp30 ligand binding and oligomerization, since oligomerization was found to be dependent on glycosylation [26] and above all, glycosylation of Asn42 was shown to have a major impact on ligand binding.

Binding of both proteins was confirmed by several methods, all of them suggesting strong binding affinity of the complex. Precise affinity measurement was performed by isothermal

titration calorimetry. Measured affinity was 5.8  $\mu\text{M}$  which is similar to the measurements found in literature where non-glycosylated NKp30 construct was used. Therefore the result comes as rather surprising since we expected higher affinity for glycosylated NKp30. This discrepancy between the result and the expectation may be caused by different affinity measurement methods used (SPR vs. ITC). Comparison of affinities of various NKp30 variants will shed more light on the interpretation of this result.

Oligomerization of NKp30 was also observed by several approaches. Small angle X-ray scattering data showed major difference between size of LBD particles and NKp30\_del particles which also corresponds to curve profile of size exclusion chromatography of these proteins (Fig. 41) and their sedimentation analysis which was done previously in our laboratory [26]. Moreover, the envelope size was shown to be dependent on the sample concentration which is supported by our previous studies [26] which show that there is dynamic equilibrium among all oligomeric forms of NKp30.

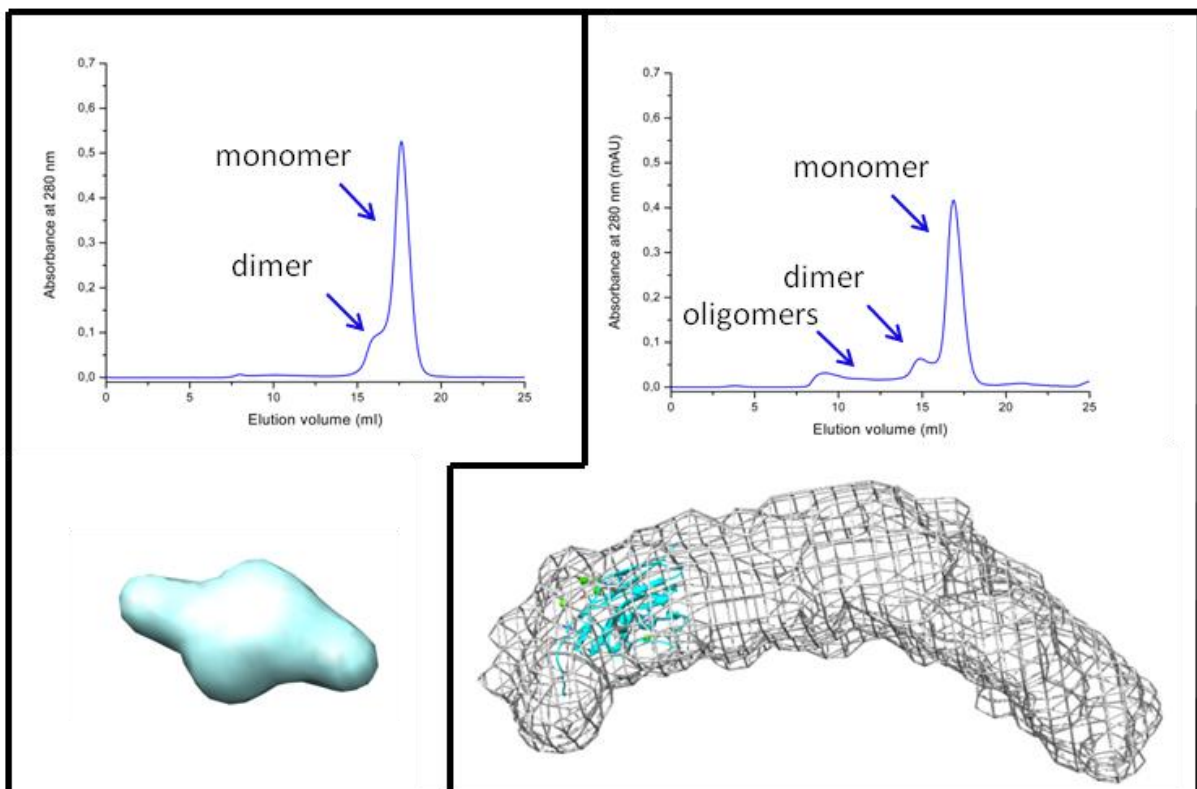


**Figure 41: Comparison of SEC and SAXS of NKp30 constructs.** Curve profiles of LBD (left) and NKp30 (right) from SEC correspond to the envelope size measured by SAXS. The size of LBD envelope (left) corresponds to LBD dimer whereas NKp30 envelope (right) is much larger and can possibly point out the shape of its oligomer.

The oligomers were also observed by electron microscopy (Fig. 42, left). The size of the particles and also their shape are similar to the particles observed previously (Fig. 42, right) [23]. However, based on the particle size, there seem to be more oligomeric forms in our EM image compared to the EM image published previously [23]. The NKp30 constructs are identical in amino acid sequence; nevertheless they differ in the glycosylation type. Our construct was produced in HEK293S GnTI<sup>-</sup> cell line which provides homogeneous glycosylation with seven monosaccharide units, while the construct in published paper was produced in Sf9 insect cell line [23] which provide also homogeneous glycosylation of similar size, yet different due to fucosylation of core N-acetylglucosamine. This difference could contribute to different shift in equilibrium among monomer and various types of NKp30 oligomers thus changing the result of electron microscopy imaging. On the other hand, previously published EM figures have clearly better resolution, probably due to better sample processing in cryo-EM measurement set-up.

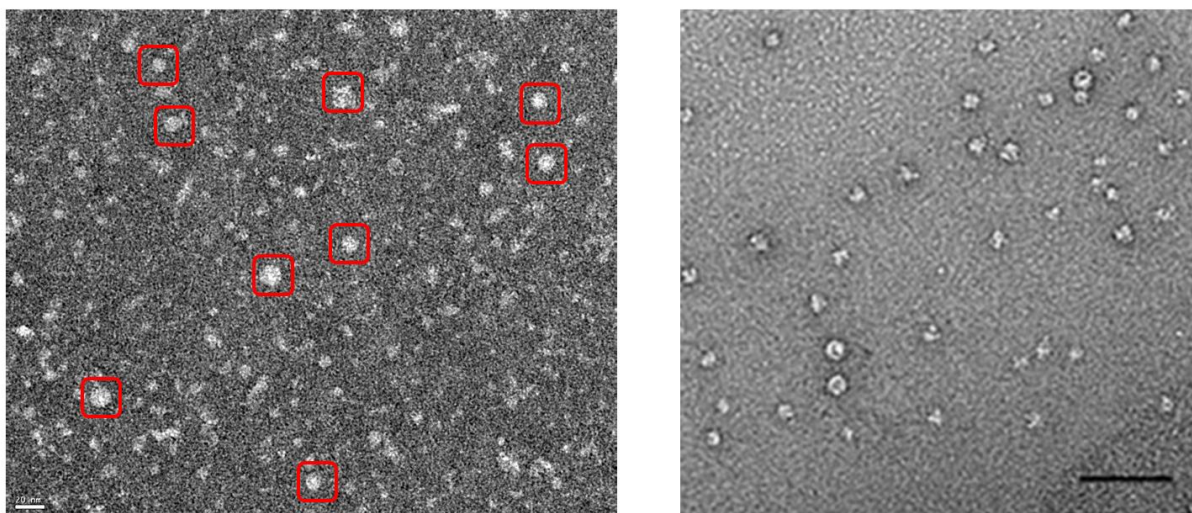


**Figure 42: Electron microscopy images of NKp30.** Comparison of previously published EM image [23] of NKp30 extracellular domain (right) and EM image obtained in this work (left). NKp30 constructs used are identical; however they differ in glycosylation type and Asn68 glycosylation site occupancy

We hoped to get more structural information by H/D exchange in combination with mass spectrometry. However, only low number of hydrogens was swapped with deuterium which calls for optimization of experimental set-up. Also it is possible that the concentration of the proteins was too low to measure significant differences between monomeric and oligomeric fractions of LBD or NKp30 (and similarly for binding of B7-H6, too).

Both electron microscopy and H/D exchange measurements could be improved by combining them with cross-linking. Although only one cross-link was detected between NKp30 and B7-H6 (chapter 5.2.1), some other sites of NKp30 were occupied by cross-linking reagents. Therefore, to study NKp30 oligomerization cross-linking could be performed at higher concentration and ideally, the change of ratio of NKp30 oligomers with change of concentration due to dynamic equilibrium would be suppressed and distinct cross-linked NKp30 oligomeric forms could be isolated by SEC and become a subject of further investigation by electron microscopy and H/D exchange, too.

The major contribution of this work reside in solution of the crystal structure of glycosylated LBD/B7H6 complex, though the model and its refinement are just preliminary. Although the structures of NKp30 alone [14] and in complex with B7-H6 [15] have already been solved, they did not explain the role of the oligomerization or glycosylation in B7-H6 binding. In the structure of NKp30, the dimeric structure of the protein is visible, however it is not clear whether the dimer is disrupted by B7-H6 binding or is stable upon binding, too. The published structure of the complex shows the interaction interface but the NKp30 dimer is not visible in the structure. Moreover, the NKp30 constructs used for the X-ray structural analysis were always produced in bacteria and thus possessed no glycosylation [14, 15].

Herein we present the first structure of NKp30/B7-H6 complex with visible dimer of NKp30. The dimer possesses the same two-fold symmetry as the published dimer of NKp30 (PID 3NOI), though slight differences can be seen (Fig. 43, p. 78). The major difference is that in the published structure of NKp30 dimer, the two molecules are in more open orientation towards each other, whilst NKp30 dimer with bound B7-H6 possesses closer conformation. This effect could be a result of conformational changes of NKp30 upon B7-H6 binding.

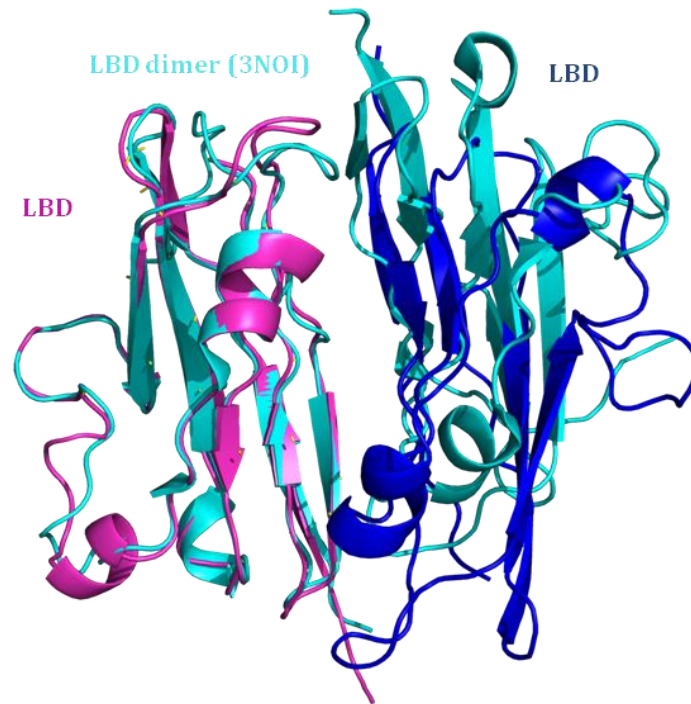


**Figure 43: NKp30 dimer alignment.** The structural differences between published and recently solved structure may be result of NKp30 conformational change upon B7-H6 binding.

Moreover, in comparison to published structure of NKp30/B7-H6 complex (PID 3PV6), one more B7-H6 molecule (two together) is in contact with NKp30 in our structure. The first NKp30/B7-H6 complex (previously termed as LBD\_A and B7-H6\_A) has similar orientation and binding interface as in already published structure (PID 3PV6) and major difference lies in B7-H6 C-terminal Ig domain orientation. There is no interaction between N- and C-terminal Ig domain of B7-H6, therefore this structural difference could be an effect and also a preliminary evidence of the C-terminal domain flexibility. The interface between second B7-H6 (B7-H6\_B) and NKp30 (LBD\_A) is very small, which suggest that this is rather a crystallographic contact with no biological relevance. Yet it is interesting that this contact is in close proximity to Asn121 of LBD, glycosylation of which has been previously shown to improve B7-H6 binding. While this might suggest biological relevance of this protein-protein interaction, such arrangement is probably impossible in the intercellular space (Fig. 44, p. 79; Fig. 45, p. 80). If the NKp30 molecules created dimer on the cell surface and both of the molecules in dimer bound two molecules of B7-H6, it would be sterically impossible for NKp30 to be attached onto the cell surface, even though 12 additional amino acids which correspond to NKp30 stalk domain are missing in the structure. However; it would be



beneficial to perform NKp30 point mutation at this interaction site to confirm or disprove the relevance of this contact.

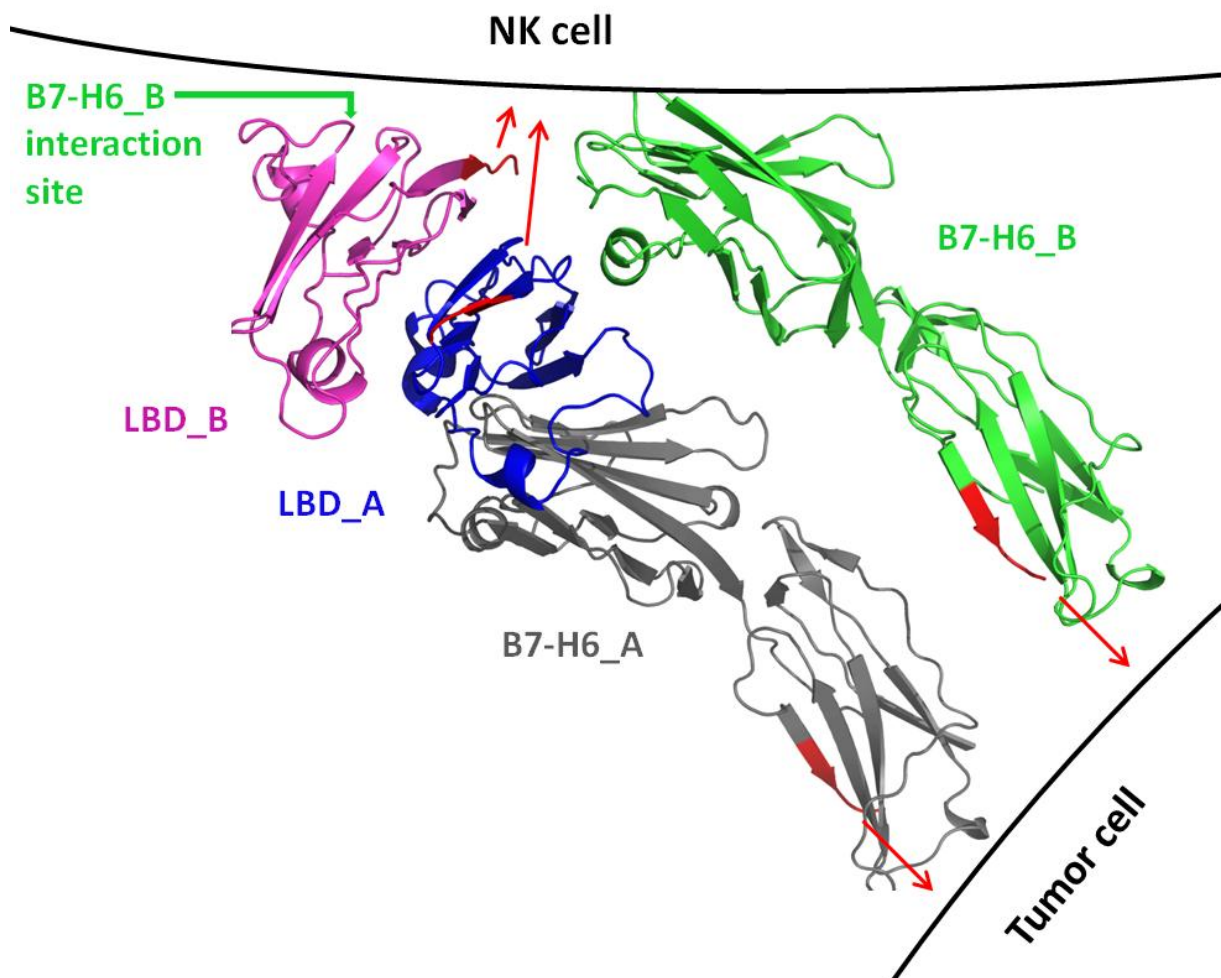


**Figure 44: Asymmetric model of NKp30/B7-H6 molecular arrangement in intracellular space.** The binding of B7-H6\_B to LBD\_A presumably does not have any biological relevance as with this arrangement, the second LBD molecule (LBD-B in this case) could not bind B7-H6 (B7-H6\_B) at the same interaction interface as LBD\_A/B7-H6\_A and no dimer-dimer structure could be formed. C-termini of all proteins are shown in red.

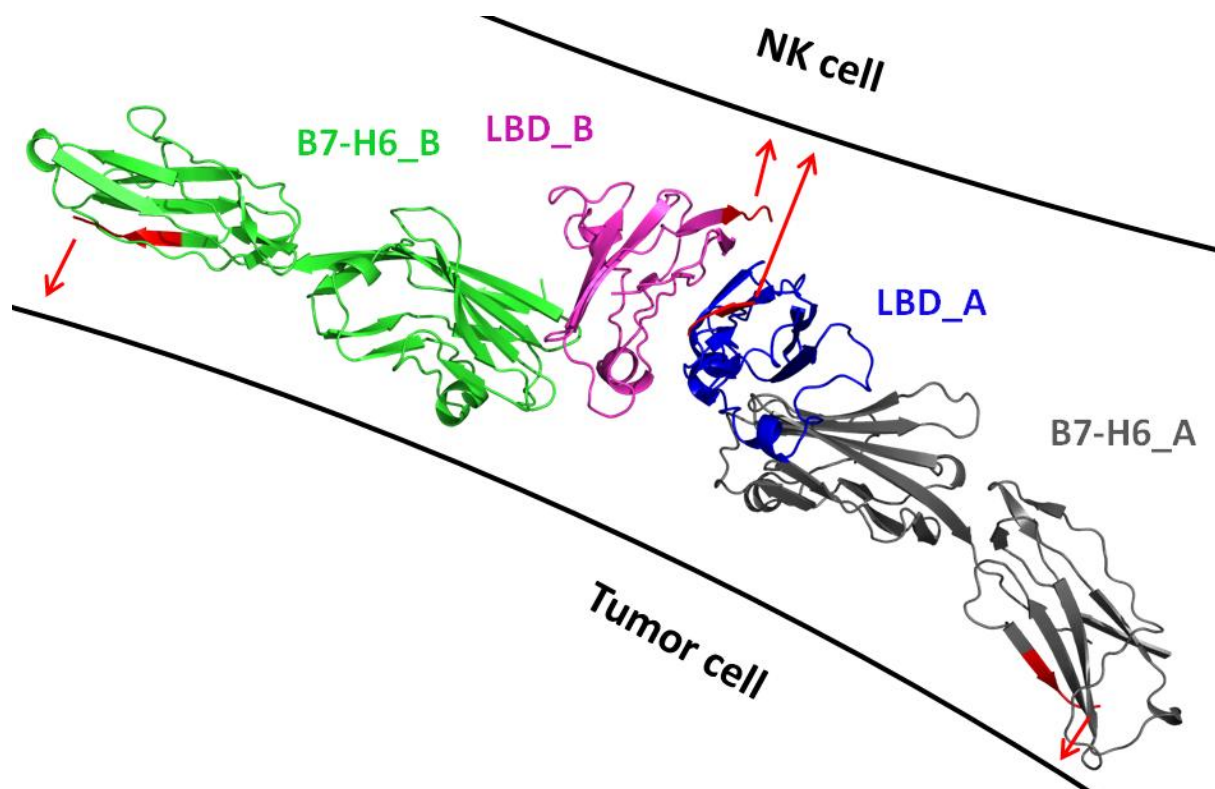


**Figure 45: Suggested model of NKp30/B7-H6 molecular arrangement in intracellular space.** In this case, each LBD molecule binds B7-H6 at the same interaction interface creating symmetric dimer-dimer structure. Interestingly, this type of interaction would probably bring membranes of both cells in close proximity which in turn might be relevant for mechanism of signal transduction and/or NK cell activation. C-termini of all proteins are shown in red.

For further research, it would be interesting to obtain crystal structure of NKp30/B7-H6 with NKp30 stalk domain, which is present just in proximity of glycosylation site Asn42 of the dimeric partner NKp30 molecule. For this purpose, the suggested follow-up is optimization of NKp30 storage buffer condition and crystallization of the complex using seeding with grown LBD/B7-H6 crystals. Also crystallization of the present LBD/B7-H6 complex could be optimized yet (sample homogeneity, protein ratio, crystallization reagents) to obtain structure with higher resolution with visible electron densities of whole N-linked oligosaccharide chains. Apart from that the ultimate goal of this project will be to put observations obtained on molecular level with individual solubilized proteins into cellular context and eventually, to observe and study NKp30 oligomerization and its ligand binding on living cells.



## 7. CONCLUSIONS

- Extracellular portion of membrane protein B7-H6 (construct B7-H6\_2, D25 - L245) was expressed in HEK293 cell line and purified.
- Protein characterization discovered incorrect disulfide bridge formation.
- Mutated form of B7-H6\_2 (C212S, termed mB7H6\_2) was expressed in HEK293 cell line and purified.
- Correct disulfide bridges formation was confirmed and occupancy of glycosylation sites was characterized.
- Conditions of B7-H6 deglycosylation were optimized.
- Binding of NKp30 and LBD to B7-H6 was confirmed and preliminary results of affinity measurement were obtained.
- Oligomers of NKp30 were observed by multiple techniques.
- Complex of glycosylated LBD and deglycosylated B7-H6 was crystallized and diffraction data were collected to 3.4 Å resolution.
- Preliminary crystal structure of the LBD/B7-H6 complex was solved.

## 8. LITERATURE

- [1] V. Hořejší, J. Bartůňková, T. Brdička and R. Špišek, *Základy imunologie*, Praha: Triton, 2013.
- [2] Bio-Rad Laboratories, Inc., "NK Cells Mini Review", cited at July 20, 2016, retrieved from <https://www.bio-rad-antibodies.com/nkcells-minireview.html>.
- [3] T. D. Holmes and Y. T. Bryceson, "Natural killer cell memory in context," *Semin Immunol.*, Electronic Collection, 2016.
- [4] M. M. Tu, A. B. Mahmoud and A. P. Makrigiannis, "Licensed and Unlicensed NK Cells: Differential Roles in Cancer and Viral control," *Front Immunol.*, vol. 7:166, Electronic collection, 2016.
- [5] A. Mandal and C. Viswanathan, "Natural killer cells: In health and disease," *Hematol Oncol Stem Cell Ther.*, vol. 8, no. 2, pp. 47-55, 2015.
- [6] H. J. Pegram, D. M. Andrews, M. J. Smyth, P. K. Darcy and M. H. Kershaw, "Activating and inhibitory receptors of natural killer cells," *Nature*, vol. 89, no. 2, pp. 216-24, 2011.
- [7] P. H. Kruse, J. Matta, S. Ugolini and E. Vivier, "Natural cytotoxicity receptors and their ligands," *Immunol Cell Biol.*, vol. 92, no. 3, pp. 221-9, 2013.
- [8] J. Back, E. L. Malchiodi, S. Cho, L. Scarpellino, P. Schneider, M. C. Kerzic, R. A. Mariuzza and W. Held, "Distinct conformations of Ly49 natural killer cell receptors mediate MHC class I recognition in trans and cis," *Immunity*, vol. 31, no. 4, pp. 598-608, 2009.
- [9] O. Hershkovitz, M. Jarahian, A. Zilka, A. Bar-Ilan, G. Landau, S. Jivov, Y. Tekoah, R. Glicklis, J. T. Gallagher, S. C. Hofmann, H. Zer, O. Mandelboim, C. Watzl, F. Momburg and A. Porgador, "Altered glycosylation of recombinant NKp30 hampers binding to heparan sulfate: a lesson for the use of recombinant immunoreceptors as an immunological tool," *Glycobiology*, vol. 18, no. 1, pp. 28-41, 2008.

- [10] W. Wang, H. Guo, J. Geng, X. Zheng, H. Wei, R. Sun and Z. Tian, "Tumor-released Galectin-3, a soluble inhibitory ligand of human NKp30, plays an important role in tumor escape from NK cell attack," *J Biol Chem.*, vol. 289, no. 48, pp. 33311-9, 2014.
- [11] P. Höglund and P. Brodin, "Current perspectives of natural killer cell education by MHC class I molecules," *Nat Rev Immunol.*, vol. 10, no. 10, pp. 724-34, 2010.
- [12] D. Pende, S. Parolini, A. Pessino, S. Sivori, R. Augugliaro, L. Morelli, E. Marcenaro, L. Accame, A. Malaspina, R. Biassoni, C. Bottino, L. Moretta and A. Moretta, "Identification and Molecular Characterization of NKp30, a Novel Triggering Receptor Involved in Natural Cytotoxicity Mediated by Human Natural Killer Cells," *J Exp Med.*, vol. 190, no. 10, pp. 1505-16, 1999.
- [13] T. Kaifu, B. Escalière, L. N. Gastinel, E. Vivier and M. Baratin, "B7-H6/NKp30 interaction: a mechanism of alerting NK cells against tumors," *Cell Mol Life Sci*, vol. 68, no. 21, pp. 3531-9, 2011.
- [14] M. G. Joyce, P. Tran, M. A. Zhuravleva, J. Jaw, M. Colonna and P. D. Sun, "Crystal structure of human natural cytotoxicity receptor NKp30 and identification of its ligand binding site," *Proc Natl Acad Sci U S A.*, vol. 108, no. 15, pp. 6223-8, 2011.
- [15] Y. Li, Q. Wang and R. A. Mariuzza, "Structure of the human activating natural cytotoxicity receptor NKp30 bound to its tumor cell ligand B7-H6," *J Exp Med.*, vol. 208, no. 4, pp. 703-14, 2011.
- [16] N. F. Delahaye and e. al., "Alternatively spliced NKp30 isoforms affect the prognosis of gastrointestinal stromal tumors," *Nat Med.*, vol. 17, no. 6, pp. 700-7, 2011.
- [17] E. Mavoungou, J. Held, L. Mewono and P. G. Kremsner, "A Duffy binding-like domain is involved in the NKp30-mediated recognition of Plasmodium falciparum-parasitized erythrocytes by natural killer cells," *J Infect Dis.*, vol. 195, no. 10, pp. 1521-31, 2007.
- [18] T. I. Arnon, H. Achdout, O. Levi, G. Markel, N. Saleh, G. Katz, R. Gazit, T. Gonen-Gross, J. Hanna, E. Nahari, A. Porgador, A. Honigman, B. Plachter, D. Mevorach, D. G. Wolf and O.

- Mandelboim, "Inhibition of the NKp30 activating receptor by pp65 of human cytomegalovirus," *Nat Immunol.*, vol. 6, no. 5, pp. 515-23, 2005.
- [19] J. Binici and J. Koch, "BAG-6, a jack of all trades in health and disease," *Cell Mol Life Sci.*, vol. 71, no. 10, pp. 1829-37, 2014.
- [20] C. S. Brandt, M. Baratin, E. C. Yi, J. Kennedy, Z. Gao, B. Fox, B. Haldeman, C. D. Ostrander, T. Kaifu, C. Chabannon, A. Moretta, R. West, W. Xu, E. Vivier and S. D. Levin, "The B7 family member B7-H6 is a tumor cell ligand for the activating natural killer cell receptor NKp30 in humans," *J Exp Med.*, vol. 206, no. 7, pp. 1495-503, 2009.
- [21] E. Schlecker, N. Fiegler, A. Arnold, P. Altevogt, S. Rose-John, G. Moldenhauer, A. Sucker, A. Paschen, E. P. von Strandmann, S. Textor and A. Cerwenka, "Metalloprotease-Mediated Tumor Cell Shedding of B7-H6, the ligand of the natural killer cell-activating receptor NKp30," *Cancer Res*, vol. 74, no. 13, pp. 3429-40, 2014.
- [22] J. Hartmann, T. V. Tran, J. Kaudeer, K. Oberle, J. Hermann, I. Quagliano, T. Abel, A. Cohnen, V. Gatterdam, A. Jacobs, B. Wollscheid, R. Tampé, C. Watzl, A. Diefenbach and J. Koch, "The stalk domain and the glycosylation status of the activating natural killer cell receptor NKp30 are important for ligand binding," *J Biol Chem.*, vol. 287, no. 37, pp. 31527-39, 2012.
- [23] J. Hermann, H. Berberich, J. Hartmann, S. Beyer, K. Davies and J. Koch, "Homooligomerization of the activating natural killer cell receptor NKp30 ectodomain increases its binding affinity for cellular ligands," *J Biol Chem.*, vol. 289, no. 2, pp. 765-77, 2014.
- [24] P. J. Reeves, N. C. Callewaert and H. G. Khorana, "Structure and function in rhodopsin: High-level expression of rhodopsin with restricted and homogeneous N-glycosylation by a tetracycline-inducible N-acetylglucosaminyltransferase I-negative HEK293S stable mammalian cell line," *Proc Natl Acad Sci U S A.*, vol. 99, no. 21, pp. 13419-24, 2002.
- [25] J. Binici, J. Hartmann, J. Herrmann, C. Schreiber, S. Beyer, G. Güler, V. Vogel, F. Tumulka, R. Abele, W. Mäntele and J. Koch, "A soluble fragment of the tumor antigen BCL2-associated athanogene 6 (BAG-6) is essential and sufficient for inhibition of NKp30

- receptor-dependent cytotoxicity of natural killer cells," *J Biol Chem.*, vol. 288, no. 48, pp. 34295-303, 2013.
- [26] B. Kalousková, "Preparation of glycosylated form of human immunoreceptor," Bachelor thesis, Faculty of Science, Charles University in Prague, 2014.
- [27] J. Matta, M. Baratin, L. Chiche, J. M. Forel, C. Cognet, G. Thomas, C. Farnarier, C. Piperoglou, L. Papazian, D. Cahussabel, S. Ugolini, F. Vély and E. Vivier, "Induction of B7-H6, a ligand for the natural killer cell-activating receptor NKp30, in inflammatory conditions," *Blood*, vol. 122, no. 3, pp. 394-404, 2013.
- [28] S. Pesce, G. Tabellini, C. Cantoni, O. Patrizi, D. Coltrini, F. Rampinelli, J. Matta, E. Vivier, A. Moretta, S. Parolini and E. Marcenaro, "B7-H6-mediated downregulation of NKp30 in NK cells contributes to ovarian carcinoma immune escape," *Oncoimmunology*, vol. 4, no. 4, Electronic collection, 2015.
- [29] J. Guo, C. Guo, Z. He, Z. Liu, Y. Wang and Y. Mou, "Clinical significance of B7-H6 protein expression in astrocytoma," *Onco Targets Ther.*, vol. 9, pp. 3291-97, 2016.
- [30] X. Zhang, G. Zhang, Y. Qin, R. Bai and J. Huang, "B7-H6 expression in non-small cell lung cancers," *Int J Clin Exp Pathol.*, vol. 7, no. 10, pp. 6936-42, 2014.
- [31] X. J. Chen, J. Shen, G. B. Zhang and W. C. Chen, "B7-H6 protein expression has no prognostic significance in human gastric carcinoma," *Pathol Oncol Res.*, vol. 20, no. 1, pp. 203-7, 2014.
- [32] Y. Zhou, Y. Xu, L. Chen, B. Xu, C. Wu and J. Jiang, "B7-H6 expression correlates with cancer progression and patient's survival in human ovarian cancer," *Int J Clin Exp Pathol.*, vol. 8, no. 8, pp. 9428-33, 2015.
- [33] S. Rusakiewicz and e. al., "NCR3/NKp30 contributes to pathogenesis in primary Sjögren's syndrome," *Sci Transl Med.*, vol. 24, no. 5, Electronic collection, 2014.
- [34] F. Bisio, F. Bozzano, F. Marras, A. Di Biagio, L. Moretta and A. De Maria, "Successfully treated HIV-infected patients have differential expression of NK cell receptors (NKp46

- and NKp30) according to AIDS status at presentation," *Immunol Lett.*, vol. 152, no. 1, pp. 16-24, 2013.
- [35] Y. Zou, T. Chen, M. Han, H. Wang, W. Yan, G. Song, Z. Wu, X. Wang, C. Zhu, X. Luo and Q. Ning, "Increased killing of liver NK cells by Fas/Fas ligand and NKG2D/NKG2D ligand contributes to hepatocyte necrosis in virus-induced liver failure," *J Immunol.*, vol. 184, no. 1, pp. 466-75, 2010.
- [36] S. Mantovani, D. Mele, B. Oliviero, G. Barbarini, S. Varchetta and M. U. Mondelli, "NKp30 isoforms in patients with chronic hepatitis C virus infection," *Immunology*, vol. 146, no. 2, pp. 234-42, 2015.
- [37] M. Semeraro and e. al., "Clinical impact of the NKp30/B7-H6 axis in high-risk neuroblastoma patients," *Sci Transl Med.*, vol. 7, no. 283, Electronic collection, 2015.
- [38] A. Shemesh, D. Tirosh, E. Sheiner, N. Benshalom-Tirosh, M. Brusilovsky, R. Segev, B. Rosental and A. Porgador, "First Trimester Pregnancy Loss and the Expression of Alternatively Spliced NKp30 Isoforms in Maternal Blood and Placental Tissue," *Front Immunol.*, vol. 6, p. 189, 2015.
- [39] G. Cao, J. Wang, X. Zheng, H. Wei, Z. Tian and R. Sun, "Tumor Therapeutics Work as Stress Inducers to Enhance Tumor Sensitivity to Natural Killer (NK) Cell Cytolysis by Up-regulating NKp30 Ligand B7-H6.," *J Biol Chem.*, vol. 290, no. 50, pp. 29964-73, 2015.
- [40] C. Kellner, A. Günther, A. Humpe, R. Repp, K. Klausz, S. Derer, T. Valerius, M. Ritgen, M. Brüggemann, J. G. van de Winkel, P. W. Parren, M. Kneba, M. Gramatzki and M. Peipp, "Enhancing natural killer cell-mediated lysis of lymphoma cells by combining therapeutic antibodies with CD20-specific immunoligands engaging NKG2D or NKp30," *Oncoimmunology*, vol. 5, no. 1, Electronic collection, 2015.
- [41] M. Peipp, S. Derer, S. Lohse, M. Staudinger, K. Klausz, T. Valerius, M. Gramatzki and C. Kellner, "HER2-specific immunoligands engaging NKp30 or NKp80 trigger NK-cell-mediated lysis of tumor cells and enhance antibody-dependent cell-mediated cytotoxicity," *Oncotarget.*, vol. 6, no. 31, pp. 32075-88, 2015.

- [42] M. Wu, T. Zhang, A. T. Gacerez, T. A. Coupet, L. R. DeMars and C. L. Sentman, "B7H6-specific bispecific T cell engagers (BiTEs) lead to tumor elimination and host anti-tumor immunity," *J Immunol.*, vol. 194, no. 11, pp. 5305-5311, 2015.
- [43] T. I. Arnon, G. Markel, A. Bar-Ilan, J. Hanna, E. Fima, F. Benchetrit, A. Cerwenka, D. Benharroch, N. Sion-Vardy, A. Porgador and O. Mandelboim, "Harnessing Soluble NK Cell Killer Receptors for the Generation of Novel Cancer Immune Therapy," *PLoS ONE*, vol. 3, no. 5, Electronic collection, 2008.
- [44] T. Zhang, M. Wu and C. L. Sentman, "An NKp30-based chimeric antigen receptor promotes T-cell effector functions and anti-tumor efficacy in vivo," *J Immunol.*, vol. 189, no. 5, pp. 2290-99, 2012.
- [45] M. Phillips, F. Romeo, C. Bitsaksis and D. Sabatino, "B7H6 Derived Peptides Trigger TNF- $\alpha$  Dependent Immunostimulatory Activity of Lymphocytic NK92-M1 Cells," *Biopolymers*, Ahead of print, 2016.
- [46] B. Besse and e. al., "Dendritic cell-derived exosomes as maintenance immunotherapy after first line chemotherapy in NSCLC," *Oncoimmunology*, vol. 5, no. 4, Electronic collection, 2016.
- [47] EX-CELL™ 293 Serum-Free Medium for HEK 293 Cells, cited on August 9, 2016, retrieved from [http://www.sigmaaldrich.com/content/dam/sigmaaldrich/docs/Sigma/Product\\_Information\\_Sheet/p24571.pdf](http://www.sigmaaldrich.com/content/dam/sigmaaldrich/docs/Sigma/Product_Information_Sheet/p24571.pdf).
- [48] S. Pažický, "Preparation of expression vectors for receptor NKp30 and its ligands B7-H6 and BAG-6," Bachelor thesis, Faculty of Nature Science, Charles University, 2014.
- [49] Gel/PCR DNA Fragments Extraction Kit, cited on August 9, 2016, retrieved from <http://www.geneaid.com/sites/default/files/DF13.pdf>.
- [50] High-Speed Plasmid Mini Kit, cited on August 9, 2016, retrieved from <http://www.geneaid.com/sites/default/files/PD13.pdf>.

- [51] E. Gasteiger, C. Hoogland, A. Gattiker, S. Duvaud, M. R. Wilkins, R. D. Appel and A. Bairoch, "Protein Identification and Analysis Tools on the ExpASY Server," in *The Proteomics Protocols Handbook*, Humana Press, 2005, pp. 571-607.
- [52] SENDTERP software, cited on August 2, 2016, retrieved from <http://www.jphilo.mailway.com/default.htm>.
- [53] SEDFIT software, cited on August 2, 2016, retrieved from <http://www.analyticalultracentrifugation.com/tutorials.htm>.
- [54] P. V. Konarev, V. V. Volkov, A. V. Sokolova, M. H. J. Koch and D. I. Svergun, "PRIMUS: a Windows PC-based system for small-angle scattering data analysis," *J. Appl. Crystallogr.*, vol. 36, pp. 1277-82, 2003.
- [55] Uniprot website, cited on August 2, 2016, retrieved from <http://www.uniprot.org/uniprot/Q68D85>.
- [56] D. Svergun, C. Barberato and M. H. J. Koch, "a Program to Evaluate X-ray Solution Scattering of Biological Macromolecules from Atomic Coordinates," *J. Appl. Cryst.*, vol. 28, pp. 768-73, 1995.



Svoluji k zapůjčení této práce pro studijní účely a prosím, aby byla řádně vedena evidence vypůjčovatelů.

Jméno a příjmení, adresa	Číslo OP	Datum vypůjčení	Poznámka